IL-33 drives polyfunctionality and antitumor activity of a unique ST2+ NK cell population

Isabelle Treilleux, Marie-cecile Michallet, Jenny Valladeau-Guilemond, Antoine Marçais, Thierry Walzer, Philippe Krebs, Adelheid Cerwenka, Margaux Hubert, Christophe Caux, Nathalie Bendriss-Vermare

IL-33 drives polyfunctionality and antitumor activity of a unique ST2+ NK cell population

Anaïs Eberhardt[1], Elena Blanc[1], Valentin Picant[1], Vincent Alcazer[1], Yamila Rocca[1], Maude Ardin[1], Aurélien Voissière[1], Fanny Onodi[1], Céline Rodriguez[1], Laurie Tonon[2], Benjamin Estavoyer[1], Lyvia Moudombi[1], Emily Charrier[3], Xi Wang[4,5], Ana Stojanovic[6], Tilman Rau[7], Olivier Tredan[8], Isabelle Treilleux[8], Marie-Cécile Michallet[1], Jenny Valladeau-Guilemond[1], Antoine Marçais[3], Thierry Walzer[3], Philippe Krebs[7], Adelheid Cerwenka[6,9], Margaux Hubert[1], Christophe Caux[1,10], Nathalie Bendriss-Vermare[1,10]*

[1] Centre de Recherche en Cancérologie de Lyon, INSERM U1052, CNRS UMR5286, Université de Lyon, Université Lyon 1, Centre Léon Bérard, F-69000 Lyon, France.

[2] Fondation Synergie-Lyon-Cancer, 28, rue Laennec, 69008 Lyon, France

[3] CIRI, Centre International de Recherche en Infectiologie Lyon, France; INSERM, U1111, Lyon, France; École Normale Supérieure de Lyon, Lyon, France; Université Lyon 1, Lyon, France; and CNRS, UMR 5308, Lyon, France.

[4] State Key Laboratory of Reproductive Medicine, Nanjing Medical University, Nanjing 211166, China

[5] Division of Cellular Immunology, German Cancer Research Center, 69120 Heidelberg, Germany

[6] Department of Immunobiochemistry, Mannheim Institute for Innate Immunoscience (MI3), Heidelberg University, 68167 Mannheim, Germany

[7] Institute of Pathology, University of Bern, Bern, Switzerland.

[8] Department of Medical Oncology, Centre Léon Bérard, F-69000 Lyon, France.

[9] European Center for Angioscience (ECAS), Medical Faculty Mannheim, University of Heidelberg, 68167 Mannheim, Germany

[10]These authors contributed equally

*Corresponding author. Email: nathalie.bendriss-vermare@lyon.unicancer.fr

One sentence summary: The IL-33/IL-33R(ST2)/NK cell axis is a key determinant of cancer immunity and immunotherapy.

Abstract

Natural Killer (NK) cell subsets differ to ensure complementary and crucial roles in tumor immunosurveillance. Their biology is critically regulated by cytokines. Here, we show that IL-33 synergizes with IL-12 to strongly activate a subset of $CD56^{dim}$ NK cells acquiring ST2 expression. Transcriptomic and biological analysis of human $ST2^{+}$ $CD56^{dim}$ NK cells revealed a distinct intermediate differentiation state between canonical $CD56^{bright}$ and $CD56^{dim}$ NK cells, combining high proliferative properties, cytokines/chemokines production, and cytotoxicity. NK cells expressing ST2 protein or exhibiting a ST2-linked transcriptional signature were identified in human and mouse tumors. Accordingly, IL-12 unleashes human breast tumor $ST2^{+}$ NK cell potential to produce IFN-γ in response to IL-33 and IL-33/IL-12 co-injection resulted in a NK-dependent IFN-γ secretion and anti-tumor effects in murine mammary tumors. An *IL33^{hi}-NK*^{hi} score in solid tumors correlated with increased progression-free patient survival. Our findings thus identify polyfunctional $ST2^{+}$ NK cells which effector functions can be harnessed by IL-33 to boost anti-tumor immunity.

Keywords: NK cells, IL-33, ST2/IL1RL1, cancer immunosurveillance, cancer immunotherapy

Introduction

Natural Killer (NK) cells are major innate effector cells involved in host defense against viral infections and tumors *(1)*. NK cells have evolved into a spectrum of effector subsets, including the main CD56^{bright} and CD56^{dim} subsets in humans, diverging in terms of phenotype, function, location, and responsiveness to activating stimuli to ensure complementary roles in innate immune responses *(2)*. Indeed, CD56^{bright} NK cells are predominant in lymphoid tissues, secrete high levels of cytokines and chemokines including Interferon-gamma (IFN)-γ, Tumor Necrosis Factor-alpha (TNF-α), CCL3/4 (Macrophage Inflammatory Protein 1 α/β), and CCL5 (RANTES) and undergo robust proliferation after cytokine stimulation *(3)*. Conversely, CD56^{dim} NK cells are the largest circulating population, show a greater cytotoxic ability but a lower cytokine production and proliferation compared to CD56^{bright} NK cells *(2)*. CD56^{dim} NK cells also express the activating Fc receptor CD16, endowing them with antibody-dependent cellular cytotoxicity (ADCC) function, a central mechanism in antibody-based antitumor therapies *(4)*.

Developmental relationships between NK cell subsets remain partially solved, with CD56^{dim} NK cells likely originating from differentiated CD56^{bright} NK cells *(5, 6)*, and evidences of intermediate subsets corroborating this developmental trajectory *(7)*. CD56^{dim} NK cells can then give rise to a variety of phenotypically and functionally distinct subsets including terminally differentiated CD56^{dim} CD57^{+} *(8, 9)*, memory-like/adaptive *(10)* or hypo-responsive exhausted-like NK cells *(11)*. These NK cell subsets are characterized by distinct transcriptional programs *(12, 13)* regulated by profound epigenetic modifications and chromatin re-arrangements *(14, 13)*. Therefore, NK cell diversity is broader than originally depicted and delineates functionally distinct subsets, which may be alternatively exploited for the development of therapeutic strategies *(15)*.

NK cells are highly potent in tumor elimination by directly killing cancer cells and supporting effective innate and adaptive antitumor immune responses *(16)*. Many tumor cells express high levels of ligands for activating NK cell receptors, leading to efficient recognition by NK cells *(17)*. Accordingly, high intratumoral infiltration by NK cells is associated with improved prognosis for cancer patients *(18–*

20). However, chronic exposure to activating signals, presence of inhibitory ligands and immunosuppressive molecules in tumor microenvironment favor NK cells dysfunction, leading to tumor escape *(21)*. In this context, NK cells are emerging as promising targets for cancer therapy with a growing number of therapeutic agents aiming to unleash their full antitumor potential.

The activation of NK cells depends on the signaling balance between activating and inhibitory receptors. However, numerous cytokines such as Interleukin(IL)-2 *(22)*, IL-12 *(23)*, IL-15 *(24)*, IL-18 *(25)*, and type I IFN *(26)* also regulate NK cell maturation, activation, and survival by acting alone or in cooperation. The identification of cytokines (*i.e.* IL-21, IL-23, IL-27, IL-33) regulating NK cells is continually increasing *(27)*. The IL-1-like cytokine IL-33 is constitutively expressed in the nucleus of non-immune cells at epithelial barriers *(28)*. In response to tissue injury, cellular stress, and inflammation, IL-33 is released and functions as an alarmin by activating immune cells expressing its heterodimeric receptor, composed of ST2 (encoded by *IL1RL1* gene) and ILRAcP accessory chain *(29)*. The IL-33/ST2 axis was originally described to support type 2 immunity *(30)*. Also, studies showed a pivotal role of the IL-33/ST2 pathway on the biology of a subset of regulatory T cells (Tregs) constitutively expressing ST2 and involved in tissue repair *(31)* and immunomodulation *(32)*. In contrast, IL-33 is now emerging as a regulator of Th1 responses during viral infection and chronic immune pathologies in mice, enhancing IFN-γ production in $CD4^+$ cells, $CD8^+$ T cells, and NK/NKT cells that acquire ST2 expression under inflammatory conditions *(33–35)*. However, the role of IL-33/ST2 axis in human NK cell subsets biology remains scarcely addressed and its impact on tumor development has revealed opposing effects depending on the tumor type and the microenvironment *(36)*. Indeed, IL-33 can contribute to tumor progression and metastasis by promoting immune cell-dependent (*i.e.*, recruitment of immune suppressive cells, activation of type 2-mediated inflammation, and inhibition of effector CD8 T and NK cells) and immune cell-independent (i.e., tumor angiogenesis, cancer cell stemness, tumor cell proliferation) mechanisms. In contrast, systemic and/or local production of IL-33 can inhibit tumor growth and metastasis by enhancing both adaptive (*i.e.*, effector Th1 and CD8 T cells) and innate (*i.e.*, NK cells, DCs, and eosinophils) immune responses.

In this study, we evaluated the role of IL-33 in NK cell biology in physiological and tumor context in human and mouse models. We found that IL-12 upregulates ST2 expression on a subset of human NK cells, in a STAT4-dependent pathway, promoting NK cell activation by IL-33. Following IL-33 stimulation, human $ST2^{+}$ NK cells displayed polyfunctional activity featuring increased secretory and cytotoxic functions as well as a higher proliferative ability. RNA sequencing (RNA-seq) analysis identified human $ST2^{+}$ $CD56^{dim}$ NK cells as an unprecedently characterized intermediate population between canonical $CD56^{bright}$ and $ST2^{-}$ $CD56^{dim}$ NK cells. We also identified NK cells expressing ST2 protein in human breast tumors or exhibiting an ST2-linked transcriptional signature in human and mouse tumor public scRNA-seq datasets. In accordance, IL-12 unleashes the potential of $ST2^{+}$ NK cells from the blood and tumor tissue of breast cancer patients to respond to IL-33 by producing IFN-γ. In a murine mammary tumor model, IL-33 and IL-12 combination had a potent NK-dependent antitumor effect associated with IFN-γ production. Finally, pan-cancer analysis in TCGA database showed that an *IL33*^{hi}*-NK*^{hi} score correlates with good prognosis in several solid cancers including breast cancer. Therefore, our results reveal $ST2^{+}$ NK cells as a hitherto unappreciated polyfunctional subset potentially involved in tumor immune surveillance and identify IL-33 as a promising immunomodulator for NK cell-based cancer therapy.

Results

IL-12/STAT4 signaling drives ST2 expression on human NK cells endowed with polyfunctionality in response to IL-33

As previously reported for mouse NK cells in infectious contexts *(35)*, IL-33 was a particularly potent IFN-γ inducer in human NK cells when combined with IL-12 (from ≈500- to ≈1800-fold as compared to IL-12 alone) (Fig. 1A), similarly to IL-18, a well-known IFN-γ trigger for NK cells, and was 4-fold more potent than IL-1α/β. IL-33 also synergized with IL-2 (60-fold), IL-15 (7-fold) but not with anti-NKaR agonistic antibodies or K562 target cells (fig. S1A-C). IL-12 and IL-33 synergy was dose-dependent (fig. S1D) and IFN-γ was detected within a few hours to peak at 72 h (fig. S1H) reaching comparable levels (> 1 μg/mL) to those induced by IL-12/IL-18 co-stimulation. At low doses (1 ng/mL), IL-33 even induced higher levels of IFN-γ than IL-18, when combined with IL-12 (fig. S1D). The combination of IL-33 and IL-12 also enhanced NK cell cytotoxicity towards K562 target cells (Fig. 1B, fig. S1I), and induced their expression of CD25 and CD69 activation markers (Fig. 1C). These results indicate that IL-33, in the presence of IL-12, is nearly as effective as IL-18 to trigger polyfunctional activation of NK cells. Blocking experiments using specific antagonistic molecules against IL-1 family cytokines or receptors demonstrated that ST2 is specifically involved in the synergistic effect of IL-33 (Fig. 1D and fig. S2A) with IL-12 on IFN-γ production. The analysis of ST2 expression showed that *ST2* mRNA expression was very low in resting NK cells but increased up to 15- and 35-fold upon stimulation with IL-12 alone or combined with IL-33, respectively (Fig. 1E), to reach a plateau after 48h (fig. S2B). Levels of *IL1RAcP* co-receptor transcripts in NK cells were not similarly regulated (Fig. 1E and fig. S2B). Accordingly, ST2 protein was not detected on resting NK cells, but ~20% of NK cells, expressing intermediate CD56 levels, acquired ST2 surface expression upon IL-12 stimulation (Fig. 1F). IL-12 mainly activates STAT4-dependent transcription programs *(37)*. The treatment of IL-12-activated NK cells with lisofylline, a specific inhibitor of STAT4 phosphorylation (fig. S2C), resulted in a decrease in ST2 expression in NK cells (Fig. 1F). *In silico* analysis of the *ST2* promoter identified several potential STAT4 binding sites (fig. S2D). The binding of STAT4 to the *ST2* promoter was confirmed in IL-12-stimulated NK cells by chromatin immunoprecipitation (Fig.

1G). Taken together, these data indicate that IL-12 stimulation induces *ST2* transcription and protein expression in a subset of NK cells, through direct binding of STAT4 to the *ST2* promoter, leading to potent IFN-γ production in response to IL-33.

IL-33 is a potent activator of a subset of human CD56^{dim} NK cells in the presence of IL-12

Next, we aimed to characterize more deeply the NK cells subset acquiring ST2 expression in response to IL-12. IL-12 triggered ST2 expression selectively in ~20% of CD56^{dim} NK cells (Fig. 2A) but not in CD56^{bright} NK cells, although STAT4 activation was observed in both subsets in response to IL-12 (fig. S3A). We then used NF-κB (p65) *(38)*, MAPkinases (p38) *(39)*, and mTOR (S6) *(40)* signaling pathway activation as surrogates for ST2/IL-33 signaling. In line with ST2 expression, IL-12 and IL-33 co-stimulation of sorted NK cell subsets selectively induced p65, p38, and S6 phosphorylation exclusively in ~25% of CD56^{dim} NK cells (Fig. 2B and fig. S3B), while each cytokine alone was ineffective. In agreement, a much greater proportion of CD56^{dim} NK cells produced IFN-γ and co-expressed CD25 (Fig. 2C) or CD69 (fig. S3C) in response to IL-12 and IL-33 combination, as compared to CD56^{bright} NK cells. Coherently with CD25 expression, the highest IL-2-triggered proliferation was observed in CD56^{dim} NK cells following pre-activation with IL-12 and IL-33 combination (Fig. 2D). Of note IL-33 was more potent that IL-18 in inducing IL-2 dependent proliferation. In addition, IL-12 and IL-33 combination promoted a specific inflammatory cytokine secretion profile in CD56^{dim} NK cells (Fig. 2E), involving TNF-α, CCL3, and CCL4. As a comparison, the other IL-1s cytokines preferentially promoted the activation (Fig. 2, B and C, fig. S3B and C), the proliferation (Fig. 2D), and the cytokine production (Fig. 2E) in CD56^{bright} NK cells (for IL-1α and IL-1β) or in both NK subsets (for IL-18). CD56^{dim} NK cells represent a heterogeneous population based on CD57 and KIRs surface expression *(9, 8)*. In IL-12 context, while IL-18 preferentially triggered IFN-γ production in CD56^{bright} NK cells, the effect of IL-33 was more prominent in CD56^{dim} CD57^{-} cells NK cells (Fig. 2F), correlating with ST2 expression (Fig. 2G). Altogether these results highlight differences in the regulation of NK cell activation by IL-1s family cytokines, IL-33 being highly selective for CD56^{dim} NK cells, as summarized in Fig. 2H.

ST2^{+} NK cells show a unique transcriptional signature with intermediate features between CD56^{bright} and CD56^{dim} subsets

To further characterize human ST2^{+} NK cells, we performed RNA-seq analysis from three different donors on eight FACS-sorted NK cell subsets, based on surface expression of CD56, CD57, and ST2 following 24-hour culture in medium or IL-12 to induce ST2 expression (Fig. 3A). Principle Component Analysis (PCA) revealed that the PC1 axis (39% variance) segregated NK cells according to CD56 expression, whereas the PC2 axis (27% variance) discriminated samples according to IL-12 stimulation. Interestingly, ST2^{+} CD56^{dim} NK cells clustered together between ST2^{-} CD56^{bright} and ST2^{-} CD56^{dim} NK cells along the PC1 axis (Fig. 3B). Focusing on IL-12 culture conditions, 2,399 genes displayed differential expression between ST2^{-} CD56^{bright}, ST2^{-} CD56^{dim}, and ST2^{+} CD56^{dim} NK cells (fig. S4A). Analysis of genes specifically upregulated in each subset compared to the two others allowed us to define transcriptomic signatures specific for each NK cells subsets (Fig. 3C and Tables 1-3). The ST2^{+} CD56^{dim} NK cells signature contained 233 genes, including genes encoding surface proteins (e.g., *IL23R*, *IL1RL1*, *TRPV1, SLC16A1*, *ITGA3, MT1X*, *PTGER3*, *ULBP1*, *ICAM1*, *HPSE*, *TREML2*, *LRP8*, *EDA2R)*, secreted proteins (*VEGFA*, *GZMA, IFNG*), and transcription factors (TFs) (*DMRTA2*, *E2F2*, *E2F1*, *EZH2*, *ATF3*) (Fig. 3C, fig. S4B, and Table 1). We then evaluated the enrichment score for signatures of ST2^{-} CD56^{bright} (418 genes), ST2^{-} CD56^{dim} (396 genes), and ST2^{+} CD56^{dim} NK cells (233 genes) in each subset respectively by single sample gene set enrichment analysis (ssGSEA). Strikingly, ST2^{+} CD56^{dim} NK cells displayed an intermediate enrichment score for both ST2^{-} CD56^{bright} and ST2^{-} CD56^{dim} NK cell signatures (Fig. 3D). Indeed, besides genes specifically enriched in ST2^{+} CD56^{dim} NK cells, we also observed sets of genes encoding TFs, surface markers or soluble mediators exclusive for ST2^{-} CD56^{bright} and ST2^{-} CD56^{dim} NK cells and expressed at intermediate levels in ST2^{+} CD56^{dim} NK cells (Fig. 3E and fig. S4A). Interestingly, TFs defining the CD56^{bright} NK cell program were absent in ST2^{+} CD56^{dim} NK cells (e.g., *BACH2*, *LEF1*, *TCF7*), whereas those specifically regulating the CD56^{dim} NK cell program (e.g., *MAF*, *NFIL3*, *PRDM1*, *TBX21*, *ZBTB16*, *ZEB2*) were all (except for *NFIL3*) expressed at intermediate levels in ST2^{+} CD56^{dim} NK cells (Fig. 3E). Among

genes shared between ST2^{+} CD56^{dim} NK cells and ST2^{-} CD56^{bright} NK cells were secreted molecules (*TNF*, *XCL1*, *XCL2*, *GZMK)*; chemokine receptors (*CCR1*, *CCR5*, *CCR6*) and cytokine receptors (*IL2RA*, *IL2RB*, *IL12RB2*). Genes shared with ST2^{-} CD56^{dim} NK cells encoded differentiation markers (*FCGR3A*, *KIR2DL1*, *KIR2DL3*, *KIR3DL1*, *KIR3DL2*), chemotactic receptors (*CXCR1, CXCR2, CX3CR1*, *S1PR5*), inflammatory chemokines (*CCL3*, *CCL4*, and *CCL5*), and cytotoxic molecules (*GZMH*) (Fig. 3E). Among DEG between ST2^{-} CD56^{bright} and ST2^{-} CD56^{dim} NK cells, 75.1 % of genes displayed an intermediate expression in ST2^{+} CD56^{dim} NK cells (Fig. 3F). By using a permutation test to randomly shuffle labels of all samples (n = 1000 times) and assess samples distribution, we statistically validated the intermediate transcriptional pattern of ST2^{+} CD56^{dim} NK cells (p = 0.012) (Fig. 3F). We then performed functional enrichment analysis for gene signatures selected from Gene Ontology (GO), Hallmarks, and KEGG databases. Based on the literature *(41)* and our own data (Fig. 2E,3E, and fig. S4A), we also defined specific cytokine and homing signatures for CD56^{bright} (CYTOKINES_NKbright and HOMING_NKbright) and CD56^{dim} NK cells (CYTOKINES_NKdim and HOMING_NKdim). ST2^{+} CD56^{dim} NK cells were specifically enriched in signatures involved in cell proliferation (*i.e.* cell cycle) and metabolism (*i.e.* oxidative phosphorylation, glycolysis, PI3K/AKT/mTOR signaling), indicating their higher activation state as compared with ST2^{-} CD56^{bright} and ST2^{-} CD56^{dim} NK cells. Furthermore, ST2^{+} CD56^{dim} NK cells showed an enrichment in biological processes associated with either CD56^{bright} (*i.e.* CYTOKINES_NKbright, HOMING_NKbright, and regulation of T-helper 1 immune response) or CD56^{dim} (*i.e.* CYTOKINES_NKdim, HOMING_NKdim, and cytolysis) NK cell subsets (Fig. 3G), in line with their polyfunctionality. In agreement, the GO term associated with NK cell differentiation was progressively enriched in ST2^{+} CD56^{dim} NK and ST2^{-} CD56^{dim} NK cells, consistent with a ST2^{-} CD56^{bright}→ST2^{+} CD56^{dim} → ST2^{-} CD56^{dim} differentiation trajectory. Collins *et al.* recently reported a continuum in NK cell differentiation, with CD57^{+} CD56^{dim} NK cells representing a terminally-differentiated state *(13)*. In concordance with this study, CD57^{-} ST2^{+} CD56^{dim} NK cells expressed higher levels of genes (*LEF1*, *XCL1*, *TNF*, *GZMK*) and gene signatures/pathways of CD56^{bright} NK cells, whereas CD57^{+} ST2^{+} CD56^{dim} NK cells overexpressed genes (*FCGR3A*, *CXC3CR1*, *KIR2DL1*, *KIR2DL3*, *KIR3DL1*, KIR3DL2, NFIL3, *PRDM1*, *ZEB2*, *GZMH*) and gene signatures/pathways shared with CD56^{dim} NK cells (Fig.

3B-E,G). Altogether, this analysis revealed that ST2^{+} CD56^{dim} NK cells display a unique, highly activated, and polyfunctional profile, intermediate between IL-12-activated ST2^{-} CD56^{bright} and ST2^{-} CD56^{dim} NK cells.

ST2^{+} NK cells infiltrate tumors and are functionally competent in response to IL-33 and IL-12 activation

We then addressed the functional relevance of the ST2^{+} NK cells in cancer. First, we analyzed previously published datasets of single cell (sc)-RNAseq from NK cells infiltrating human melanoma metastases (GSE139249) *(42)* and mouse lung tumors (GSE123534) *(43)* to investigate the presence of ST2^{+} NK cells in tumor tissues. Unsupervised clustering of all sequenced intratumoral NK cells revealed nine and eight distinct clusters based on transcript signatures in human melanoma metastases and in mouse lung tumors respectively (fig. S5), with human cluster #5 and murine clusters #4 and #7 displaying a higher ssGSEA score for the 233-gene expression signature associated with ST2 expression in NK cells (representing 3%, 9.4% and 2.4% of total NK cells respectively) (Fig. 4A). By analyzing human breast tumor resections, where NK cells were detected in 85% of cases (40/46) and represented up to 7% of total infiltrating immune cells, regardless of the breast cancer molecular subtype (fig. S6A,B), we identified ST2^{+} NK cells in tumors representing ≈5 to 10% of total tumor-infiltrating NK cells, but not in patients' blood (Fig. 4B). As a surrogate for IL-33 responsiveness, we monitored p65 phosphorylation in *ex vivo*-stimulated tumor-infiltrating and circulating NK cells. While IL-33 had no effect alone, its association with IL-12 induced p65 phosphorylation in a subset of circulating and tumor-infiltrating NK cells (Fig. 4C), highlighting the potential of NK cells to respond to IL-33 in cancer patients. Consistently, IL-12 and IL-33 co-stimulation enhanced IFN-γ-production by circulating and tumor-infiltrating NK cells from breast cancer patients, as compared to IL-12 alone (Fig. 4D). Collectively, these results indicate that ST2^{+} NK cells are present in the microenvironment of different tumor types and that they can respond to IL-33 resulting in IFN-γ production, suggesting a potential antitumor function of IL-33.

Combination of IL-33 with IL-12 promotes NK cell antitumor activity *in vivo*

As for human NK cells, IL-12 was required to upregulate ST2 expression on the surface of a subset of mouse spleen NK cells (fig. S7A), which subsequently produced IFN-γ in response to IL-33 (fig. S7B). Next, using the mouse E0771 triple negative breast tumor cell line *(44)* we addressed the functional relevance *in vivo* of IL-33 NK-dependent antitumor activity. Mice were orthotopically injected in the mammary gland with E0771 tumor cells and then treated with IL-33 and IL-12 alone or in combination via peritumoral injection (Fig. 5A). We observed a marked reduction in primary tumor growth in IL-12/IL-33 co-treated mice compared to the control group and, and to a lesser extent, to IL-12 or IL-33 monotherapy (Fig. 5A). Consistently, co-injection of IL-12 and IL-33 increased long-term survival of tumor-bearing mice (Fig. 5B). These antitumor effects were linked to higher levels of systemic IFN-γ (Fig. 5C). Strikingly, the effects of IL-33/IL-12 co-treatment on tumor growth, survival, and IFN-γ production were abrogated when NK cells were depleted (Fig. 5D-F) while they were maintained in T and B cell-deficient *Rag2*-KO mice, in an NK cell-dependent manner (fig. S8A-C). Altogether, these results demonstrate that IL-12 and IL-33 co-stimulation induces anti-tumor NK cell functions *in vivo*.

_An NK_^{hi}-_IL33_^{hi} score predicts improved cancer patients survival

To assess the clinical relevance of our findings, we analyzed *IL33* and *IL1RL1* (ST2) gene expression in human cancers using The Cancer Genome Atlas (TCGA) transcriptomic database. Although detected in virtually all cancer types, *IL33* expression was lower in tumor as compared to adjacent non-tumoral tissue in 13/30 cancers, including invasive breast carcinoma (IBC), while it was upregulated in five cancers (Fig. 6A). Similarly, *IL1RL1* was downregulated in 20/30 cancers as compared to adjacent normal tissues, with some cancers displaying barely detectable *IL1RL1* expression (Fig. 6A). These observations suggest a protective role of the IL-33/ST2 pathway in human cancers. We confirmed the presence of IL-33 soluble protein in 95% of breast tumor supernatants, with the highest levels detected in luminal tumors compared to Her2^{+} and triple negative tumors (Fig. 6B). While absent from the nuclei of tumor cells, IL-33 was expressed in the nuclei of epithelial cells from normal acini, of endothelial cells as previously reported *(45)*, and of isolated stromal cells morphologically resembling immune cells or

cancer-associated fibroblasts (Fig. 6C). Further analysis from public transcriptomic datasets from microdissected tissues *(46, 47)* confirmed that *IL33* expression was mainly restricted to the stroma, and higher in non-tumoral tissue and early non-invasive lesions (DCIS) compared to advanced IBC (Fig. 6D), consistent with a loss of IL-33 expression in cancer cells during breast tumorigenesis. In addition, we found that the expression of *IL33* and *IL1RL1* in TCGA data sets for human cancers was frequently associated with an improved Progression-Free Survival (PFS) (fig. S9A-C). Notably, in breast cancer, *IL33*-based patient stratification was independently prognostic when adjusted for age, molecular subtype, and tumor stage (fig. S9D).

We then examined whether high *IL33* expression in conjunction with a high *NK* cell infiltration predicted improved patients survival as compared with these parameters considered separately. TCGA clinical cases were stratified as $IL33^{high}$ *vs* $IL33^{low}$ expression and as NK^{high} *vs* NK^{low} score, using a previously defined NK cell gene signature *(48)* (Table 4). NK^{hi} tumors displayed higher expression of *IL33*, indicating a positive association between these two parameters (Fig. 7A). An NK^{high}-$IL33^{high}$ score was associated with improved PFS in six cancers including breast cancer (BRCA), whereas NK^{high}-$IL33^{low}$ score had no prognostic value with the exception of Liver Hepatocellular Carcinoma (LIHC) (Fig. 7, B and C, and fig. S9E). Notably, multivariate analysis in breast cancer patients highlighted that an NK^{high}-$IL33^{high}$ score remained a marker of better PFS regardless of the molecular subtype, the stage of the disease, and the age of patients (Fig. 7D). Altogether, these results reveal a strong favorable prognostic value of the IL-33/ST2 axis in particular when associated with a high *NK* score in several cancers including breast cancer.

Discussion

Previous studies have established the important role for IL-33 in type 2 immunity, but its contribution to type 1 immune responses remains poorly understood *(36)*. Indeed, the role of IL-33/ST2 pathway in antitumor immunity remains elusive, in particular through NK cell modulation. Our results demonstrate that a specific subset of human $CD56^{dim}$ NK cells express ST2 in response to IL-12 and is endowed with polyfunctional activity in response to IL-33. This unique subset represents an intermediate differentiation stage between less mature secretory $CD56^{bright}$ and more differentiated cytotoxic $CD56^{dim}$ NK cells, with high activation potential and anti-tumor activity. Indeed, tumor-infiltrating NK cells were found to express ST2 and to produce IFN-γ in response to IL-12/IL-33 co-activation. Accordingly, IL-33 and IL-12 combination inhibits mammary tumor development in mice in an NK cell-dependent manner and an $IL33^{hi}/NK^{hi}$ transcriptomic score predicts better survival in breast cancer and other cancers. These findings uncover an important role for $ST2^{+}$ NK cells in antitumor immunity which is relevant in cancer immune surveillance and cancer immunotherapy.

Our data indicate that IL-33 by itself is not able to activate NK cells. Indeed, ST2 protein expression in human and mouse NK cells requires IL-12, in agreement with previous works but only shown at the transcriptional level *(33)*. Mechanistically, we show that IL-12 induces and stabilizes *ST2* expression in human NK cells through a direct binding of STAT4 in *ST2* promoter, corroborating previous results in mouse Th1 cells *(49)*. IL-12 appears as the most potent signal to enable NK cells to respond to IL-33, highlighting a major role of STAT4 as a master regulator of ST2 expression. Synergistic activity with IL-12 was also reported for other members of the IL-1 cytokine family, such as IL-18. Indeed, IL-12 and IL-18 coactivation induces STAT4/c-jun complexes which bind to *IFNG* promoter *(50)* and activates p38-MAPK pathway which enhances stability of *IFNG* transcripts in human NK cells *(51)*. Similarly, IL-33 was shown to activate c-jun *(52)* and p38-MAPK (our results and *(53)*), therefore, IL-33 and IL-12 synergy likely acts through pathways similar to those described for IL-18 to trigger high IFN-γ production by NK cells. However, our study identifies specific regulation of NK cell functions by IL-33 compared to other IL-1 family cytokines including IL-18. Indeed, IL-33 was unique in its ability to induce the concomitant

secretion of IFN-γ and a broad spectrum of pro-inflammatory cytokines and chemokines in CD56^{dim} NK cells. In addition, while CD56^{dim} NK cells are known for their low proliferative ability *(54)*, only IL-33 strongly potentiates their IL-2-triggered proliferation, consistent with the upregulation of CD25. Our findings therefore highlight differences in NK cell subsets' ability to respond to IL-1 family members upon co-stimulation with IL-12, with unique activation features acquired in response to IL-33.

Our results show that IL-12-induced ST2^{+} NK cells stand as an intermediate stage between conventional CD56^{bright} and CD56^{dim} NK cells, with a mixed transcriptomic profile, consistent with their polyfunctional activity in response to IL-12 and IL-33. Previous studies reported NK cell differentiation intermediates, based on their surface expression of CD94/NKG2A, CD62L, CX3CR1, KIRs and CD57 *(9, 8, 7, 55)* and transcriptional and epigenetic programs governing differentiation from immature CD56^{bright} to terminally differentiated CD56^{dim} *(56, 12, 13)*. ST2 expression is restricted to human CD56^{dim} NK cells, although IL-12/STAT4 signaling is active in CD56^{bright} NK cells, suggesting differences in transcriptional regulation by STAT4 among NK cells subsets, as previously evidenced for adaptive memory NK cells *(14)*. Genes encoding BACH2 and TCF7, master transcription factors of CD56^{bright} NK cells, were specifically downregulated in ST2^{+} NK cells and might therefore act as transcriptional repressors preventing ST2 expression in CD56^{bright} NK cells, as previously shown to inhibit CD56^{dim} transcriptional program *(13)*. The absence of CD56^{bright} specific transcription factors in ST2^{+} NK cells argue for a differentiation model were ST2 is upregulated on NK cells after they first lose the transcription factors governing the CD56^{bright} subset. Furthermore, ST2 expression was preferentially observed in a subset of CD57^{-} CD56^{dim} NK cells and lost during terminal differentiation alongside with the acquisition of CD57. Together, our results point toward a model in which ST2^{+} CD56^{dim} NK cells originate from CD56^{bright} NK cells to emerge as an intermediate stage between CD56^{bright} and terminally differentiated CD56^{dim} CD57^{+} NK cells.

We also report NK cells expressing ST2 protein and exhibiting an ST2-linked transcriptional signature in human and mouse tumors. Of note, we previously reported significant levels of IL-12p40

and IL-12p70 in supernatants obtained from advanced breast tumor *(57)* that may be released in tumors by activated DCs *(58)* to locally license NK cells to respond to IL-33 by inducing ST2 expression. IL-12 may also be produced in tumor-draining lymph nodes by DCs, in close vicinity with NK cells. Interestingly, a recent study suggested that DC-derived IL-12 is essential for the anti-tumor activity of NK cells *(59)*, while NK cell-derived IFN-γ sustains the production of IL-12 by cDC1 *(60)*, hence delineating a positive feedback loop. In this context, loss of IL-12 expression in advanced tumors may represent an escape mechanism preventing NK cells' activation by IL-33. In conclusion, we suggest that NK cells are fine-tuned by the cytokine microenvironment with IL-12 driving IL-33 activity towards an anti-tumor immune response via NK cells.

Our study reveals that IL-33 protein is present in human breast tumors. Nevertheless, we document a frequent downregulation of *IL33* expression in tumors and a positive impact of *IL33* expression on patients' survival in several cancer types, including breast cancer. Consistently, previous studies reported a positive prognostic impact of IL-33 in hepatocarcinoma, kidney, salivary glands or prostate cancers *(61–63)* and IL-33 levels are inversely correlated with tumor grade and tumor size in lung adenocarcinomas *(64)* and osteosarcomas *(65)*. These observations support an anti-tumor role for endogenous IL-33 that could be released in the microenvironment of early-stage tumors following cell death and stress. Furthermore, our analysis of TCGA database reveal a strong favorable prognostic value of IL-33 in particular when associated with a high *NK* score in several cancers, including breast cancer, independently of other clinical parameters, highlighting a selective advantage of combined IL-33 and NK cells. Our observation complements recent findings showing that a *NK-IL18-IFNG*^{high} signature has a positive prognosis value for cancer patients' survival *(43)*. Although NK cells in advanced solid tumors are characterized by a dysfunctional state *(21)*, we show here that *ex vivo* stimulation with IL-33 and IL-12 triggered IFN-γ production by human breast tumor-infiltrating NK cells. Consistently, our *in vivo* study demonstrates a potent antitumor role for IL-33/IL-12 on primary mammary tumor growth in mice via the activation of tumor-infiltrating NK cell resulting in systemic IFN-γ production, in line with previous

reports following ectopic expression of IL-33 *(66)* or systemic administration of IL-33 *(67, 68)*. Systemic IL-33 was also shown to inhibit the development of metastatic tumor in 4T1 mouse model in an NK cell-dependent manner *(68)*. Together, these results highlight the potential of IL-33 as a novel therapeutic strategy to promote NK cells anti-tumor activity.

In conclusion, our analysis of human and mouse tissues identifies a novel NK cell subset upregulating ST2 upon IL-12 activation, which display high proliferative abilities and polyfunctionality. IL-33/ST2 axis plays a protective role in cancer and is of clinical relevance for cancer patients' outcome. Our results also reveal a promising role of $ST2^+$ NK cells to be harnessed for cancer treatment. Deciphering NK cell differentiation paths and identifying stimuli promoting distinct maturation stages and functions is crucial to achieve tailored harnessing of NK cell features for therapeutic benefit in a variety of pathological contexts.

Acknowledgments

RNA sequencing was performed by the genomic platform of the CRCL supported by the SiRIC-LYriCAN program (grant INCa-DGOS-Inserm_12563). Cell sorting was performed at the flow cytometry facility of the CRCL. Mouse experiments were performed at the P-PAC animal facility of the CRCL.

We thank S. Boyault, J. Auclair, and C. Audoynaud for performing RNA sequencing. We thank M. Pratviel, B. Vernière, and M. Sanchez for excellent technical assistance for mouse experiments. P. Battiston-Montagne and A. Jambon provided help during cell sorting. We thank Lynnette Fernandez Cuesta, Matthieu Foll, and Nicolas Alcala for their precious advice for permutation statistical test. We want to additionally thank V. Sisirak, Y. Grinberg-Bleyer, and B. Dubois for careful reading of the manuscript, helpful comments, and suggestions.

Fresh tumor samples and blood samples from breast cancer patients were provided by the tissue bank of CLB (BB-0033-00050, CRB - CLB, Lyon, France; French agreement number: AC-2019-3426).

The breast cancer immunostaining was generated by Coya Tapia (PMID: 29254793), with amended data monitoring by Rupert Langer, and stained by the Translational Research Unit in Bern. Stefan Reinhard helped for digitalization of the histology pictures.

This work was supported by the Fondation ARC pour la Recherche sur le Cancer (grant PJA20181208305 to N.B.-V.), the Institut National Du Cancer (INCA; AAP PLBIO-16-116 to A.M. and N.B.-V.), the Ligue Régionale contre le cancer (Comité du Rhône) (to N.B.-V.), the Ligue Nationale contre le cancer (EL2020.LNCC-CHC to C.C.), the LABEX DEVweCAN (ANR10-LABX-0061 to C.C.) of Université de Lyon, within the program “Investissements d’Avenir” (ANR-11-IDEX-0007) operated by the French National Research Agency (ANR), and the SIRIC LYriCAN project (grant INCa-DGOS-Inserm_12563 to C.C. and N.B.-V.).

A.E. is a recipient of a doctoral fellowship from the Ecole Normale Supérieure de Lyon (2016-2019) and 1-year extension Ph.D. Fellowship from the Labex DevWeCan, E.B. from The Région Auvergne Rhône Alpes ARC1 Santé (2013-2016), and 1-year extension Ph.D. Fellowship from Labex DevWeCan, and V.P.

from the French Government PhD Fellowship (2019-2022). A.V. is a recipient of a post-doctoral fellowship from Labex DEVweCAN and Y.R. from INCa AAP PLBIO17-187.

Author contributions

N.B.-V., A.E., E.B., and C.C. designed the study. A.E., E.B., V.P., Y.R., A.V., F.O., C.R., B.E., L.M., E.C., and T.R. did the experiments. A.E., E.B., V.A., M.A., X.W., A.S., and M.H. collected the data. A.E., E.B., V.A., and M.H. interpreted the results and prepared the manuscript. M.H. performed RNAseq data analysis. V.A., M.A., L.T., X.W., A.S., and M.H. performed TCGA data analysis. L.M., M.-C.M., J.V.-G., and A.C. provided expertise. E.C., T.W., and A.M. helped in the design of phosphosignaling analysis by flow cytometry and mouse experiments. T.R. and P.K. provided retrospective cohorts of breast tumors. O.T. and I.T. provided prospective breast tumor tissues. V.P., Y.R., A.M., T.W., and P.K. read the manuscript and provided valuable input. A.E., E.B., C.C., and N.B.-V. wrote the manuscript.

Competing interests

The authors declare no competing interests.

Fig. titles and legends

Fig. 1. IL-12/STAT4 signaling drives ST2 expression and polyfunctionality of human NK cells in response to IL-33

(A) Quantification of IFN-γ secretion by healthy donors' blood NK cells upon stimulation with IL-33, IL-18, IL-1α or IL-1β alone (10 ng/mL) or in combination with IL-12 (10 ng/mL) for 24 h. Histogram bars represent the median (n = 4 individual experiments). Friedman test with Dunn's multiple comparisons test was performed.

(B) NK cells were activated for 24 h with IL-33, IL-18, IL-1α or IL-1β alone (10 ng/mL) or in combination with IL-12 (10 ng/mL) and then co-cultured with calcein-loaded K562 target cells for 4 h at a 5:1 effector to target ratio. Calcein release in the supernatant was quantified by fluorometry to calculate lysis percentage. Results are expressed as mean + SEM (n = 9 individual experiments). One-way repeated measures ANOVA with Dunnett's multiple comparisons test against levels in medium was performed.

(C) NK cells were activated for 24 h with IL-33, IL-18, IL-1α or IL-1β alone (10 ng/mL) or in combination with IL-12 (10 ng/mL) and then stained for CD25 and CD69 (black line) or corresponding isotypic control (grey). Representative histogram plots (left) and quantification (%) (right) of $CD25^+$ or $CD69^+$ NK cells after cytokine stimulation. Symbols represent paired individual experiments (n=7). Results are expressed as mean + SEM. One-way repeated measures ANOVA with Dunnett's multiple comparisons test against levels in IL-12 was performed.

(D) IFN-γ secretion by healthy donors' blood NK cells upon stimulation for 24 h with IL-33 and IL-12 (10 ng/mL each) in the presence of anti-ST2 (10 µg/mL), anti-IL-18 (1 µg/mL) blocking antibodies, IL-1RA antagonist (100 ng/mL) or mIgG1 control antibody (1 or 10 µg/mL as control for anti-IL-18 or anti-ST2, respectively). Results are expressed as mean + SD and are representative of three individual experiments. One-way repeated measures ANOVA with Tukey's multiple comparisons test was performed.

(E) Real-time quantitative PCR (RT-qPCR) analysis of *IL1RL1* (ST2) and *IL1RAcP* mRNA expression in resting or activated NK cells with IL-12, IL-33, or the combination (10 ng/mL each for 24 h). Results are

expressed as mean + SEM of three individual experiments. Each symbol represents one donor. Two-tailed paired Student *t*-test was performed.

(F) NK cells were activated with IL-12 (10 ng/mL) in the presence or not of lisofylline (500 μM) for 24 h prior to ST2 surface expression analysis by flow cytometry. Representative dot plots (left) and quantification (%) (right) of $ST2^+$ NK cells after cytokine stimulation. One-way repeated measures ANOVA with Tukey's multiple comparisons test was performed; n = 3.

(G) p-STAT4 was immunoprecipitated in NK cells following activation or not with IL-12 (10 ng/mL) for 24 h and p-STAT4 enrichment in *ST2* promoter region was measured by RT-qPCR analysis. *PERFORIN-1 (PRF1)* and negative control sets 1 and 2 were used respectively as positive and negative controls for p-STAT4 binding. Results are expressed as mean + SEM of two individual experiments.

Fig. 2. IL-33 strongly activates a subset of $CD56^{dim}$ NK cells in the presence of IL-12

(A) Healthy donors' blood NK cells were activated with IL-12 (10 ng/mL) or not (medium) for 24 h prior to flow cytometry analysis of ST2, IL-18R1, IL-1R1 expression (grey) or corresponding isotypic control (black line). CD56 surface expression levels were used to discriminate $CD56^{bright}$ and $CD56^{dim}$ NK cells. Representative histogram plots (left) and quantification (%) (right) of $ST2^+$ NK cells after medium or IL-12 culture. Histogram bars indicate the median. Wilcoxon matched pairs signed-rank test was performed; n = 12 experiments.

(B) FACS-sorted $CD56^{bright}$ and $CD56^{dim}$ NK cells were activated with medium or IL-12 for 24 h prior to the addition of IL-33, IL-18, IL-1α or IL-1β, supplemented or not with IL-12. Each cytokine was used at 10ng/mL. p65 (NF-κB) phosphorylation was analyzed by flow cytometry 5 min after the addition of IL-1 family cytokines. Representative histogram plots (left) and quantification (%) (right) of $p\text{-}p65^+$ NK cells after cytokine activation. Histogram bars indicate the median. Two-way ANOVA with Bonferroni's multiple comparisons test was performed; n = 4 experiments.

(C) Healthy donors' blood NK cells were activated as indicated for 24 h, each cytokine was used at 10 ng/mL. CD25 surface and IFN-γ intracellular expression was analyzed by flow cytometry. CD56 surface

475 expression levels were used to discriminate CD56^{bright} and CD56^{dim} NK cells. Representative dot plots
476 (left) and quantification (%) (right) of CD25^{+} IFN-γ^{+} NK cells after cytokine activation. Histogram bars
477 indicate the median. Two-way ANOVA test with Bonferroni's multiple comparisons test was performed;
478 n = 5 experiments.
479 **(D)** FACS-sorted CD56bright and CD56dim NK cells were pre-activated as indicated, labeled with CTV,
480 and cultured in low dose IL-2 (100 UI/mL). In vitro NK cell proliferation was analyzed at day 3 for
481 CD56bright and day 6 for CD56dim NK cells. Expansion Index (Exp. Index) and Replication Index (Rep.
482 Index) determine the fold-expansion of the overall culture and of the responding cells only, respectively.
483 Data shown are representative of three individual experiments.
484 **(E)** Supernatants from FACS-sorted CD56^{bright} (empty histogram bars) and CD56^{dim} (filled histogram bars)
485 NK cells were collected to quantify cytokine and chemokine release by Luminex assay. Of note, IL-2, IL-
486 3, IL-4, IL-5, IL-10, IL-13, IL-17A, IL-22, and G-CSF were not detected (not shown). Results are expressed
487 as mean + SEM (n = 3 individual donors). One-way repeated measures ANOVA with Tukey's multiple
488 comparisons test was performed.
489 **(F)** Healthy donors' blood NK cells were activated with combinations of IL-12 and IL-33 or IL-12 and IL-
490 18 (10 ng/mL of each cytokine) for 24 h prior to flow cytometry analysis of intracellular IFN-γ expression
491 in NK cell subsets based on CD56 and CD57 surface expression. Results are expressed as mean +/- SEM
492 (n = 7 individual experiments). Two-way ANOVA with Bonferroni's multiple comparisons test was
493 performed.
494 **(G)** Healthy donors' blood NK cells were activated with IL-12 (10 ng/mL) for 24 h prior to flow cytometry
495 analysis of ST2 expression on NK cell subsets based on CD56 and CD57 surface expression. Results are
496 expressed as mean + SEM (n = 12 experiments). One-way repeated measures ANOVA with Tukey's
497 multiple comparisons test was performed.
498 **(H)** Graphical summary of biological functions differentially regulated in CD56^{bright} and CD56^{dim} NK cells
499 in response to IL-1 family cytokines (IL-33, IL-18, IL-1α and IL-1β) when combined with IL-12.
500

Fig. 3. ST2^{+} CD56^{dim} NK cells display a unique gene signature compared to CD56^{bright} and CD56^{dim} NK cells

(A) Schematic representation of FACS sorting strategy to isolate eight different subsets sorted from healthy donors' blood NK cells based on CD56, CD57 and ST2 surface expression. Three and five subsets were obtained after activation for 24 h with medium or IL-12 respectively.

(B) Principal component analysis for eight FACS-sorted NK cell subsets based on expression of the top 500 most variant genes obtained from 3 individual healthy donors.

(C) Heatmap representing upregulated genes in each sorted NK cell subset compared to the two other NK cell subsets following IL-12 activation for 24 h (n = 3 individual healthy donors). Black squares identify specific transcriptional signatures for ST2^{-} CD56^{bright}, ST2^{-} CD56^{dim} NK cells, and ST2^{+} CD56^{dim} NK cells.

(D) ssGSEA analysis of the NK signatures defined by genes specifically upregulated in each sorted NK cell subset (see Table 1) following IL-12 activation for 24 h (n = 3 individual healthy donors). Kruskal-Wallis test with Dunn multiple comparisons test was performed.

(E) Heatmap showing normalized expression for selected genes related to NK cell phenotype and functions.

(F) Sampling distribution of genes with an intermediate expression in ST2^{+} NK cells (CD56^{bright} > ST2^{+} > CD56^{dim} or CD56^{bright} < ST2^{+} < CD56^{dim}) with n = 1000 random shuffling of all sample labels. p value was computed with a permutation test.

(G) ssGSEA analysis of selected biological pathways in each sorted NK cell subset following IL-12 activation for 24 h (n = 3 individual healthy donors).

Fig. 4. Peripheral and tumor-infiltrating NK cells from breast cancer patients respond to the IL-33 and IL-12 combination

(A) Violin plots representing the distribution of ssGSEA score for ST2^{+} NK cells signature (233 genes, see Table 1) for tumor NK cell clusters identified from sc-RNAseq analysis of tumor-infiltrating NK cells isolated from (left panel) melanoma patients (GSE139249) *(42)* and (right panel) a mouse model of lung

cancer (GSE123534) *(43)*. Kruskal-Wallis test with Dunn multiple comparisons test was performed using cluster 5 for the melanoma dataset and cluster 4 (turquoise) or cluster 7 (pink) (fig. S5) as references.

(B) Flow cytometry analysis of ST2 protein expression on the surface of CD56/NKp46$^+$ NK cells among PBMCs and tumor cell suspensions from breast cancer patients (n = 6). Representative dot plots (left) and quantification (%) (right) of ST2$^+$ NK cells. Results are expressed as mean + SEM. Paired two-tailed Student *t*-test was performed.

(C) PBMCs (n = 7) and tumor cell suspensions (n = 4) from breast cancer patients were activated with medium or IL-12 for 24 h prior to the addition of medium or IL-33. p65 phosphorylation was analyzed 5 min after the addition of IL-33 by flow cytometry in CD56$^+$ CD7$^+$ NK cells. Representative histogram plots (left) and quantification (%) (right) of p-p65$^+$ NK cells after IL-12 and IL-33 combination. Results are expressed as mean + SEM. Unpaired two-tailed Student *t*-test was performed with no statistically significant difference.

(D) PBMCs and tumor cell suspensions from breast cancer patients (n = 5) were activated as indicated (10 ng/mL of each cytokine) for 24 h prior to flow cytometry analysis of intracellular IFN-γ. Representative dot plots (left) and quantification (%) (right) of IFN-γ^+ NK cells. Symbols represent individual breast cancer patients and histogram bars the median. Wilcoxon matched-pairs signed rank test was performed.

Fig. 5. The combination of IL-33 and IL-12 promotes antitumor functions in an NK-cell-dependent manner

(A) WT mice were injected intra-mammary with 2.5x10^5 E0771 cells on day 0 and then treated in the tumor area with NaCl solution (n = 6), 10 ng/mouse rmIL-12 (n = 9) or 100 ng/mouse rmIL-33 (n = 9) or in combination (n = 10) twice a week from day 2 to day 26. Primary tumor growth was monitored in mice treated with, rmIL-12, rmIL-33 or with the two cytokines. Two-way ANOVA with Tukey's multiple comparisons test was performed.

(B) Kaplan-Meier survival plots of WT mice treated with NaCl, rmIL-12, rmIL-33 or the two cytokines. Mice were sacrificed when longest side of primary tumor reached 17 mm. Log-rank test was performed and the p-value is indicated for NaCl vs rmIL-12 + rmIL-33 comparison.

(C) Serum was retrieved from blood collected at day 5, 4 h after NaCl or cytokine injection into the peritumoral area. IFN-γ concentration was measured by Elisa in the serum of mice treated with NaCl, rmIL-12, rmIL-33 or the two cytokines. Histogram bars represent the median. Kruskal Wallis test with Dunn's multiple comparisons test was performed.

(D) WT mice were injected intra-peritoneally with NaCl or anti-NK1.1 depleting antibody prior to intra-mammary injection with $2.5x10^5$ E0771 cells on day 0 and then treated in the tumor area with NaCl or a combination of 10 ng/mouse rmIL-12 and 100 ng/mouse rmIL-33 twice a week from day 2 to day 23. Primary tumor growth was monitored in non-depleted WT mice treated with NaCl (n = 4) or with rmIL-12 and rmIL-33 combination (n = 5) or in NK cell-depleted WT mice treated with NaCl (n = 5) or with rmIL-12 and rmIL-33 combination (n = 5). Two-way ANOVA with Tukey's multiple comparisons test was performed.

(E) Kaplan-Meier survival plots of non-depleted WT mice treated with NaCl (n = 4) or with a combination of rmIL-12 and rmIL-33 (n = 5) or in NK cell-depleted WT mice treated with NaCl (n = 5) or with rmIL-12 and rmIL-33 combination (n=5). Mice were sacrificed when longest side of primary tumor reached 17 mm. Log-rank test was performed and the p-value is indicated for non-depleted mice treated with rmIL-12 + rmIL-33 vs NK cell-depleted mice treated with rmIL-12 + rmIL-33.

(F) Serum was retrieved from blood collected at day 5, 4 h after NaCl or cytokine injection into the peritumoral area. IFN-γ concentration was measured by ELISA in the serum of non-depleted WT mice treated with NaCl (n = 4) or with rmIL-12 and rmIL-33 combination (n = 5) or in NK cell-depleted WT mice treated with NaCl (n = 5) or with rmIL-12 and rmIL-33 combination (n = 5). Histogram bars represent the median. Kruskal Wallis test with Dunn's multiple comparisons test was performed.

Fig. 6. IL-33 is expressed in tumors and downregulated during cancer progression

(A) *IL33* and *IL1RL1* (ST2) gene expression in tumoral (T) (orange) and normal (N) (grey) tissues extracted from TCGA and GTEX databases (ACC: Adrenocortical carcinoma, T=77, N=128; BLCA : Bladder carcinoma, T=404, N=28; BRCA : Breast invasive carcinoma, T=1095, N=291; CESC: Cervical squamous cell carcinoma and endocervical adenocarcinoma, T=306, N=13 ; CHOL: Cholangiocarcinoma, T=36, N=9; COAD : Colorectal adenocarcinoma, T=275, N=349; DLBC: Lymphoid Neoplasm Diffuse Large B-cell Lymphoma, T=47, N=337 ; ESCA: Esophageal carcinoma, T=182, N=286 ; GBM: Glioblastoma multiforme, T=163, N=207 ; HNSC : Head and neck squamous cell carcinoma, T=519, N=44 ; KICH: Kidney Chromophobe, T=66, N=53 ; KIRC : Kidney renal clear cell carcinoma, T=523, N=100 ; KIRP: Kidney renal papillary cell carcinoma, T=286, N=60 ; LGG : Brain lower grade glioma, T=518, N=207 ; LIHC: Liver hepatocellular carcinoma, T=369, N=160 ; LUAD : Lung adenocarcinoma, T=483, N=347 ; LUSC: Lung squamous cell carcinoma, T=486, N=338 ; OV : Ovarian serous cystadenocarcinoma, T=426, N=88 ; PAAD : Pancreatic adenocarcinoma, T=179, N=171 ; PCPG: Pheochromocytoma and Paraganglioma, T=182, N=3 ; PRAD: Prostate adenocarcinoma, T=492, N=152 ; READ: Rectum adenocarcinoma, T=92, N=318 ; SARC: Sarcoma, T=262, N=2 ; SKCM : Skin cutaneous melanoma, T=461, N=558 ; STAD : Stomach adenocarcinoma, T=408, N=211 ; TGCT: Testicular Germ Cell Tumors, T=137, N=165 ; THCA : Thyroid cancer, T=512, N=337; THYM: Thymoma, T=118, N=339 ; UCEC: Uterine Corpus Endometrial Carcinoma, T=174, N=91 ; UCS: Uterine Carcinosarcoma , T=57, N=78).

(B) IL-33 protein was quantified by Luminex assay in breast tumor-derived supernatants (n = 89). Kruskal-Wallis test with Dunn multiple comparisons test was performed.

(C) IL-33 expression was analyzed on breast tumor FFPE slides by Immunohistochemistry (IHC). Non-invasive Ductal Carcinoma *In Situ* (DCIS) and invasive Breast Cancer (IBC) lesions were identified based on anatomopathological tissue observations. Red arrows indicate blood vessels, orange arrows indicate peritumoral normal breast acini and green arrows indicate isolated stromal cells positive for IL-33 staining. Images are shown at 20x magnification. Dotted squares represent enlarges areas.

(D) Analysis of *IL33* expression in laser-microdissected stromal versus epithelial zones from DCIS and IBC lesions (GSE41228) *(46)* and in healthy mammary tissue versus DCIS and IBC (GSE21422) *(47)*. Kruskal-Wallis test with Steel-Dwas-Fligner multiple comparisons test was performed.

Fig. 7. An *NK*^{hi}/*IL33*^{hi} transcriptomic score is associated with improved progression-free survival

(A) Boxplots display *IL33* gene expression in NK^{hi} vs NK^{low} breast cancer patients from the TCGA database. An unpaired Student *t*-test was performed.

(B) Summary of p-values associated with the log rank test performed to evaluate prognostic value of *NK*^{high}/*IL33*^{high}, *NK*^{high}/*IL33*^{low} and *NK*^{low}/*IL33*^{high} scores as compared to *NK*^{low}/*IL33*^{low} in 32 human cancers from TCGA database (legend is the same as in panel A, MESO: Mesothelioma ; UVM: Uveal Melanoma were added). Results are represented as a bubble map showing positive (green) or negative (red) impact on progression-free survival. Dots size represents p-values obtained by log-rank test. An unpaired Student *t*-test was performed.

(C) Kaplan-Maier curves for progression-free survival for *NK*^{high}/*IL33*^{high}, *NK*^{high}/*IL33*^{low} and *NK*^{low}/*IL33*^{high} scores as compared to *NK*^{low}/*IL33*^{low} in breast cancer dataset from TCGA. p-values were obtained with log-rank test.

(D) Multivariate Cox analysis of the impact of *NK*^{high}/*IL33*^{high} score on prognosis in breast cancer patients from TCGA dataset regarding the age, molecular subtype, and stage of the tumors. p-values were obtained with log-rank test.

Tables with titles and legends

Table 1. List of ST2^{+} NK cell signature genes used in this study, Related to Fig. 3C,D,F,G, 4A

Table 2. List of ST2^{-} CD56^{bright} NK cell signature genes used in this study, Related to Fig. 3C,D,F,G

Table 3. List of ST2^{-} CD56^{dim} NK cell signature genes used in this study, Related to Fig. 3C,D,F,G

Table 4. List of NK cell signature genes used in this study (from *(48)*), Related to Fig. 7A-D, fig. S9E

Materials and Methods

Animals and in vivo tumor models.

C57BL/6J mice were purchased from Charles River Laboratories. *Rag2*-KO mice were bred and maintained at the P-PAC animal facility of the Cancer Research Center of Lyon, under specific pathogen-free conditions in accordance with all standards of animal care. Experiments were conducted with female mice aged between 8-12 weeks. All animal experiments were approved by the ethics committee (approval number CECCAPP-CLB-2019-017). Mice were orthotopically injected into the 4^{th} mammary fat pad with $5x10^4$ or $2.5x10^5$ E0771 tumor cells in 200 µL of sterile NaCl at day 0. For NK cell depletion experiments, mice were injected intra-peritoneally with 200 µg/mouse of anti-NK1.1 antibody (BioXcell) or an equivalent volume of NaCl solution one day prior to tumor cell injection and then once a week. To evaluate NK cell depletion efficiency, mice were treated with tetracaine analgesic eye drops and maintained under anesthesia using isoflurane to perform retro-orbital blood collection. Blood NK cell frequency was measured by flow cytometry. For therapeutic experiments, mice were injected with 10 ng/mouse of rmIL-12 (R&D) or 100 ng/mouse of rmIL-33 (Biolegend) alone or in combination in 50 µL directly in the tumor area twice a week from day 2 to day 26. Control mice were injected with an equal volume of NaCl solution. Tumor sizes were monitored with a digital caliper (Mitutoyo) twice a week and expressed as volume of a sphere ((smaller length)^2 × longer length) from day 9 to the end of experiments. Mice were sacrificed when longer length of the primary tumor reached > 17 mm^2. All cells were tested for mycoplasma prior to injection using MycoAlert kit (Lonza). For serum collection, blood was collected as described above on day 5, 4 h after cytokine injection. Blood was then incubated at room temperature for 30 min to allow coagulation, centrifuged at 15,000rpm for 15 min and the serum was collected and aliquoted for preservation at -80°C and IFN-γ quantification.

Tumor cell lines.

The mouse E0771 (derived from a spontaneous triple negative mammary tumor that arose in a C57BL/6 mouse) and the human K562 (originally generated from a female leukemia patient) cell lines were cultured in RPMI-1640 (Sigma) supplemented with 10% FCS (GIBCO), 2mML-glutamine, and 100 U/ml penicillin/streptomycin (ThermoFisher).

Human breast tumors and blood.

Fresh tumors and blood samples (collected in EDTA anticoagulant-containing tubes) from breast cancer patients were provided by the tissue bank of CLB (BB-0033-00050, CRB-CLB, Lyon, France, French agreement number: AC-2019-3426), after approval from the institutional review board and ethics committee (L-06-36) and patient written informed consent, in accordance with the Declaration of Helsinki. Healthy donor (HD) blood samples were obtained from the 'Etablissement Français du Sang' (Lyon). Next-generation tissue microarray (ngTMA®) (www.ngtma.com) *(69)* generated from human breast tumors was provided by the Tissue Bank Bern and approved by the Cantonal Ethics Committee of Bern (200/2014 and 2018-01502).

Human peripheral blood NK cell isolation and culture.

Peripheral Blood Mononuclear Cells (PBMCs) were isolated from whole blood of healthy donors by density gradient centrifugation on Lymphocyte Separation Medium (Eurobio). Total NK cells were purified from PBMCs by negative immune-selection using the Human NK cell isolation kit (Miltenyi) following the manufacturer's instructions and purity always exceeded 95%. Cells were cultured in RPMI GlutaMAX/10% FBS/1% penicillin-streptomycin (complete RPMI, cRPMI). Human PB NK cells were cultured in cRPMI supplemented with IL-12 (Miltenyi), IL-15 (Peprotech), IL-2 (Chiron), IFN-α2b (Schering-Plough), IL-1α (Peprotech), IL-1β (Peprotech), IL-18 (MBL) or IL-33 (Miltenyi) at concentrations indicated in Fig. legends. Anti-NKp46 and NKp30 agonist antibodies (R&D) were coated (1 µg/mL) in NUNC 96-well plates (Thermofisher) overnight at 4°C. For blocking experiments, cells were incubated

with anti-ST2 (10 µg/mL, R&D), anti-IL-18 (1 µg/mL, MBL), mIgG1 (1 or 10 µg/mL, R&D) antibodies or IL-1RA (100 ng/mL, Peprotech).

Human peripheral blood NK cell sorting

For RNA-seq analysis, MACS-purified total NK cells were stained with antibodies for CD3, CD56, CD16, CD57 (see table S1) as previously described, FACS sorted using a FACS Aria II (BD), and collected in cRPMI. Cell viability was determined by DAPI staining (1 µg/mL, Invitrogen).

Preparation of single cell suspensions from human breast tumor tissue

Sections of the resected tumor area selected by the pathologists were placed in RPMI supplemented with 100 IU/mL penicillin (Invitrogen) and 100 µg/mL streptomycin (Invitrogen). Tissues were mechanically disrupted, supernatant was collected and frozen for subsequent cytokine and chemokine quantification by Luminex assay following the manufacturer's instructions. Tumor pieces were then digested for 45 min at 37°C in RPMI supplemented with 100 IU/mL penicillin (Invitrogen) and 100 µg/mL streptomycin (Invitrogen) using 1 mg/mL of collagenase IV (Sigma Aldrich) and 20 µg/mL of DNase I (Sigma Aldrich). Digested samples were then filtered on a 70 µm cell strainer and re-suspended in cRPMI for activation and flow cytometric analysis.

***Ex vivo* stimulation of mouse splenic NK cells**

Single-cell suspensions were prepared from spleens from C57BL/6J mice (CharlesRiver) after red blood cell lysis with Pharm Lyse™ lysing buffer (BD Biosciences). Splenocytes were activated in cRPMI supplemented with IL-12 (Miltenyi), IL-1α (Miltenyi), IL-1β (Miltenyi), IL-18 (MBL) or IL-33 (Miltenyi) for 24 hr. Cells were surface stained for surface markers, fixed, and permeabilized, followed by intracellular staining of IFN-γ.

Flow cytometry

Cells were stained for the expression of surface markers using antibodies listed in table S1 for 30 min at 4°C. Cell viability was determined using Zombie dye (Biolegend) following the manufacturer's instructions. For intracellular IFN-γ staining, GolgiPlug (BD Bioscience) was added to culture media 4 h prior to the staining. Cells were stained for the expression of surface markers as previously described, fixed and permeabilized using FoxP3/Transcription Factor Staining Buffer Set (eBioscience) prior to intracellular staining for 30 min at 4°C. Cells were washed twice with PBS before acquisition on a LSRII Fortessa flow cytometer (BD Biosciences). Results were analyzed using FlowJo software (Tree Star Inc.).

Phosphorylation flow cytometry analysis

For p-STAT4 analysis, NK cells were activated or not with IL-12 (0.1 ng/mL; 1 ng/mL or 10 ng/mL) for 1 h. For p-NF-κB, p-p38 and p-S6 analysis, NK cells were activated or not with IL-12 (10 ng/mL) for 24 h. When indicated, IL-1 family members were added during 5min for p-NF-κB and p-p38 and 1 h for p-S6 analysis. Cells were then fixed with Lyse/Fix Buffer (BD Biosciences) for 10 min at 37°C and permeabilized with Perm Buffer III (BD Biosciences) for 30 min on ice following the manufacturer's instructions. Cells were then stained for 45 min at room temperature, washed, and directly acquired on a Fortessa cytometer (Becton Dickinson) as previously described.

Killing assay

PB NK cells were activated with IL-1 family members (10 ng/mL) alone or in combination with IL-12 (10 ng/mL) for 24 h and washed 3 times. K562 cells were labeled with calcein (Invitrogen) at 10 µL/mL in cRPMI for 30 min at 37°C, washed twice, and fixed with sulfinpyrazone (4 mM, Sigma-Aldrich). NK cells were incubated with K562 target cells at indicated effector:target ratios for 4 h à 37°C. Calcein release was measured using Clariostar (Labtech) and the percentage of specific lysis was calculated as followed:

$$\% \text{ of lysis} = ((Fluo_{measured} - Fluo_{spontaneous\ release})) / ((Fluo_{max} - Fluo_{spontaneous\ release})) \times 100$$

Proliferation assay

NK cells were stained with 5 µM Cell Trace Violet (CTV) (Invitrogen) for 20 min at room temperature, washed twice, and activated with IL-1 family members (10 ng/mL) with or without IL-12 (10 ng/mL) for 24 h in RMPI supplemented with 20% human AB serum. After three washes, IL-2 (100 UI/mL, Chiron) was added and CTV signal was analyzed by flow cytometry on day 3 and 6 for $CD56^{bright}$ and $CD56^{dim}$, respectively.

IFN-γ ELISAs

Human IFN-γ levels were measured in culture supernatants using the human IFN-γ ELISA kit (R&D) following the manufacturer's instructions. Mouse IFN-γ levels were measured in serum using the Extra Sensitive IFN gamma Mouse ELISA Kit (ThermoFischer) following the manufacturer's instructions.

Luminex immunoassay

Culture supernatants of activated NK cells were harvested to perform IFN-γ, TNF-α, GM-CSF, IL-8, CCL3 (MIP-1α), CCL4 (MIP-1β), CCL5 (RANTES), IL-2, IL-3, IL-4, IL-5, IL-6, IL-10, IL-13, IL-17A, IL-22, and G-CSF quantification using a human Bio-plex PRO assay (Biorad) following the manufacturer's instructions and acquired with the Luminex200 instrument (Luminex).

mRNA isolation and quantitative PCR

Total RNA extraction was performed using NucleoSpin RNA Kit (Macherey-Nagel) following the manufacturer's instructions. Reverse transcription was performed with the iScript Reverse Transcription kit (BioRad) using 350 ng total RNA extract. Real Time quantitative PCR (RT-qPCR) analysis was performed using TaqMan gene expression assay with *ST2* and *IL-1RAcP* specific primers (Hs00249384_m1 and Hs00895050_m1 respectively, Life Technologies). Normalization of ST2 expression was performed using GADD45a (Hs00169255_m1, Life Technologies) expression.

***ST2* promoter region analysis**

The human *ST2* gene sequence was obtained from Gen-Bank and then submitted to Eukaryotic Promoter Databank (EPD)*(70)* to identify the promoter region. Putative binding sites for transcription factors in the *ST2*-regulating region were identified using the PROMO database *(71)*.

p-STAT4 Chromatin Immunoprecipitation (Ch-IP)

PB NK cells were stimulated or not with IL-12 as previously described and Ch-IP was performed using ChIP-IT PBMCs Kit (Active Motif) according to the manufacturer's instructions. Briefly, cells were cross-linked with 1% formaldehyde then sonicated on ice for 6 min (6 cycles of 1 min; 30 s on / 30 s off) at 4°C using a water bath-sonicator (Diagenode). Chromatin fragments were reverse cross-linked overnight at 65°C, and 500 ng of each input DNA was run on a 1% agarose gel to confirm that fragment size ranged between 200 and 1500 bp. p-STAT4 immunoprecipitation was performed overnight at 4°C using anti-p-STAT4 antibody (Cell signaling). p-STAT4 immunoprecipitation was validated by Western blot using pre- and post-immunoprecipitated samples stained with anti-p-STAT4 (Cell Signaling). Isolated DNA fragments were purified and quantitative PCR analysis was performed using 1 µg of DNA as template. Primers for *ST2* promoter region were extracted from*(72)* and we used *PRF1* (Cell Signaling) and Negative Primer Set 1 and 2 (Active Motif) as positive and negative controls for p-STAT4 binding (see table S1 for sequences). The Ct Value of each sample was normalized to input DNA fraction and fold-change for p-STAT4 binding was calculated using ΔΔct method. qPCR analysis was conducted in triplicate for each sample.

RNA-seq

PB NK cells were FACS-sorted as described above. 400,000 cells from each population were resuspended in 350 µL TCL lysis buffer (Qiagen) supplemented with 1 % β-mercaptoethanol. Total RNA extraction was performed using the Single Cell RNA Purification Kit (Norgen) following the manufacturer's instructions, including an additional treatment with rDNAse (Qiagen) to avoid DNA contamination. RNA quality was addressed using 4200 TapeStation (Agilent) automated electrophoresis with RIN always exceeding 8,

and total RNA was quantified using Qubit™4 Fluorometer (ThermoFischer). Reverse transcription and DNA amplification was performed with SmartSeqV4 (Takara) using 10 ng of RNA as template. DNA library was prepared with Nextera XT DNA library Prep kit (Illumina), hybridized on NovaSeqS1 Flow cell and sequenced on NovaSeq sequencing platform (Illumina) with a paired-end protocol. Raw sequencing reads were aligned on the human genome (GRCh38) with STAR (v2.7.3a) and the annotation of known genes from gencode v33. Gene expression was quantified using Salmon (v1.1.0) and the annotation of protein coding genes from gencode v33.

RNA-seq bioinformatics analysis

All analyses were performed in R programming language (v3.6.3). DESeq2 (v1.26.0) was used to normalize raw counts, to generate principal component analysis (PCA) plots based on the 500 most variable genes and to identify differentially-expressed genes (DEGs). To identify NK subset signatures, DEGs between one subset and the two other subsets of NK cells were filtered considering a log2 fold change (LFC) > 1 and an adjusted p-value < 0.001, resulting in 234 genes enriched in $ST2^{+}$, 396 genes enriched in $CD56^{dim}$ and 418 genes enriched in $CD56^{bright}$ NK cells. These signatures were scored by ssGSEA using the GSVA package. The Morpheus tool (Broad Institute) was used to generate a heatmap representing the relative expression of these DEGs, using an unsupervised hierarchical clustering of genes and samples based on the one minus Pearson correlation metric. To evaluate the intermediate state of $ST2^{+}$ NK cells compared with $CD56^{bright}$ and $CD56^{dim}$ NK cells, DEGs between one subset and the two other subsets of NK cells were filtered considering a log2 fold change (LFC) > 1 and an adjusted p-value < 0.05. The Morpheus tool (Broad Institute) was used to generate a heatmap representing their relative expression. For this heatmap, genes were classified as follows: upregulated DEGs in $CD56^{bright}$ NK cells (n = 828 genes), downregulated DEGs in $CD56^{dim}$ NK cells (n = 1,348 genes), upregulated DEGs in $ST2^{+}$ NK cells (n = 547 genes), downregulated DEGs in $CD56^{bright}$ NK cells (n = 1,009 genes) and upregulated DEGs in $CD56^{dim}$ NK cells (n = 1,024 genes). Intermediate transcriptional profile of $ST2^{+}$ NK cells was validated using a permutation resampling strategy. Briefly, among all genes differentially

expressed between $CD56^{bright}$ and $CD56^{dim}$ NK cells, the observed number of genes with an intermediate expression in $ST2^{+}$ NK cells ($CD56^{bright} > ST2^{+} > CD56^{dim}$ or $CD56^{bright} < ST2^{+} < CD56^{dim}$) was evaluated and compared to a sampling distribution obtained after n = 1000 permutations of sample labels. p value was computed with a permutation statistical test.

Analysis of cancer patient data

Upper-quartile normalized expression (UQN) and clinical outcome datasets from The Cancer Genome Atlas (TCGA) were downloaded from the Pan-Cancer Atlas (https://www.cancer.gov/about-nci/organization/ccg/research/structural-genomics/tcga) for 33 tumor types: adrenocortical carcinoma (ACC), bladder urothelial carcinoma (BLCA), breast invasive carcinoma (BRCA), cervical carcinoma (CESC), cholangiosarcoma (CHOL), colorectal adenocarcinoma (COAD), diffuse large B-cell lymphoma (DLBC), esophageal carcinoma (ESCA), glioblastoma multiforme (GBM), head and neck squamous cell carcinoma (HNSC), kidney chromophobe carcinoma (KICH), kidney clear renal cell carcinoma (KIRC), kidney papillary cell carcinoma (KIRP), lower grade glioma (LGG), liver hepatocellular carcinoma (LIHC), lung adenocarcinoma (LUAD), lung squamous cell carcinoma (LUSC), mesothelioma (MESO), ovarian serous cystadenocarcinoma (OV), pancreatic adenocarcinoma (PAAD), paraganglioma & pheochromocytoma (PCPG), prostate adenocarcinoma (PRAD), rectum adenocarcinoma (READ), sarcoma (SARC), skin cutaneous metastatic melanoma (SKCM), stomach adenocarcinoma (STAD), testicular germ cell cancer (TGCT), thyroid carcinoma (THCA), thymoma (THYM), uterine corpus endometrial carcinoma (UCEC), uterine carcinosarcoma (UCS) and uveal melanoma (UVM) to compare gene expression in tumor *versus* peritumoral healthy tissue. For breast cancer analysis, tumors were further stratified according to their molecular subtype to analyze IL-33 log2 (RSEM+1) normalized expression and clinical impact. Overall survival analyses and plots were performed with R software v 3.6.0, using the packages survival and survminer. For each gene, patients were stratified into terciles according to normalized gene expression levels in log2 (RSEM+1) to compare top (*i.e.* high) and bottom (*i.e.* low) terciles. The log-rank test was used to determine statistical significance for overall survival

between the two groups of patients. For multivariate analysis in the breast cancer dataset, a cox model including the main prognostic factors (age, molecular subtype and stage) was used. Gender was removed from the model due to the low number of males in the study.

IL-33 immunohistochemistry on FFPE human breast tumor ngTMA

IL-33 staining was performed automatically using a BOND RX autostainer (Leica Biosystems). Sections were first deparaffinized and antigen was retrieved using Tris buffer (pH 9.0) for 30 min at 95°C. Sections were then stained with goat anti-human IL-33 (R&D Systems, # AF3625; dilution of 1:400 for 30 min) primary antibody. A rabbit anti-goat antibody (Agilent, # E0466) was used as secondary antibody, at a dilution of 1:400 for 15 min. Specific binding of primary antibodies was visualized using a polymer-based visualization system with horseradish peroxidase as the enzyme and 3,3-diaminobenzidine (DAB) as a brown chromogen for IL-33. Sections were counterstained with hematoxylin, dehydrated and mounted with Tissue-Tek Glas Mounting Medium (Sakura). Slides were scanned in high resolution on whole slide scanners Panoramic 250 Flash (3DHISTECH) or NanoZoomer S360 (Hamamatsu).

Data analysis and statistics

Statistical analyses were performed using the GraphPad software and tests conducted are indicated in the Fig. legends. P-values lower than 0.05 were considered to be significant, with stars corresponding to * $p < 0.05$; ** $p < 0.01$; *** $p < 0.001$ and **** $p < 0.0001$. If no stars are indicated, no statistically significant difference was found.

Data Availability

The bulk RNA-seq data generated during this study are deposited in Gene Expression Omnibus repository (GEO) with accession number GEO: GSE199134. The raw and processed data are publicly available as of the date of publication. Accession numbers are listed in the table S1. This paper does not report original code. The RNA-seq data from laser-microdissected stromal versus epithelial zones from

DCIS and IBC lesions *(46, 47)* and from healthy mammary tissue versus DCIS and IBC *(46, 47)* were downloaded from GEO with accession number GEO: GSE41228 and GSE21422 respectively. The scRNA-seq data derived from NK cells infiltrating human melanoma metastases *(42)* and mouse lung tumors *(43)* were downloaded from GEO with accession number GEO: GSE139249 and GSE123534, respectively. The Cancer Genome Atlas data were downloaded from Firehose (https://gdac.broadinstitute.org/). Genes Signatures used in this study are listed in Tables 1-3.

867 **List of Supplementary Materials**

868 Fig. S1. IL-33 in combination with IL-12 strongly activates NK cell secretory and cytotoxic functions

869 Fig. S2. IL-12 induces ST2 expression on a subset of NK cells in a STAT4-dependent manner

870 Fig. S3. IL-33 preferentially activates a subset of $CD56^{dim}$ NK cells

871 Fig. S4. $ST2^{+}$ NK cells display a unique gene signature compared to $CD56^{bright}$ and $CD56^{dim}$ NK cells

872 Fig. S5. Unsupervised clustering of sc-RNAseq datasets

873 Fig. S6. Gating strategy to identify NK cells in tumor cell suspensions by flow cytometry

874 Fig. S7 | IL-12 sensitizes mouse splenic NK cells to the production of IFN-γ in response to IL-33

875 Fig. S8. Antitumoral effect of IL-33 and IL-12 combination is dependent on NK cells in *Rag2*-KO mice

876 Fig. S9. IL-33 is associated with increased overall patient survival for several cancers

877 Table S1. Reagent and resources table

878

879 **References**

880

881 1. E. Vivier, E. Tomasello, M. Baratin, T. Walzer, S. Ugolini, Functions of natural killer cells. *Nat.*
882 *Immunol.* **9**, 503–510 (2008).

883 2. A. G. Freud, B. L. Mundy-Bosse, J. Yu, M. A. Caligiuri, The Broad Spectrum of Human Natural Killer
884 Cell Diversity. *Immunity* **47**, 820–833 (2017).

885 3. A. Poli, T. Michel, M. Thérésine, E. Andrès, F. Hentges, J. Zimmer, CD56bright natural killer (NK) cells:
886 an important NK cell subset. *Immunology* **126**, 458–465 (2009).

887 4. C. Lo Nigro, M. Macagno, D. Sangiolo, L. Bertolaccini, M. Aglietta, M. C. Merlano, NK-mediated
888 antibody-dependent cell-mediated cytotoxicity in solid tumors: biological evidence and clinical
889 perspectives. *Ann Transl Med* **7** (2019), doi:10.21037/atm.2019.01.42.

890 5. C. Romagnani, K. Juelke, M. Falco, B. Morandi, A. D'Agostino, R. Costa, G. Ratto, G. Forte, P. Carrega,
891 G. Lui, R. Conte, T. Strowig, A. Moretta, C. Münz, A. Thiel, L. Moretta, G. Ferlazzo, CD56brightCD16-
892 killer Ig-like receptor- NK cells display longer telomeres and acquire features of CD56dim NK cells upon
893 activation. *J. Immunol.* **178**, 4947–4955 (2007).

894 6. N. D. Huntington, N. Legrand, N. L. Alves, B. Jaron, K. Weijer, A. Plet, E. Corcuff, E. Mortier, Y.
895 Jacques, H. Spits, J. P. Di Santo, IL-15 trans-presentation promotes human NK cell development and
896 differentiation in vivo. *J. Exp. Med.* **206**, 25–34 (2009).

897 7. J. Yu, H. C. Mao, M. Wei, T. Hughes, J. Zhang, I. Park, S. Liu, S. McClory, G. Marcucci, R. Trotta, M. A.
898 Caligiuri, CD94 surface density identifies a functional intermediary between the CD56bright and
899 CD56dim human NK-cell subsets. *Blood* **115**, 274–281 (2010).

900 8. N. K. Björkström, P. Riese, F. Heuts, S. Andersson, C. Fauriat, M. A. Ivarsson, A. T. Björklund, M.
901 Flodström-Tullberg, J. Michaëlsson, M. E. Rottenberg, C. A. Guzmán, H.-G. Ljunggren, K.-J. Malmberg,
902 Expression patterns of NKG2A, KIR, and CD57 define a process of CD56dim NK-cell differentiation
903 uncoupled from NK-cell education. *Blood* **116**, 3853–3864 (2010).

9. S. Lopez-Vergès, J. M. Milush, S. Pandey, V. A. York, J. Arakawa-Hoyt, H. Pircher, P. J. Norris, D. F. Nixon, L. L. Lanier, CD57 defines a functionally distinct population of mature NK cells in the human CD56dimCD16+ NK-cell subset. *Blood* **116**, 3865–3874 (2010).

10. T. E. O'Sullivan, J. C. Sun, L. L. Lanier, Natural Killer Cell Memory. *Immunity* **43**, 634–645 (2015).

11. S. J. Judge, W. J. Murphy, R. J. Canter, Characterizing the Dysfunctional NK Cell: Assessing the Clinical Relevance of Exhaustion, Anergy, and Senescence. *Front Cell Infect Microbiol* **10**, 49 (2020).

12. A. Crinier, P. Milpied, B. Escalière, C. Piperoglou, J. Galluso, A. Balsamo, L. Spinelli, I. Cervera-Marzal, M. Ebbo, M. Girard-Madoux, S. Jaeger, E. Bollon, S. Hamed, J. Hardwigsen, S. Ugolini, F. Vély, E. Narni-Mancinelli, E. Vivier, High-Dimensional Single-Cell Analysis Identifies Organ-Specific Signatures and Conserved NK Cell Subsets in Humans and Mice. *Immunity* **49**, 971-986.e5 (2018).

13. P. L. Collins, M. Cella, S. I. Porter, S. Li, G. L. Gurewitz, H. S. Hong, R. P. Johnson, E. M. Oltz, M. Colonna, Gene Regulatory Programs Conferring Phenotypic Identities to Human NK Cells. *Cell* **176**, 348-360.e12 (2019).

14. C. M. Lau, N. M. Adams, C. D. Geary, O.-E. Weizman, M. Rapp, Y. Pritykin, C. S. Leslie, J. C. Sun, Epigenetic control of innate and adaptive immune memory. *Nat. Immunol.* **19**, 963–972 (2018).

15. J. A. Myers, J. S. Miller, Exploring the NK cell platform for cancer immunotherapy. *Nat Rev Clin Oncol* **18**, 85–100 (2021).

16. N. D. Huntington, J. Cursons, J. Rautela, The cancer–natural killer cell immunity cycle. *Nat Rev Cancer* **20**, 437–454 (2020).

17. D. H. Raulet, N. Guerra, Oncogenic stress sensed by the immune system: role of natural killer cell receptors. *Nat Rev Immunol* **9**, 568–580 (2009).

18. S. Rusakiewicz, M. Semeraro, M. Sarabi, M. Desbois, C. Locher, R. Mendez, N. Vimond, A. Concha, F. Garrido, N. Isambert, L. Chaigneau, V. Le Brun-Ly, P. Dubreuil, I. Cremer, A. Caignard, V. Poirier-Colame, K. Chaba, C. Flament, N. Halama, D. Jäger, A. Eggermont, S. Bonvalot, F. Commo, P. Terrier, P. Opolon, J.-F. Emile, J.-M. Coindre, G. Kroemer, N. Chaput, A. Le Cesne, J.-Y. Blay, L. Zitvogel, Immune

infiltrates are prognostic factors in localized gastrointestinal stromal tumors. *Cancer Res.* **73**, 3499–3510 (2013).

19. K. C. Barry, J. Hsu, M. L. Broz, F. J. Cueto, M. Binnewies, A. J. Combes, A. E. Nelson, K. Loo, R. Kumar, M. D. Rosenblum, M. D. Alvarado, D. M. Wolf, D. Bogunovic, N. Bhardwaj, A. I. Daud, P. K. Ha, W. R. Ryan, J. L. Pollack, B. Samad, S. Asthana, V. Chan, M. F. Krummel, A natural killer-dendritic cell axis defines checkpoint therapy-responsive tumor microenvironments. *Nat. Med.* **24**, 1178–1191 (2018).

20. J. Cursons, F. Souza-Fonseca-Guimaraes, M. Foroutan, A. Anderson, F. Hollande, S. Hediyeh-Zadeh, A. Behren, N. D. Huntington, M. J. Davis, A Gene Signature Predicting Natural Killer Cell Infiltration and Improved Survival in Melanoma Patients. *Cancer Immunol Res* **7**, 1162–1174 (2019).

21. B. Cózar, M. Greppi, S. Carpentier, E. Narni-Mancinelli, L. Chiossone, E. Vivier, Tumor-Infiltrating Natural Killer Cells. *Cancer Discov* (2020), doi:10.1158/2159-8290.CD-20-0655.

22. G. Trinchieri, M. Matsumoto-Kobayashi, S. C. Clark, J. Seehra, L. London, B. Perussia, Response of resting human peripheral blood natural killer cells to interleukin 2. *J. Exp. Med.* **160**, 1147–1169 (1984).

23. M. Kobayashi, L. Fitz, M. Ryan, R. M. Hewick, S. C. Clark, S. Chan, R. Loudon, F. Sherman, B. Perussia, G. Trinchieri, Identification and purification of natural killer cell stimulatory factor (NKSF), a cytokine with multiple biologic effects on human lymphocytes. *J. Exp. Med.* **170**, 827–845 (1989).

24. W. E. Carson, J. G. Giri, M. J. Lindemann, M. L. Linett, M. Ahdieh, R. Paxton, D. Anderson, J. Eisenmann, K. Grabstein, M. A. Caligiuri, Interleukin (IL) 15 is a novel cytokine that activates human natural killer cells via components of the IL-2 receptor. *J. Exp. Med.* **180**, 1395–1403 (1994).

25. H. Okamura, H. Tsutsi, T. Komatsu, M. Yutsudo, A. Hakura, T. Tanimoto, K. Torigoe, T. Okura, Y. Nukada, K. Hattori, Cloning of a new cytokine that induces IFN-gamma production by T cells. *Nature* **378**, 88–91 (1995).

26. L. Müller, P. Aigner, D. Stoiber, Type I Interferons and Natural Killer Cell Regulation in Cancer. *Front Immunol* **8**, 304 (2017).

954 27. G. M. Konjević, A. M. Vuletić, K. M. Mirjačić Martinović, A. K. Larsen, V. B. Jurišić, The role of
955 cytokines in the regulation of NK cells in the tumor environment. *Cytokine* **117**, 30–40 (2019).
956 28. C. Garlanda, C. A. Dinarello, A. Mantovani, The interleukin-1 family: back to the future. *Immunity*
957 **39**, 1003–1018 (2013).
958 29. C. Cayrol, J.-P. Girard, Interleukin-33 (IL-33): A nuclear cytokine from the IL-1 family. *Immunological*
959 *Reviews* **281**, 154–168 (2018).
960 30. F. Y. Liew, J.-P. Girard, H. R. Turnquist, Interleukin-33 in health and disease. *Nat. Rev. Immunol.* **16**,
961 676–689 (2016).
962 31. W. Kuswanto, D. Burzyn, M. Panduro, K. K. Wang, Y. C. Jang, A. J. Wagers, C. Benoist, D. Mathis,
963 Poor Repair of Skeletal Muscle in Aging Mice Reflects a Defect in Local, Interleukin-33-Dependent
964 Accumulation of Regulatory T Cells. *Immunity* **44**, 355–367 (2016).
965 32. L. D. Faustino, J. W. Griffith, R. A. Rahimi, K. Nepal, D. L. Hamilos, J. L. Cho, B. D. Medoff, J. J. Moon,
966 D. A. A. Vignali, A. D. Luster, Interleukin-33 activates regulatory T cells to suppress innate γδ T cell
967 responses in the lung. *Nat Immunol* **21**, 1371–1383 (2020).
968 33. M. D. Smithgall, M. R. Comeau, B.-R. Park Yoon, D. Kaufman, R. Armitage, D. E. Smith, IL-33
969 amplifies both Th1- and Th2-type responses through its activity on human basophils, allergen-reactive
970 Th2 cells, iNKT and NK Cells. *Int Immunol* **20**, 1019–1030 (2008).
971 34. W. V. Bonilla, A. Fröhlich, K. Senn, S. Kallert, M. Fernandez, S. Johnson, M. Kreutzfeldt, A. N.
972 Hegazy, C. Schrick, P. G. Fallon, R. Klemenz, S. Nakae, H. Adler, D. Merkler, M. Löhning, D. D.
973 Pinschewer, The Alarmin Interleukin-33 Drives Protective Antiviral CD8+ T Cell Responses. *Science* **335**,
974 984–989 (2012).
975 35. J. T. Clark, D. A. Christian, J. A. Gullicksrud, J. A. Perry, J. Park, M. Jacquet, J. C. Tarrant, E. Radaelli, J.
976 Silver, C. A. Hunter, G. T. Belz, C. V. Rothlin, M. R. Starkey, Eds. IL-33 promotes innate lymphoid cell-
977 dependent IFN-γ production required for innate immunity to Toxoplasma gondii. *eLife* **10**, e65614
978 (2021).

979 36. G. K. Dwyer, L. M. D'Cruz, H. R. Turnquist, Emerging Functions of IL-33 in Homeostasis and
980 Immunity. *Annual Review of Immunology* **40**, null (2022).
981 37. G. Trinchieri, Interleukin-12 and the regulation of innate resistance and adaptive immunity. *Nature*
982 *Reviews Immunology* **3**, 133–146 (2003).
983 38. J. Schmitz, A. Owyang, E. Oldham, Y. Song, E. Murphy, T. K. McClanahan, G. Zurawski, M. Moshrefi,
984 J. Qin, X. Li, D. M. Gorman, J. F. Bazan, R. A. Kastelein, IL-33, an interleukin-1-like cytokine that signals
985 via the IL-1 receptor-related protein ST2 and induces T helper type 2-associated cytokines. *Immunity*
986 **23**, 479–490 (2005).
987 39. D. E. Ochayon, A. Ali, P. C. Alarcon, D. Krishnamurthy, L. C. Kottyan, M. T. Borchers, S. N. Waggoner,
988 IL-33 promotes type 1 cytokine expression via p38 MAPK in human NK cells. *J. Leukoc. Biol.* (2020),
989 doi:10.1002/JLB.3A0120-379RR.
990 40. R. J. Salmond, A. S. Mirchandani, A.-G. Besnard, C. C. Bain, N. C. Thomson, F. Y. Liew, IL-33 induces
991 innate lymphoid cell–mediated airway inflammation by activating mammalian target of rapamycin. *J*
992 *Allergy Clin Immunol* **130**, 1159-1166.e6 (2012).
993 41. N. K. Björkström, H.-G. Ljunggren, J. Michaëlsson, Emerging insights into natural killer cells in
994 human peripheral tissues. *Nat Rev Immunol* **16**, 310–320 (2016).
995 42. L. F. de Andrade, Y. Lu, A. Luoma, Y. Ito, D. Pan, J. W. Pyrdol, C. H. Yoon, G.-C. Yuan, K. W.
996 Wucherpfennig, Discovery of specialized NK cell populations infiltrating human melanoma metastases.
997 *JCI Insight* **4**, 133103 (2019).
998 43. J. Ni, X. Wang, A. Stojanovic, Q. Zhang, M. Wincher, L. Bühler, A. Arnold, M. P. Correia, M. Winkler,
999 P.-S. Koch, V. Sexl, T. Höfer, A. Cerwenka, Single-Cell RNA Sequencing of Tumor-Infiltrating NK Cells
1000 Reveals that Inhibition of Transcription Factor HIF-1α Unleashes NK Cell Activity. *Immunity* **52**, 1075-
1001 1087.e8 (2020).
1002 44. M. M. Tu, M. M. A. Rahim, C. Sayed, A. B. Mahmoud, A. P. Makrigiannis, Immunosurveillance and
1003 Immunoediting of Breast Cancer via Class I MHC Receptors. *Cancer Immunol Res* **5**, 1016–1028 (2017).

45. C. Moussion, N. Ortega, J.-P. Girard, The IL-1-like cytokine IL-33 is constitutively expressed in the nucleus of endothelial cells and epithelial cells in vivo: a novel “alarmin”? *PLoS ONE* **3**, e3331 (2008).

46. S. Lee, S. Stewart, I. Nagtegaal, J. Luo, Y. Wu, G. Colditz, D. Medina, D. C. Allred, Differentially expressed genes regulating the progression of ductal carcinoma in situ to invasive breast cancer. *Cancer Res* **72**, 4574–4586 (2012).

47. C. Kretschmer, A. Sterner-Kock, F. Siedentopf, W. Schoenegg, P. M. Schlag, W. Kemmner, Identification of early molecular markers for breast cancer. *Molecular Cancer* **10**, 15 (2011).

48. J. P. Böttcher, E. Bonavita, P. Chakravarty, H. Blees, M. Cabeza-Cabrerizo, S. Sammicheli, N. C. Rogers, E. Sahai, S. Zelenay, C. Reis e Sousa, NK Cells Stimulate Recruitment of cDC1 into the Tumor Microenvironment Promoting Cancer Immune Control. *Cell* **172**, 1022-1037.e14 (2018).

49. C. Baumann, W. V. Bonilla, A. Fröhlich, C. Helmstetter, M. Peine, A. N. Hegazy, D. D. Pinschewer, M. Löhning, T-bet- and STAT4-dependent IL-33 receptor expression directly promotes antiviral Th1 cell responses. *Proc. Natl. Acad. Sci. U.S.A.* **112**, 4056–4061 (2015).

50. M. Nakahira, H.-J. Ahn, W.-R. Park, P. Gao, M. Tomura, C.-S. Park, T. Hamaoka, T. Ohta, M. Kurimoto, H. Fujiwara, Synergy of IL-12 and IL-18 for IFN-gamma gene expression: IL-12-induced STAT4 contributes to IFN-gamma promoter activation by up-regulating the binding activity of IL-18-induced activator protein 1. *Journal of immunology (Baltimore, Md. : 1950)* **168**, 1146–53 (2002).

51. A. Mavropoulos, G. Sully, A. P. Cope, A. R. Clark, Stabilization of IFN-gamma mRNA by MAPK p38 in IL-12- and IL-18-stimulated human NK cells. *Blood* **105**, 282–288 (2005).

52. M. Fang, Y. Li, K. Huang, S. Qi, J. Zhang, W. Zgodzinski, M. Majewski, G. Wallner, S. Gozdz, P. Macek, A. Kowalik, M. Pasiarski, E. Grywalska, L. Vatan, N. Nagarsheth, W. Li, L. Zhao, I. Kryczek, G. Wang, Z. Wang, W. Zou, L. Wang, IL33 Promotes Colon Cancer Cell Stemness via JNK Activation and Macrophage Recruitment. *Cancer Res.* **77**, 2735–2745 (2017).

53. D. E. Ochayon, A. Ali, P. C. Alarcon, D. Krishnamurthy, L. C. Kottyan, M. T. Borchers, S. N. Waggoner, IL-33 promotes type 1 cytokine expression via p38 MAPK in human NK cells. *J Leukoc Biol* **107**, 663–671 (2020).

1030 54. C. T. Lutz, A. Karapetyan, A. Al-Attar, B. J. Shelton, K. J. Holt, J. H. Tucker, S. R. Presnell, Human
1031 natural killer cells proliferate and die in vivo more rapidly than T cells in healthy young and elderly
1032 adults. *J Immunol* **186**, 4590–4598 (2011).
1033 55. I. Hamann, N. Unterwalder, A. E. Cardona, C. Meisel, F. Zipp, R. M. Ransohoff, C. Infante-Duarte,
1034 Analyses of phenotypic and functional characteristics of CX3CR1-expressing natural killer cells.
1035 *Immunology* **133**, 62–73 (2011).
1036 56. J. Hanna, P. Bechtel, Y. Zhai, F. Youssef, K. McLachlan, O. Mandelboim, Novel insights on human NK
1037 cells' immunological modalities revealed by gene expression profiling. *J. Immunol.* **173**, 6547–6563
1038 (2004).
1039 57. M. Hubert, E. Gobbini, C. Couillault, T.-P. V. Manh, A.-C. Doffin, J. Berthet, C. Rodriguez, V. Ollion, J.
1040 Kielbassa, C. Sajous, I. Treilleux, O. Tredan, B. Dubois, M. Dalod, N. Bendriss-Vermare, C. Caux, J.
1041 Valladeau-Guilemond, IFN-III is selectively produced by cDC1 and predicts good clinical outcome in
1042 breast cancer. *Sci Immunol* **5** (2020), doi:10.1126/sciimmunol.aav3942.
1043 58. L. Zitvogel, G. Kroemer, CD103+ dendritic cells producing interleukin-12 in anticancer
1044 immunosurveillance. *Cancer Cell* **26**, 591–593 (2014).
1045 59. D. Mittal, D. Vijayan, E. M. Putz, A. R. Aguilera, K. A. Markey, J. Straube, S. Kazakoff, S. L. Nutt, K.
1046 Takeda, G. R. Hill, N. Waddell, M. J. Smyth, Interleukin-12 from CD103+ Batf3-Dependent Dendritic
1047 Cells Required for NK-Cell Suppression of Metastasis. *Cancer Immunol Res* **5**, 1098–1108 (2017).
1048 60. Y. O. Alexandre, S. Ghilas, C. Sanchez, A. Le Bon, K. Crozat, M. Dalod, XCR1+ dendritic cells promote
1049 memory CD8+ T cell recall upon secondary infections with Listeria monocytogenes or certain viruses.
1050 *Journal of Experimental Medicine* **213**, 75–92 (2015).
1051 61. S. M. Brunner, C. Rubner, R. Kesselring, M. Martin, E. Griesshammer, P. Ruemmele, T. Stempfl, A.
1052 Teufel, H. J. Schlitt, S. Fichtner-Feigl, Tumor-infiltrating, interleukin-33-producing effector-memory
1053 CD8(+) T cells in resected hepatocellular carcinoma prolong patient survival. *Hepatology* **61**, 1957–
1054 1967 (2015).

62. I. Saranchova, J. Han, H. Huang, F. Fenninger, K. B. Choi, L. Munro, C. Pfeifer, I. Welch, A. W. Wyatt, L. Fazli, M. E. Gleave, W. A. Jefferies, Discovery of a Metastatic Immune Escape Mechanism Initiated by the Loss of Expression of the Tumour Biomarker Interleukin-33. *Sci Rep* **6**, 30555 (2016).

63. M. Rössle, G. Cathomas, L. Bonapace, M. Sachs, S. Dehler, M. Storz, G. Huber, H. Moch, T. Junt, K. D. Mertz, Interleukin-33 Expression Indicates a Favorable Prognosis in Malignant Salivary Gland Tumors. *Int. J. Surg. Pathol.* **24**, 394–400 (2016).

64. M. Yang, Y. Feng, C. Yue, B. Xu, L. Chen, J. Jiang, B. Lu, Y. Zhu, Lower expression level of IL-33 is associated with poor prognosis of pulmonary adenocarcinoma. *PLOS ONE* **13**, e0193428 (2018).

65. R. Koster, O. A. Panagiotou, W. A. Wheeler, E. Karlins, J. M. Gastier-Foster, S. R. Caminada de Toledo, A. S. Petrilli, A. M. Flanagan, R. Tirabosco, I. L. Andrulis, J. S. Wunder, N. Gokgoz, A. Patiño-Garcia, F. Lecanda, M. Serra, C. Hattinger, P. Picci, K. Scotlandi, D. M. Thomas, M. L. Ballinger, R. Gorlick, D. A. Barkauskas, L. G. Spector, M. Tucker, D. H. Belynda, M. Yeager, R. N. Hoover, S. Wacholder, S. J. Chanock, S. A. Savage, L. Mirabello, Genome-wide association study identifies the GLDC/IL33 locus associated with survival of osteosarcoma patients. *Int. J. Cancer* **142**, 1594–1601 (2018).

66. X. Gao, X. Wang, Q. Yang, X. Zhao, W. Wen, G. Li, J. Lu, W. Qin, Y. Qi, F. Xie, J. Jiang, C. Wu, X. Zhang, X. Chen, H. Turnquist, Y. Zhu, B. Lu, Tumoral expression of IL-33 inhibits tumor growth and modifies the tumor microenvironment through CD8+ T and NK cells. *J. Immunol.* **194**, 438–445 (2015).

67. A. Long, D. Dominguez, L. Qin, S. Chen, J. Fan, M. Zhang, D. Fang, Y. Zhang, T. M. Kuzel, B. Zhang, Type 2 Innate Lymphoid Cells Impede IL-33–Mediated Tumor Suppression. *The Journal of Immunology* (2018), doi:10.4049/jimmunol.1800173.

68. L. Qi, Q. Zhang, Y. Miao, W. Kang, Z. Tian, D. Xu, W. Xiao, F. Fang, Interleukin-33 activates and recruits natural killer cells to inhibit pulmonary metastatic cancer development. *Int. J. Cancer* **146**, 1421–1434 (2020).

69. C. Laedrach, B. Salhia, N. Cihoric, I. Zlobec, C. Tapia, Immunophenotypic profile of tumor buds in breast cancer. *Pathol Res Pract* **214**, 25–29 (2018).

70. R. Dreos, G. Ambrosini, R. C. Périer, P. Bucher, The Eukaryotic Promoter Database: expansion of EPDnew and new promoter analysis tools. *Nucleic Acids Res* **43**, D92-96 (2015).

71. D. Farré, R. Roset, M. Huerta, J. E. Adsuara, L. Roselló, M. M. Albà, X. Messeguer, Identification of patterns in biological sequences at the ALGGEN server: PROMO and MALGEN. *Nucleic Acids Research* **31**, 3651–3653 (2003).

72. Y. Baba, K. Maeda, T. Yashiro, E. Inage, K. Kasakura, R. Suzuki, F. Niyonsaba, M. Hara, A. Tanabe, H. Ogawa, K. Okumura, Y. Ohtsuka, T. Shimizu, C. Nishiyama, GATA2 is a critical transactivator for the human IL1RL1/ST2 promoter in mast cells/basophils: opposing roles for GATA2 and GATA1 in human IL1RL1/ST2 gene expression. *J. Biol. Chem.* **287**, 32689–32696 (2012).

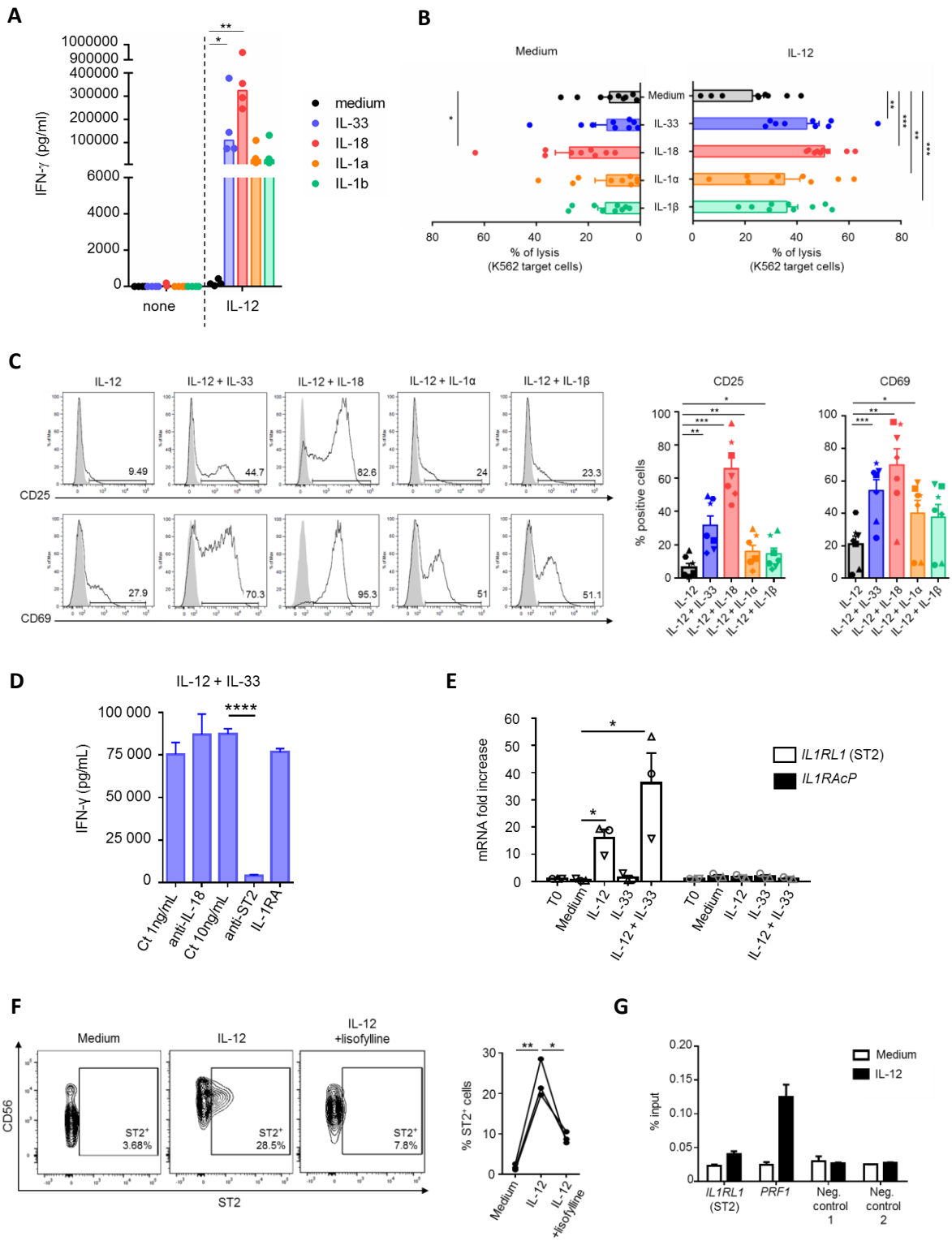

Fig. 1. IL-12/STAT-4 signaling drives ST2 expression and polyfunctionality of human NK cells in response to IL-33

(A) Quantification of IFN-γ secretion by healthy donors' blood NK cells upon stimulation with IL-33, IL-18, IL-1α or IL-1β alone (10 ng/mL) or in combination with IL-12 (10 ng/mL) for 24 h. Histogram bars

represent the median (n = 4 individual experiments). Friedman test with Dunn's multiple comparisons test was performed.

(B) NK cells were activated for 24 h with IL-33, IL-18, IL-1α or IL-1β alone (10 ng/mL) or in combination with IL-12 (10 ng/mL) and then co-cultured with calcein-loaded K562 target cells for 4 h at a 5:1 effector to target ratio. Calcein release in the supernatant was quantified by fluorometry to calculate lysis percentage. Results are expressed as mean + SEM (n = 9 individual experiments). One-way repeated measures ANOVA with Dunnett's multiple comparisons test against levels in medium was performed.

(C) NK cells were activated for 24 h with IL-33, IL-18, IL-1α or IL-1β alone (10 ng/mL) or in combination with IL-12 (10 ng/mL) and then stained for CD25 and CD69 (black line) or corresponding isotypic control (grey). Representative histogram plots (left) and quantification (%) (right) of $CD25^+$ or $CD69^+$ NK cells after cytokine stimulation. Symbols represent paired individual experiments (n=7). Results are expressed as mean + SEM. One-way repeated measures ANOVA with Dunnett's multiple comparisons test against levels in IL-12 was performed.

(D) IFN-γ secretion by healthy donors' blood NK cells upon stimulation for 24 h with IL-33 and IL-12 (10 ng/mL each) in the presence of anti-ST2 (10 μg/mL), anti-IL-18 (1 μg/mL) blocking antibodies, IL-1RA antagonist (100 ng/mL) or mIgG1 control antibody (1 or 10 μg/mL as control for anti-IL-18 or anti-ST2, respectively). Results are expressed as mean + SD and are representative of three individual experiments. One-way repeated measures ANOVA with Tukey's multiple comparisons test was performed.

(E) Real-time quantitative PCR (RT-qPCR) analysis of *IL1RL1* (ST2) and *IL1RAcP* mRNA expression in resting or activated NK cells with IL-12, IL-33, or the combination (10 ng/mL each for 24 h). Results are expressed as mean + SEM of three individual experiments. Each symbol represents one donor. Two-tailed paired Student *t*-test was performed.

(F) NK cells were activated with IL-12 (10 ng/mL) in the presence or not of lisofylline (500 μM) for 24 h prior to ST2 surface expression analysis by flow cytometry. Representative dot plots (left) and

quantification (%) (right) of $ST2^+$ NK cells after cytokine stimulation. One-way repeated measures ANOVA with Tukey's multiple comparisons test was performed; n = 3.

(G) p-STAT4 was immunoprecipitated in NK cells following activation or not with IL-12 (10 ng/mL) for 24 h and p-STAT4 enrichment in *ST2* promoter region was measured by RT-qPCR analysis. *PERFORIN-1 (PRF1)* and negative control sets 1 and 2 were used respectively as positive and negative controls for p-STAT4 binding. Results are expressed as mean + SEM of two individual experiments.

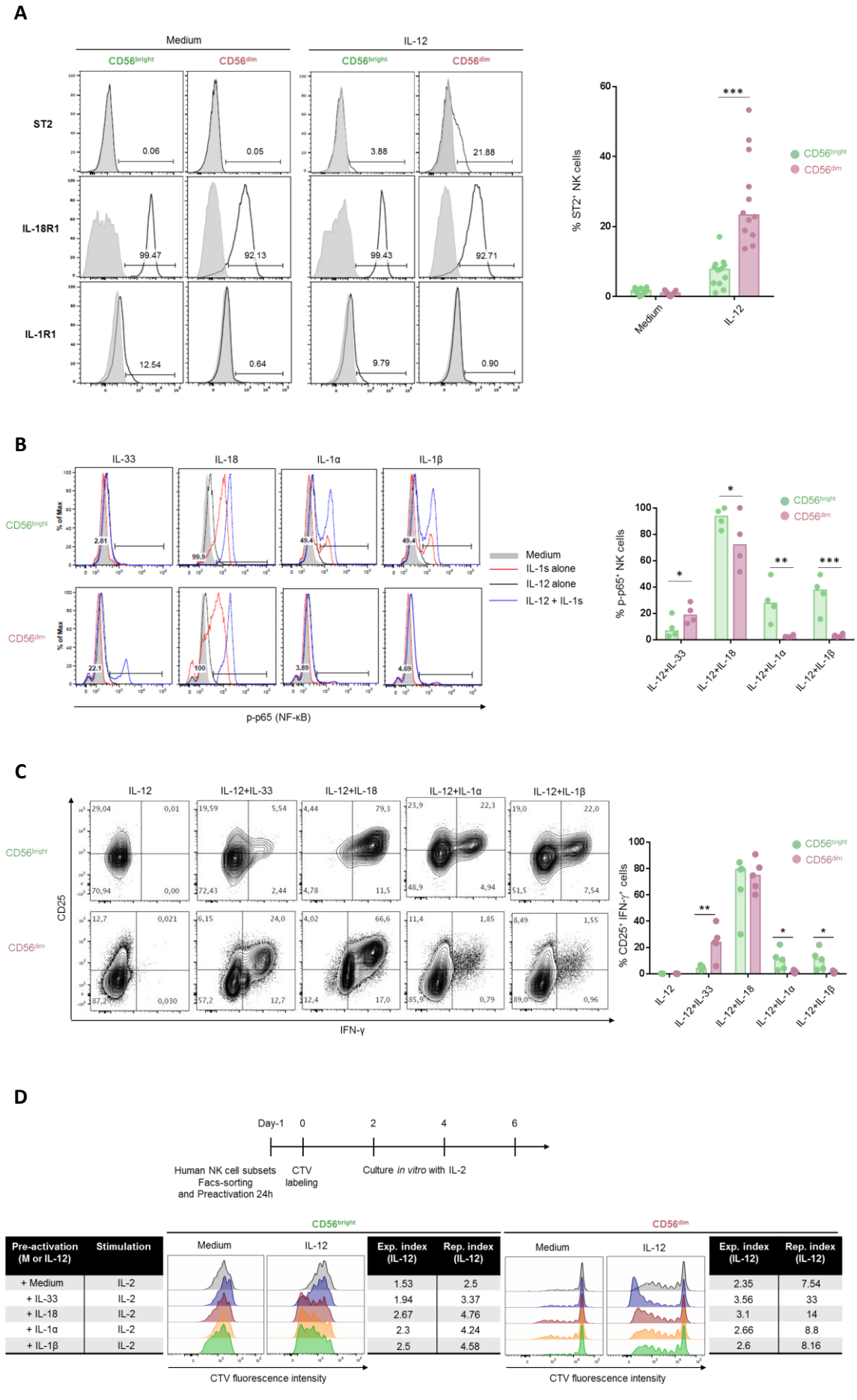

Pre-activation (M or IL-12)	Stimulation	CD56bright Exp. index (IL-12)	CD56bright Rep. index (IL-12)	CD56dim Exp. index (IL-12)	CD56dim Rep. index (IL-12)
+ Medium	IL-2	1.53	2.5	2.35	7.54
+ IL-33	IL-2	1.94	3.37	3.56	33
+ IL-18	IL-2	2.67	4.76	3.1	14
+ IL-1α	IL-2	2.3	4.24	2.66	8.8
+ IL-1β	IL-2	2.5	4.58	2.6	8.16

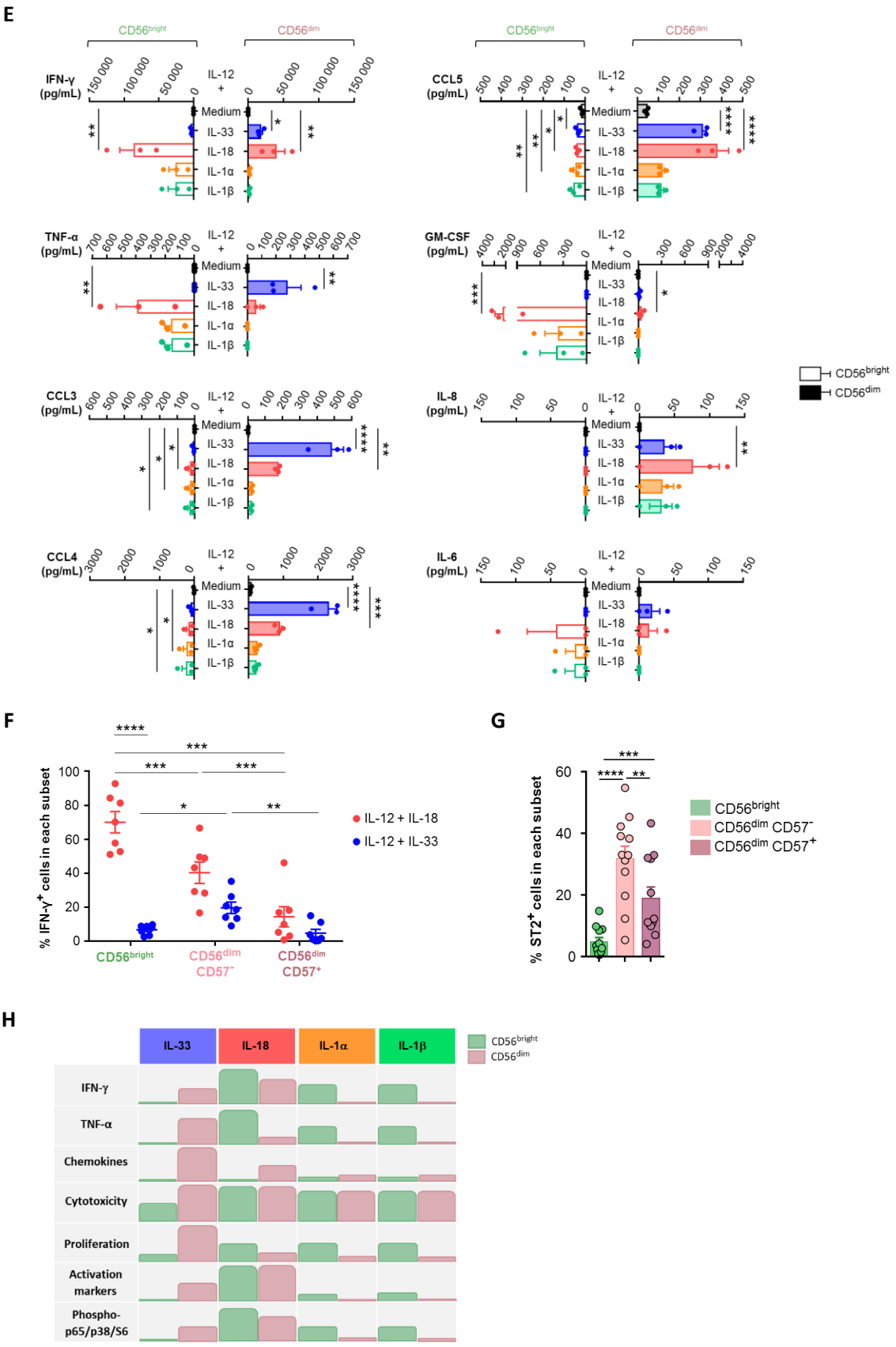

Fig. 2. IL-33 strongly activates a subset of CD56^{dim} NK cells in the presence of IL-12

(A) Healthy donors' blood NK cells were activated with IL-12 (10 ng/mL) or not (medium) for 24 h prior to flow cytometry analysis of ST2, IL-18R1, IL-1R1 expression (grey) or corresponding isotypic control (black line). CD56 surface expression levels were used to discriminate $CD56^{bright}$ and $CD56^{dim}$ NK cells. Representative histogram plots (left) and quantification (%) (right) of $ST2^{+}$ NK cells after medium or IL-12 culture. Histogram bars indicate the median. Wilcoxon matched pairs signed-rank test was performed; n = 12 experiments.

(B) FACS-sorted $CD56^{bright}$ and $CD56^{dim}$ NK cells were activated with medium or IL-12 for 24 h prior to the addition of IL-33, IL-18, IL-1α or IL-1β, supplemented or not with IL-12. Each cytokine was used at 10ng/mL. p65 (NF-κB) phosphorylation was analyzed by flow cytometry 5 min after the addition of IL-1 family cytokines. Representative histogram plots (left) and quantification (%) (right) of $p\text{-}p65^{+}$ NK cells after cytokine activation. Histogram bars indicate the median. Two-way ANOVA with Bonferroni's multiple comparisons test was performed; n = 4 experiments.

(C) Healthy donors' blood NK cells were activated as indicated for 24 h, each cytokine was used at 10 ng/mL. CD25 surface and IFN-γ intracellular expression was analyzed by flow cytometry. CD56 surface expression levels were used to discriminate $CD56^{bright}$ and $CD56^{dim}$ NK cells. Representative dot plots (left) and quantification (%) (right) of $CD25^{+}$ $IFN\text{-}\gamma^{+}$ NK cells after cytokine activation. Histogram bars indicate the median. Two-way ANOVA test with Bonferroni's multiple comparisons test was performed; n = 5 experiments.

(D) FACS-sorted $CD56^{bright}$ and $CD56^{dim}$ NK cells were pre-activated as indicated, labeled with CTV, and cultured in low dose IL-2 (100 UI/mL). *In vitro* NK cell proliferation was analyzed at day 3 for $CD56^{bright}$ and day 6 for $CD56^{dim}$ NK cells. Expansion Index (Exp. Index) and Replication Index (Rep. Index) determine the fold-expansion of the overall culture and of the responding cells only, respectively. Data shown are representative of three individual experiments.

(E) Supernatants from FACS-sorted $CD56^{bright}$ (empty histogram bars) and $CD56^{dim}$ (filled histogram bars) NK cells were collected to quantify cytokine and chemokine release by Luminex assay. Of note, IL-2, IL-3, IL-4, IL-5, IL-10, IL-13, IL-17A, IL-22, and G-CSF were not detected (not shown). Results are expressed

as mean + SEM (n = 3 individual donors). One-way repeated measures ANOVA with Tukey's multiple comparisons test was performed.

(F) Healthy donors' blood NK cells were activated with combinations of IL-12 and IL-33 or IL-12 and IL-18 (10 ng/mL of each cytokine) for 24 h prior to flow cytometry analysis of intracellular IFN-γ expression in NK cell subsets based on CD56 and CD57 surface expression. Results are expressed as mean +/- SEM (n = 7 individual experiments). Two-way ANOVA with Bonferroni's multiple comparisons test was performed.

(G) Healthy donors' blood NK cells were activated with IL-12 (10 ng/mL) for 24 h prior to flow cytometry analysis of ST2 expression on NK cell subsets based on CD56 and CD57 surface expression. Results are expressed as mean + SEM (n = 12 experiments). One-way repeated measures ANOVA with Tukey's multiple comparisons test was performed.

(H) Graphical summary of biological functions differentially regulated in $CD56^{bright}$ and $CD56^{dim}$ NK cells in response to IL-1 family cytokines (IL-33, IL-18, IL-1α and IL-1β) when combined with IL-12.

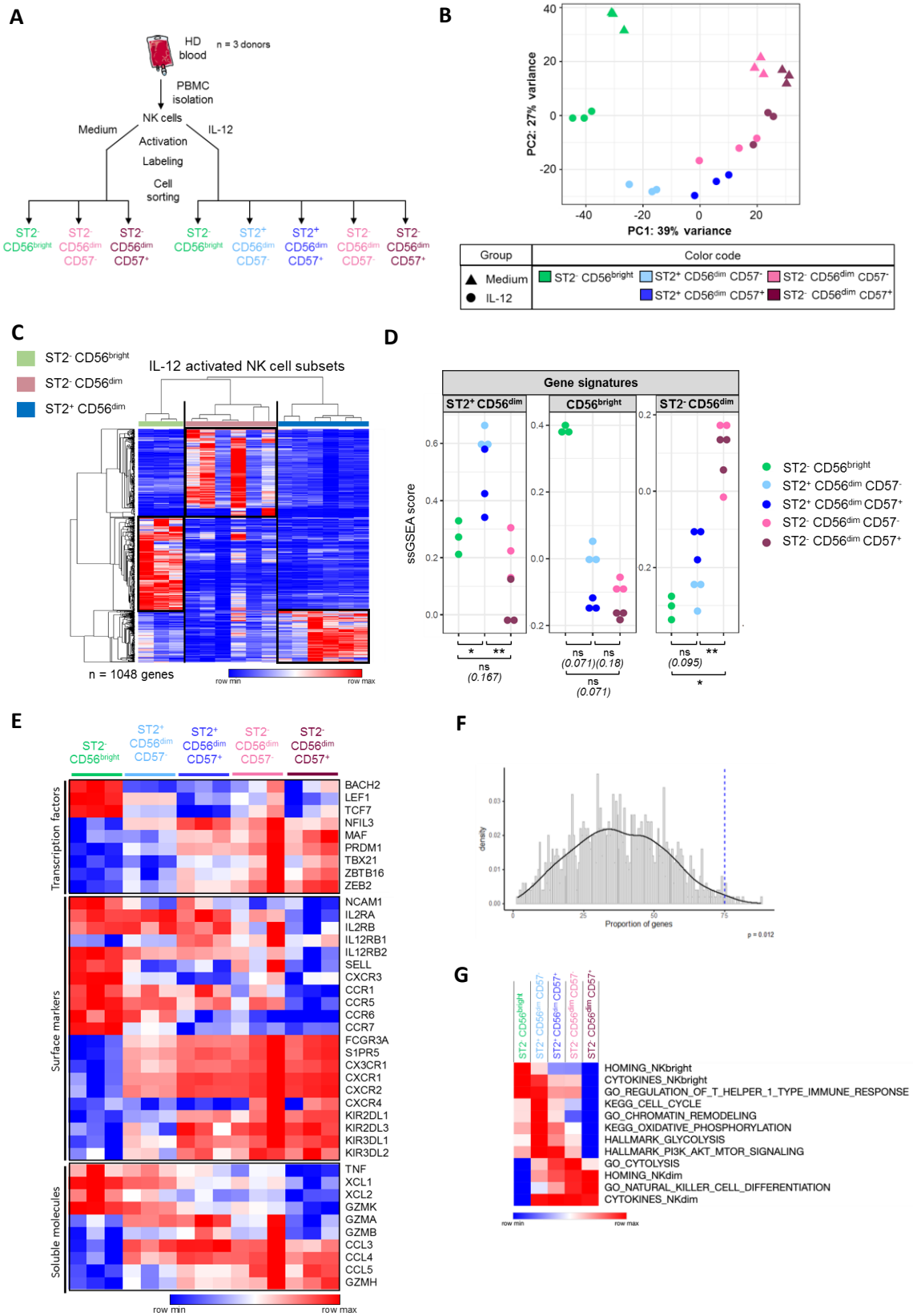

Fig. 3. ST2^{+} CD56^{dim} NK cells display a unique gene signature compared to CD56^{bright} and CD56^{dim} NK cells

(A) Schematic representation of FACS sorting strategy to isolate eight different subsets sorted from healthy donors' blood NK cells based on CD56, CD57 and ST2 surface expression. Three and five subsets were obtained after activation for 24 h with medium or IL-12 respectively.

(B) Principal component analysis for eight FACS-sorted NK cell subsets based on expression of the top 500 most variant genes obtained from 3 individual healthy donors.

(C) Heatmap representing upregulated genes in each sorted NK cell subset compared to the two other NK cell subsets following IL-12 activation for 24 h (n = 3 individual healthy donors). Black squares identify specific transcriptional signatures for $ST2^-$ $CD56^{bright}$, $ST2^-$ $CD56^{dim}$ NK cells, and $ST2^+$ $CD56^{dim}$ NK cells.

(D) ssGSEA analysis of the NK signatures defined by genes specifically upregulated in each sorted NK cell subset (see Table 1) following IL-12 activation for 24 h (n = 3 individual healthy donors). Kruskal-Wallis test with Dunn multiple comparisons test was performed.

(E) Heatmap showing normalized expression for selected genes related to NK cell phenotype and functions.

(F) Sampling distribution of genes with an intermediate expression in $ST2^+$ NK cells ($CD56^{bright}$ > $ST2^+$ > $CD56^{dim}$ or $CD56^{bright}$ < $ST2^+$ < $CD56^{dim}$) with n = 1000 random shuffling of all sample labels. p value was computed with a permutation test.

(G) ssGSEA analysis of selected biological pathways in each sorted NK cell subset following IL-12 activation for 24 h (n = 3 individual healthy donors).

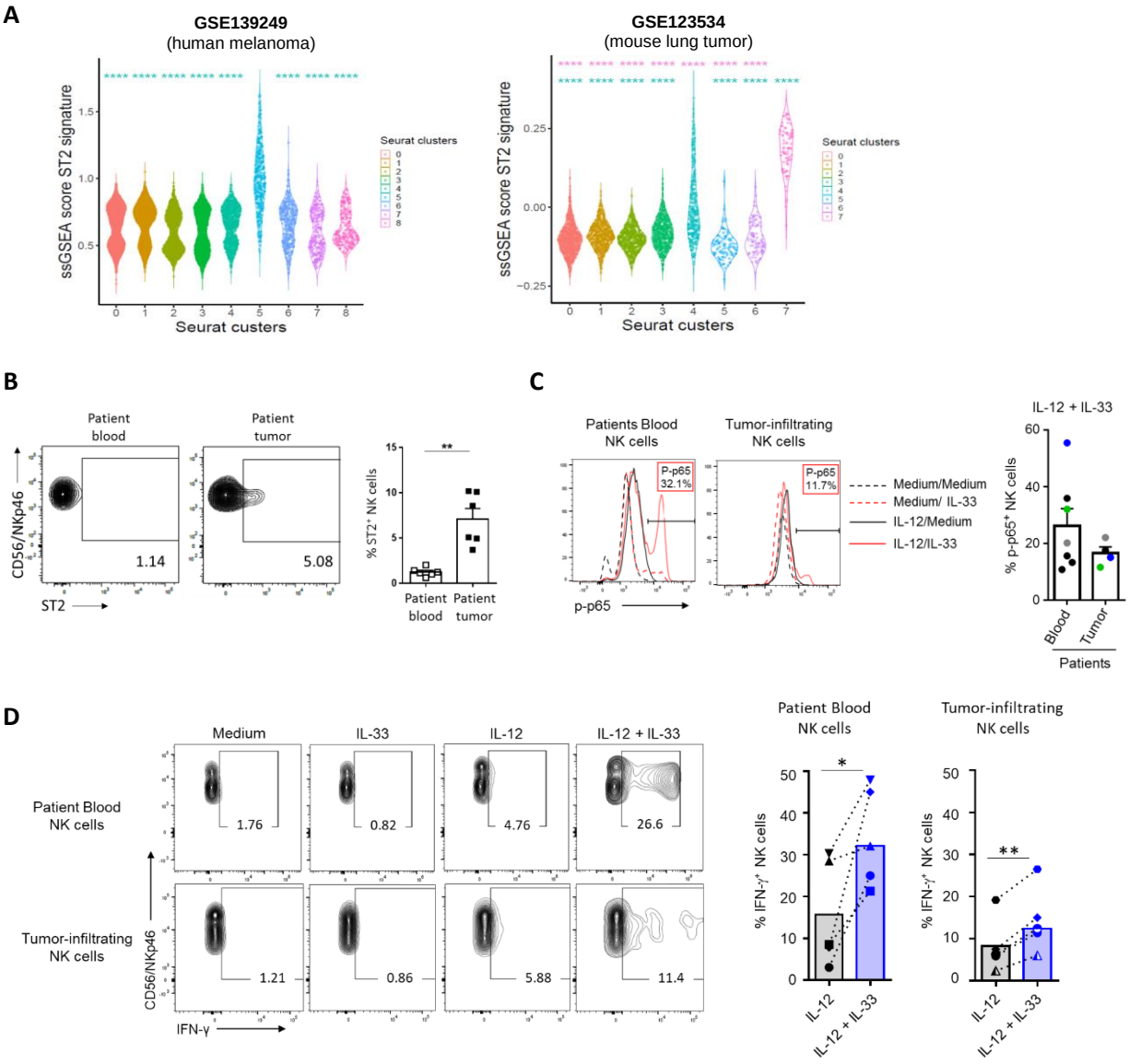

Fig. 4. Peripheral and tumor-infiltrating NK cells from breast cancer patients respond to the IL-33 and IL-12 combination

(A) Violin plots representing the distribution of ssGSEA score for ST2^{+} NK cells signature (233 genes, see Table 1) for tumor NK cell clusters identified from sc-RNAseq analysis of tumor-infiltrating NK cells isolated from (left panel) melanoma patients (GSE139249) *(42)* and (right panel) a mouse model of lung cancer (GSE123534) *(43)*. Kruskal-Wallis test with Dunn multiple comparisons test was performed using cluster 5 for the melanoma dataset and cluster 4 (turquoise) or cluster 7 (pink) (fig.S5) as references.

(B) Flow cytometry analysis of ST2 protein expression on the surface of CD56/NKp46$^+$ NK cells among PBMCs and tumor cell suspensions from breast cancer patients (n = 6). Representative dot plots (left) and quantification (%) (right) of ST2$^+$ NK cells. Results are expressed as mean + SEM. Paired two-tailed Student *t*-test was performed.

(C) PBMCs (n = 7) and tumor cell suspensions (n = 4) from breast cancer patients were activated with medium or IL-12 for 24 h prior to the addition of medium or IL-33. p65 phosphorylation was analyzed 5 min after the addition of IL-33 by flow cytometry in CD56$^+$ CD7$^+$ NK cells. Representative histogram plots (left) and quantification (%) (right) of p-p65$^+$ NK cells after IL-12 and IL-33 combination. Results are expressed as mean + SEM. Unpaired two-tailed Student *t*-test was performed with no statistically significant difference.

(D) PBMCs and tumor cell suspensions from breast cancer patients (n = 5) were activated as indicated (10 ng/mL of each cytokine) for 24 h prior to flow cytometry analysis of intracellular IFN-γ. Representative dot plots (left) and quantification (%) (right) of IFN-γ^+ NK cells. Symbols represent individual breast cancer patients and histogram bars the median. Wilcoxon matched-pairs signed rank test was performed.

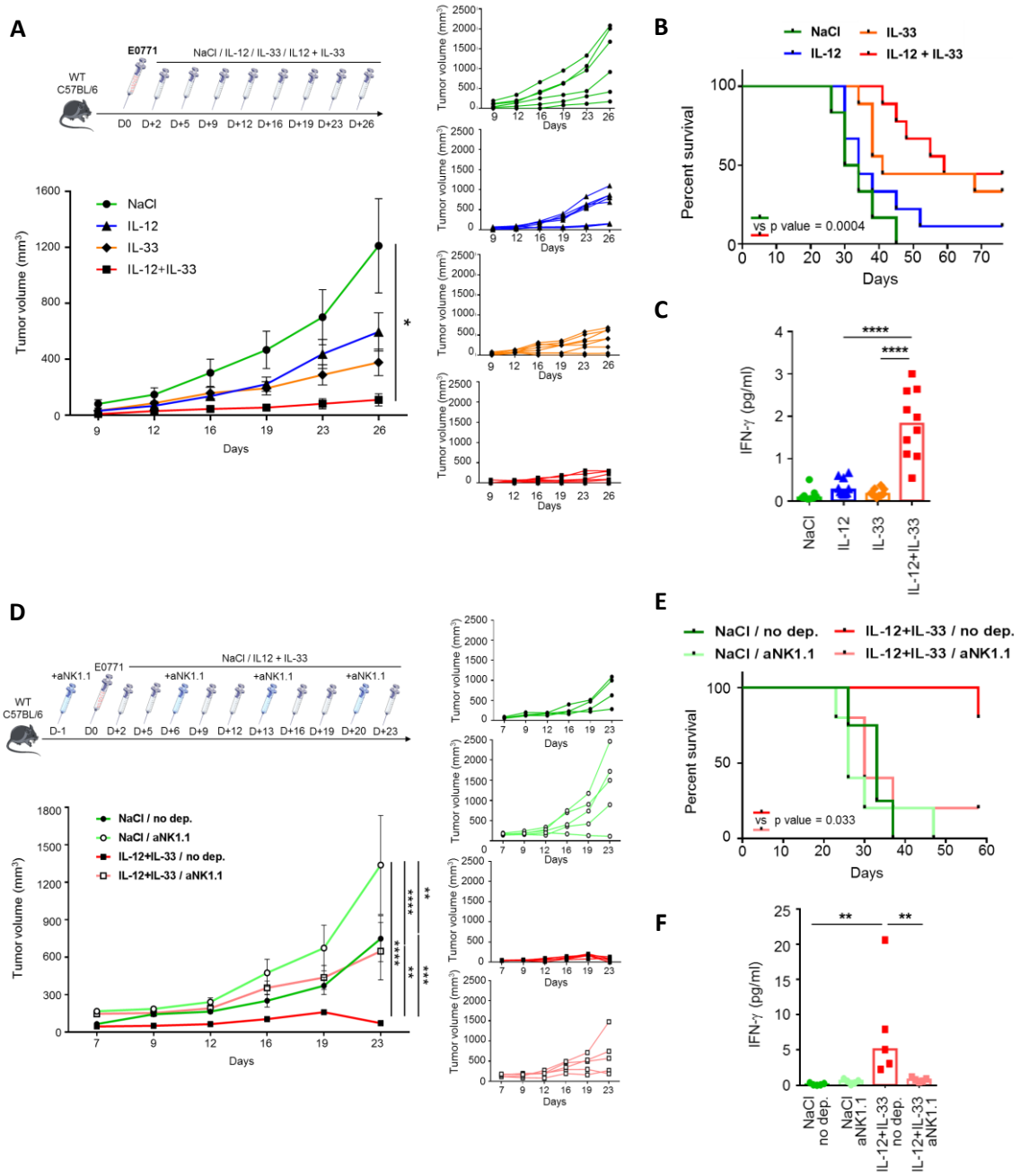

Fig. 5. The combination of IL-33 and IL-12 promotes antitumor functions in an NK-cell-dependent manner

(A) WT mice were injected intra-mammary with 2.5x10^5 E0771 cells on day 0 and then treated in the tumor area with NaCl solution (n = 6), 10 ng/mouse rmIL-12 (n = 9) or 100 ng/mouse rmIL-33 (n = 9) or in combination (n = 10) twice a week from day 2 to day 26. Primary tumor growth was monitored in mice treated with, rmIL-12, rmIL-33 or with the two cytokines. Two-way ANOVA with Tukey's multiple comparisons test was performed.

(B) Kaplan-Meier survival plots of WT mice treated with NaCl, rmIL-12, rmIL-33 or the two cytokines. Mice were sacrificed when longest side of primary tumor reached 17 mm. Log-rank test was performed and the p-value is indicated for NaCl vs rmIL-12 + rmIL-33 comparison.

(C) Serum was retrieved from blood collected at day 5, 4 h after NaCl or cytokine injection into the peritumoral area. IFN-γ concentration was measured by Elisa in the serum of mice treated with NaCl, rmIL-12, rmIL-33 or the two cytokines. Histogram bars represent the median. Kruskal Wallis test with Dunn's multiple comparisons test was performed.

(D) WT mice were injected intra-peritoneally with NaCl or anti-NK1.1 depleting antibody prior to intra-mammary injection with $2.5x10^5$ E0771 cells on day 0 and then treated in the tumor area with NaCl or a combination of 10 ng/mouse rmIL-12 and 100 ng/mouse rmIL-33 twice a week from day 2 to day 23. Primary tumor growth was monitored in non-depleted WT mice treated with NaCl (n = 4) or with rmIL-12 and rmIL-33 combination (n = 5) or in NK cell-depleted WT mice treated with NaCl (n = 5) or with rmIL-12 and rmIL-33 combination (n = 5). Two-way ANOVA with Tukey's multiple comparisons test was performed.

(E) Kaplan-Meier survival plots of non-depleted WT mice treated with NaCl (n = 4) or with a combination of rmIL-12 and rmIL-33 (n = 5) or in NK cell-depleted WT mice treated with NaCl (n = 5) or with rmIL-12 and rmIL-33 combination (n=5). Mice were sacrificed when longest side of primary tumor reached 17 mm. Log-rank test was performed and the p-value is indicated for non-depleted mice treated with rmIL-12 + rmIL-33 vs NK cell-depleted mice treated with rmIL-12 + rmIL-33.

(F) Serum was retrieved from blood collected at day 5, 4 h after NaCl or cytokine injection into the peritumoral area. IFN-γ concentration was measured by ELISA in the serum of non-depleted WT mice treated with NaCl (n = 4) or with rmIL-12 and rmIL-33 combination (n = 5) or in NK cell-depleted WT mice treated with NaCl (n = 5) or with rmIL-12 and rmIL-33 combination (n = 5). Histogram bars represent the median. Kruskal Wallis test with Dunn's multiple comparisons test was performed.

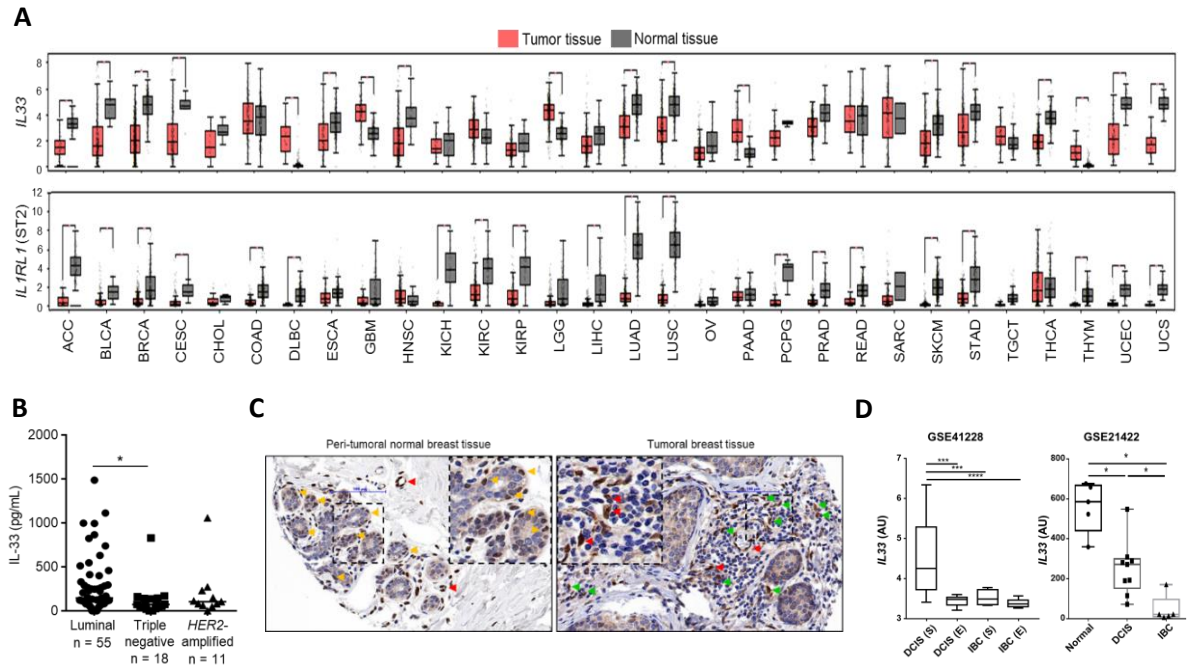

Fig. 6. IL-33 is expressed in tumors and downregulated during cancer progression

(A) *IL33* and *IL1RL1* (ST2) gene expression in tumoral (T) (orange) and normal (N) (grey) tissues extracted from TCGA and GTEX databases (ACC: Adrenocortical carcinoma, T=77, N=128; BLCA : Bladder carcinoma, T=404, N=28; BRCA : Breast invasive carcinoma, T=1095, N=291; CESC: Cervical squamous cell carcinoma and endocervical adenocarcinoma, T=306, N=13 ; CHOL: Cholangiocarcinoma, T=36, N=9; COAD : Colorectal adenocarcinoma, T=275, N=349; DLBC: Lymphoid Neoplasm Diffuse Large B-cell Lymphoma, T=47, N=337 ; ESCA: Esophageal carcinoma, T=182, N=286 ; GBM: Glioblastoma multiforme, T=163, N=207 ; HNSC : Head and neck squamous cell carcinoma, T=519, N=44 ; KICH: Kidney Chromophobe, T=66, N=53 ; KIRC : Kidney renal clear cell carcinoma, T=523, N=100 ; KIRP: Kidney renal papillary cell carcinoma, T=286, N=60 ; LGG : Brain lower grade glioma, T=518, N=207 ; LIHC: Liver hepatocellular carcinoma, T=369, N=160 ; LUAD : Lung adenocarcinoma, T=483, N=347 ; LUSC: Lung squamous cell carcinoma, T=486, N=338 ; OV : Ovarian serous cystadenocarcinoma, T=426, N=88 ; PAAD : Pancreatic adenocarcinoma, T=179, N=171 ; PCPG: Pheochromocytoma and Paraganglioma, T=182, N=3 ; PRAD: Prostate adenocarcinoma, T=492, N=152 ; READ: Rectum adenocarcinoma, T=92, N=318 ; SARC: Sarcoma, T=262, N=2 ; SKCM : Skin cutaneous melanoma, T=461, N=558 ; STAD : Stomach adenocarcinoma, T=408, N=211 ; TGCT: Testicular Germ Cell Tumors, T=137, N=165 ; THCA : Thyroid

cancer, T=512, N=337; THYM: Thymoma, T=118, N=339 ; UCEC: Uterine Corpus Endometrial Carcinoma, T=174, N=91 ; UCS: Uterine Carcinosarcoma , T=57, N=78).

(B) IL-33 protein was quantified by Luminex assay in breast tumor-derived supernatants (n = 89). Kruskal-Wallis test with Dunn multiple comparisons test was performed.

(C) IL-33 expression was analyzed on breast tumor FFPE slides by Immunohistochemistry (IHC). Non-invasive Ductal Carcinoma *In Situ* (DCIS) and invasive Breast Cancer (IBC) lesions were identified based on anatomopathological tissue observations. Red arrows indicate blood vessels, orange arrows indicate peritumoral normal breast acini and green arrows indicate isolated stromal cells positive for IL-33 staining. Images are shown at 20x magnification. Dotted squares represent enlarges areas.

(D) Analysis of *IL33* expression in laser-microdissected stromal versus epithelial zones from DCIS and IBC lesions (GSE41228) *(46)* and in healthy mammary tissue versus DCIS and IBC (GSE21422) *(47)*. Kruskal-Wallis test with Steel-Dwas-Fligner multiple comparisons test was performed.

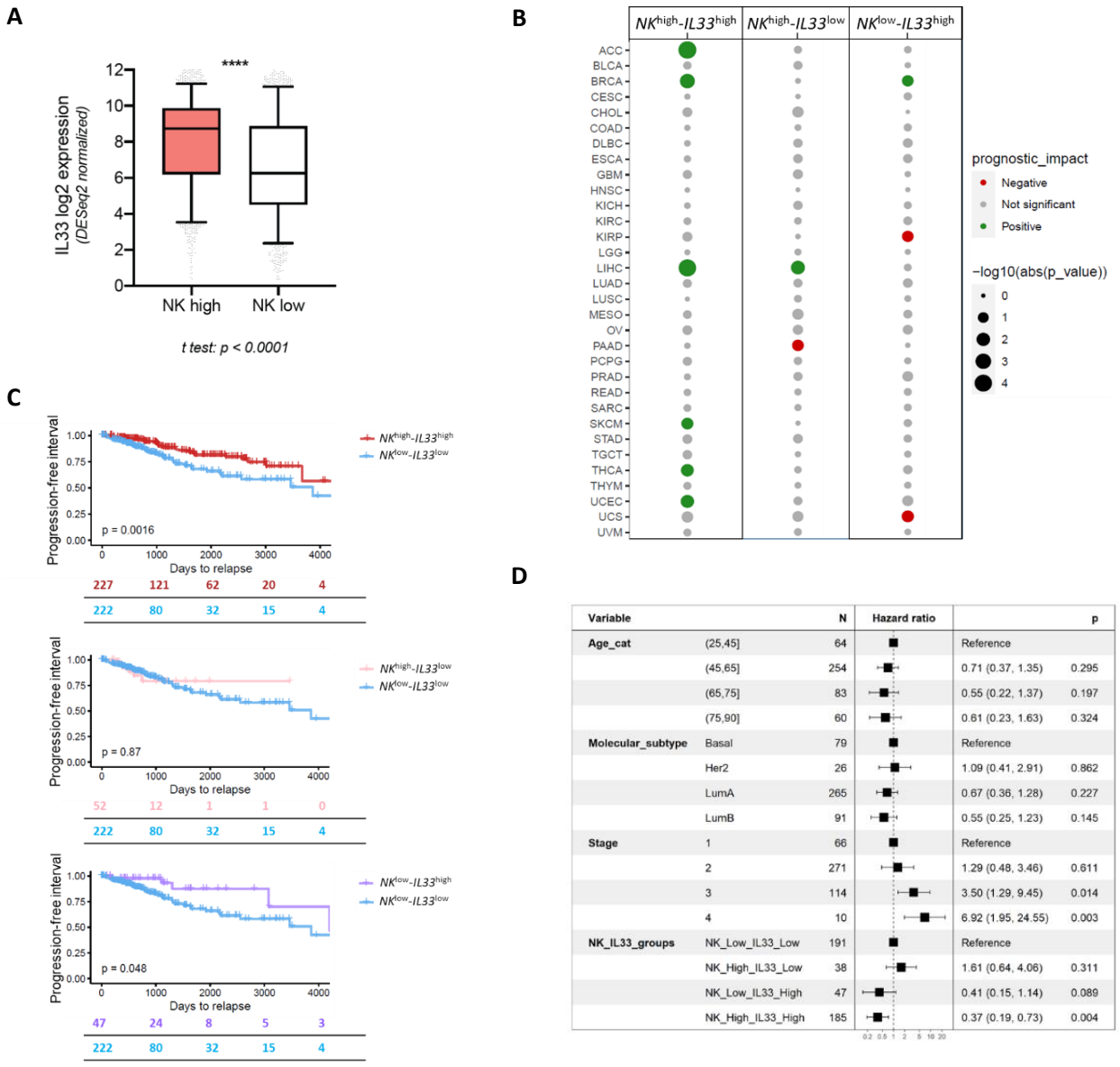

Fig. 7. An *NK*^{hi}/*IL33*^{hi} transcriptomic score is associated with improved progression-free survival

(A) Boxplots display *IL33* gene expression in NK^{hi} vs NK^{low} breast cancer patients from the TCGA database. An unpaired Student *t*-test was performed.

(B) Summary of p-values associated with the log rank test performed to evaluate prognostic value of *NK*^{high}/*IL33*^{high}, *NK*^{high}/*IL33*^{low} and *NK*^{low}/*IL33*^{high} scores as compared to *NK*^{low}/*IL33*^{low} in 32 human cancers from TCGA database (legend is the same as in panel A, MESO: Mesothelioma ; UVM: Uveal Melanoma were added). Results are represented as a bubble map showing positive (green) or negative (red) impact

on progression-free survival. Dots size represents p-values obtained by log-rank test. An unpaired Student *t*-test was performed.

(C) Kaplan-Maier curves for progression-free survival for $NK^{high}/IL33^{high}$, $NK^{high}/IL33^{low}$ and $NK^{low}/IL33^{high}$ scores as compared to $NK^{low}/IL33^{low}$ in breast cancer dataset from TCGA. p-values were obtained with log-rank test.

(D) Multivariate Cox analysis of the impact of $NK^{high}/IL33^{high}$ score on prognosis in breast cancer patients from TCGA dataset regarding the age, molecular subtype, and stage of the tumors. p-values were obtained with log-rank test.

Table 1. List of ST2^{+} NK cell signature genes used in this study, Related to Fig. 3C,D,F,G, 4A

gene	baseMean	log2FoldChange	lfcSE	stat	pvalue	padj
IL23R	840,503787	2,42322895	0,24889705	9,81765284	9,45E-23	8,62E-19
TRPV1	585,713744	1,5368841	0,1666148	9,18767638	4,01E-20	1,46E-16
IL1RL1	1126,7443	2,61252558	0,29381202	9,01318107	2E-19	5,21E-16
NDFIP2	620,975976	1,96393908	0,2429768	8,14409229	3,82E-16	4,35E-13
VEGFA	800,797748	2,08492082	0,27235779	7,70971428	1,26E-14	9,58E-12
DESI1	1249,1091	1,1262011	0,14710845	7,65517735	1,93E-14	1,34E-11
FRMD4B	1643,87039	1,81739229	0,24219981	7,53071051	5,05E-14	2,79E-11
DMRTA2	122,468676	3,05535882	0,41505092	7,31571058	2,56E-13	1,11E-10
FAM89A	545,929495	1,18540785	0,16358858	7,24271616	4,4E-13	1,82E-10
CDC7	1128,13727	1,06925225	0,15213337	7,02091227	2,2E-12	6,82E-10
STRIP2	140,760635	1,29741714	0,1881047	6,89072171	5,55E-12	1,33E-09
NCS1	468,813606	2,07555351	0,31228121	6,84559957	7,62E-12	1,76E-09
SLC16A1	1512,26695	1,9475331	0,28782674	6,72865566	1,71E-11	3,55E-09
CLU	915,149362	1,8992889	0,28769004	6,59283755	4,31E-11	7,36E-09
CHAC2	356,999118	1,25300861	0,19181008	6,53944106	6,17E-11	1,01E-08
ZNF367	984,442668	1,89172016	0,28799764	6,51164619	7,43E-11	1,18E-08
PSAT1	3785,47966	1,67376617	0,26455322	6,44648195	1,14E-10	1,71E-08
GLB1L2	151,981654	1,46163105	0,22563266	6,44192863	1,18E-10	1,75E-08
WDR76	1241,79085	1,43758613	0,2229631	6,43924506	1,2E-10	1,77E-08
CYCS	7640,67913	1,02715495	0,16080527	6,38946825	1,66E-10	2,32E-08
ITGA3	253,34202	1,30398949	0,20420147	6,38357806	1,73E-10	2,39E-08
MT1X	692,256455	1,30721854	0,20490144	6,36783592	1,92E-10	2,55E-08
C4orf46	658,702544	1,03853939	0,16290331	6,3707641	1,88E-10	2,55E-08
CDKN2A	155,551181	1,68677994	0,26579413	6,34882571	2,17E-10	2,85E-08
WEE1	2447,37932	1,44249365	0,22840625	6,28343908	3,31E-10	4,14E-08

FANCB	202,276777	1,19938518	0,19410873	6,18297309	6,29E-10	7,21E-08
ODC1	3337,57699	1,214216	0,19669728	6,16936299	6,86E-10	7,72E-08
PMAIP1	3335,93606	1,18029835	0,19394516	6,13557786	8,49E-10	9,34E-08
MCM3	10000,7616	1,06949838	0,17412227	6,13221471	8,67E-10	9,35E-08
LIMK2	3104,25713	1,15832666	0,18776431	6,12878921	8,86E-10	9,5E-08
MCM5	9509,01304	1,19770655	0,19494071	6,12424439	9,11E-10	9,66E-08
FANCC	557,126559	1,17140782	0,19204919	6,10582487	1,02E-09	1,07E-07
CTNNAL1	508,701126	1,79673214	0,29391591	6,09584392	1,09E-09	1,11E-07
GINS4	525,980957	1,73755156	0,28580647	6,05885887	1,37E-09	1,34E-07
ANKRD9	504,828651	1,19109652	0,19590466	6,05394548	1,41E-09	1,37E-07
GZMA	74121,1277	1,08182451	0,17931976	6,04154076	1,53E-09	1,46E-07
NMB	106,524871	1,14403357	0,19049991	5,99940616	1,98E-09	1,81E-07
TMEM106C	2456,27398	1,26007271	0,21005254	5,98257723	2,2E-09	1,99E-07
MT1E	44,050544	1,95169574	0,32328037	5,95810717	2,55E-09	0,00000022
CENPS-CORT	55,7971453	2,46977763	0,41342915	5,95115155	2,66E-09	2,27E-07
PRXL2A	237,702271	1,05442176	0,17889782	5,94511089	2,76E-09	2,34E-07
MCM7	14752,7609	1,37191183	0,2297699	5,94314722	2,8E-09	2,36E-07
CSTF2	2575,74527	1,09307847	0,18452897	5,9067807	3,49E-09	2,78E-07
PACSIN3	25,0768206	2,26253594	0,38409283	5,83189903	5,48E-09	0,0000004
FAM222A	180,250612	1,40349469	0,23981944	5,80219939	6,55E-09	4,57E-07
AL121985.1	40,7926711	1,16589314	0,20293076	5,75067325	8,89E-09	5,85E-07
MARCHF3	783,211555	1,17359882	0,20479762	5,73444119	9,78E-09	6,32E-07
TIMELESS	4418,15331	1,08590411	0,18925965	5,72959812	1,01E-08	6,49E-07
AL354718.3	26,2533188	1,7417743	0,29946638	5,72789903	1,02E-08	6,53E-07
ACTN1	1511,11114	1,74503563	0,30449433	5,72027976	1,06E-08	6,79E-07
CCDC74A	251,973341	1,31883746	0,2376231	5,71927486	1,07E-08	0,00000068
GINS3	467,902103	1,33967219	0,23328208	5,71328543	1,11E-08	6,94E-07
H4C2	16,5518026	1,95322135	0,34238088	5,70051711	1,19E-08	7,43E-07

AL133215.2	30,1675575	1,42266749	0,25229359	5,63269336	1,77E-08	0,00000101
WDHD1	1158,87928	1,46188406	0,26192838	5,5726197	2,51E-08	0,00000137
PPIF	4031,87853	1,15942507	0,20940214	5,55032627	2,85E-08	0,00000153
TUBB	35257,5275	1,17169715	0,21471365	5,44816951	5,09E-08	0,00000244
PTGER3	1122,67732	1,94573883	0,35633685	5,42295615	5,86E-08	0,00000274
NUDT1	1001,90806	1,00733025	0,18719371	5,38299465	7,33E-08	0,00000331
CCDC167	992,092596	1,07088026	0,20061089	5,34769926	8,91E-08	0,00000382
PGD	6735,92045	1,48019965	0,27474308	5,3438772	9,1E-08	0,00000388
AL645939.6	104,812089	1,27138805	0,23475732	5,33692254	9,45E-08	0,00000396
RPP25	367,831914	1,47390104	0,27692459	5,32409178	1,01E-07	0,00000418
HDAC9	472,156038	1,47723458	0,28428291	5,3202141	1,04E-07	0,00000427
RPS6KL1	45,2426705	1,51043197	0,28647669	5,30331887	1,14E-07	0,00000452
C17orf58	532,027454	1,01441751	0,19141547	5,30104302	1,15E-07	0,00000454
SLC43A3	1071,36813	1,13990933	0,21499718	5,27929886	0,00000013	0,00000504
SNORD3A	146,092244	1,13049166	0,21362145	5,27808359	1,31E-07	0,00000506
MTFP1	1468,3341	1,157943	0,21913998	5,27760423	1,31E-07	0,00000506
ZNRF1	3820,68738	1,16731492	0,2234197	5,2740492	1,33E-07	0,00000511
PPFIA3	324,368873	1,55820112	0,29729033	5,27239408	1,35E-07	0,00000515
UCK2	2079,14805	1,13481736	0,21676644	5,22789662	1,71E-07	0,00000624
AC011447.3	57,3186488	1,11553004	0,21343931	5,22242262	1,77E-07	0,00000638
HASPIN	554,208648	1,68583729	0,32282234	5,21282615	1,86E-07	0,00000661
ULBP1	149,625849	1,51410848	0,29748326	5,21097287	1,88E-07	0,00000665
SLC6A9	187,199925	1,70333199	0,33635265	5,18997273	0,00000021	0,00000735
RPA3	1636,73819	1,00311422	0,19366157	5,1705612	2,33E-07	0,00000798
ARHGAP11B	278,264429	1,20368016	0,23432331	5,16331317	2,43E-07	0,00000825
CHAC1	481,352013	1,23939592	0,24088971	5,14265704	2,71E-07	0,00000902
CDK4	3873,60144	1,11749802	0,21784441	5,12557997	2,97E-07	0,00000971
LRR1	920,996475	1,0036983	0,19575589	5,12386851	2,99E-07	0,00000974

AP1S1	105,27595	1,0450958	0,20455019	5,11990457	3,06E-07	0,00000991
SHMT2	9828,60995	1,1975069	0,23618809	5,10614466	3,29E-07	0,0000106
DNAJC9	3188,18598	1,22199097	0,2387053	5,09616228	3,47E-07	0,000011
PSMC3IP	350,481732	1,4581779	0,28547784	5,0661719	4,06E-07	0,0000126
GLP1R	296,527103	1,49740713	0,30734149	5,03306041	4,83E-07	0,0000144
ICAM1	6843,1637	1,04169586	0,20732701	5,03330967	4,82E-07	0,0000144
TCF19	2640,77586	1,43029337	0,2832562	5,02682044	4,99E-07	0,0000147
CHPF	3180,3357	1,13623626	0,22647359	5,02329478	5,08E-07	0,000015
UACA	101,587297	1,28522978	0,25825954	4,97927636	6,38E-07	0,0000182
HPSE	246,082026	1,25104351	0,24899855	4,96053958	7,03E-07	0,0000195
ZNF90	85,3883948	1,07121192	0,21718338	4,94198616	7,73E-07	0,0000211
CHD5	40,98575	2,40552677	0,45150459	4,93564678	7,99E-07	0,0000216
STEAP1	38,756016	1,82746385	0,36064085	4,92882198	8,27E-07	0,000022
TMEM97	753,470908	1,44688755	0,29464752	4,9218635	8,57E-07	0,0000226
PCNA	5824,63591	1,46770467	0,29734296	4,91964178	8,67E-07	0,0000228
DHCR7	2278,22228	1,01502954	0,20677943	4,91212558	9,01E-07	0,0000235
ATAD2	3755,90616	1,2943769	0,26245318	4,90082092	9,54E-07	0,0000246
CKS2	1407,44132	1,31951811	0,26895317	4,89882553	9,64E-07	0,0000248
DSN1	1613,8097	1,02750526	0,21012032	4,88135299	0,00000105	0,0000265
POLD3	1710,94088	1,00011605	0,20433338	4,88106533	0,00000106	0,0000265
PHLDA3	77,6403238	1,36984895	0,27522185	4,87388501	0,00000109	0,0000272
AC079209.1	41,3225837	1,8582839	0,39181777	4,86322585	0,00000115	0,0000283
CENPP	386,136493	1,29006839	0,26693782	4,84742954	0,00000125	0,0000303
PKM	24972,8962	1,13454211	0,23415197	4,83603007	0,00000132	0,0000319
TESC	1490,65093	1,18929034	0,2514482	4,83364582	0,00000134	0,0000322
MCM6	4653,0983	1,57235012	0,32417432	4,82704181	0,00000139	0,000033
MSH6	3869,11953	1,05660942	0,21928593	4,80328372	0,00000156	0,0000361
RFC4	1553,09963	1,031953	0,21441157	4,78866885	0,00000168	0,0000385

CHAF1A	2149,62629	1,28745474	0,27220876	4,72032172	0,00000235	0,0000514
H2AC13	51,7125691	1,05210436	0,22268468	4,70945125	0,00000248	0,0000537
SPTY2D1OS	42,2396604	1,29347563	0,27513413	4,70686789	0,00000252	0,0000543
GPT2	960,333544	1,47635661	0,30788401	4,69049231	0,00000273	0,0000578
MCM4	6340,26235	1,63367485	0,34634032	4,68454086	0,00000281	0,0000591
NDC80	776,695235	1,29472715	0,27563296	4,67623182	0,00000292	0,000061
GMNN	934,054353	1,43630881	0,30640338	4,67506347	0,00000294	0,0000613
E2F2	802,219169	1,65972969	0,3514081	4,66431846	0,0000031	0,0000641
P2RX5-TAX1BP3	1342,34518	1,52101022	0,3204367	4,66403728	0,0000031	0,0000642
PDLIM1	1187,47176	1,03361573	0,2224437	4,6617062	0,00000314	0,0000647
TMEM154	574,226839	1,00573313	0,2150905	4,64587086	0,00000339	0,0000683
CHEK1	825,482205	1,73191025	0,36953111	4,64538288	0,00000339	0,0000683
TREML2	235,222525	1,45436846	0,32219791	4,64228458	0,00000345	0,000069
EME1	314,144262	1,57289255	0,33841067	4,62692244	0,00000371	0,0000731
MCM2	8689,40083	1,61040092	0,34557034	4,62485422	0,00000375	0,0000737
GINS2	1161,25528	1,8507702	0,39762798	4,61960492	0,00000384	0,0000753
ORC6	684,604254	1,57585647	0,33937762	4,61923814	0,00000385	0,0000753
EPOP	77,9565208	1,32065759	0,28593559	4,61440444	0,00000394	0,0000769
POLD2	3182,659	1,11906962	0,24281803	4,60941177	0,00000404	0,0000783
TMPO-AS1	283,780703	1,71981254	0,36963206	4,59856749	0,00000425	0,0000818
IFNG	6396,66052	1,45636818	0,31848246	4,58996006	0,00000443	0,0000847
RASD1	606,327077	1,55681397	0,33333489	4,58647174	0,00000451	0,0000858
DHCR24	7856,12245	1,11331258	0,24256226	4,58412271	0,00000456	0,0000863
TFDP1	4133,97738	1,30153913	0,28366491	4,57958167	0,00000466	0,0000877
AP1S3	369,438627	1,3518563	0,29480193	4,56559322	0,00000498	0,0000928
BRCA1	930,477735	1,39840757	0,30518946	4,56130619	0,00000508	0,0000945
SLC7A1	2343,405	1,10529514	0,24349859	4,55492539	0,00000524	0,0000965
DHFR	2151,02731	1,55704343	0,33954021	4,5402195	0,00000562	0,00010235

ATAD5	805,154511	1,10530992	0,2427956	4,53887588	0,00000566	0,00010269
RANP1	16,5239844	1,32440045	0,28989191	4,51475446	0,00000634	0,00011231
BZW1P2	22,4181532	1,12484237	0,47018698	4,51482661	0,00000634	0,00011231
S100P	87,3413641	1,82640658	0,3899944	4,51308538	0,00000639	0,00011298
STAP2	242,784642	1,09058482	0,24286098	4,51313801	0,00000639	0,00011298
FEN1	5528,4219	1,38578289	0,30732008	4,49108564	0,00000709	0,00012315
E2F1	2025,17146	1,7319208	0,38283899	4,47953839	0,00000748	0,00012825
AMOTL1	496,757411	1,02596064	0,22667277	4,47446543	0,00000766	0,00013064
TUBAP2	38,2765439	1,53130728	0,34105492	4,47299192	0,00000771	0,00013098
DTYMK	2010,46089	1,02403528	0,22848002	4,47138208	0,00000777	0,00013168
NET1	461,954204	1,2765251	0,28560765	4,46968512	0,00000783	0,00013211
CENPN	782,642068	1,53981103	0,34494963	4,46054026	0,00000818	0,00013737
AC092718.4	63,7504111	1,4920021	0,33635788	4,45531478	0,00000838	0,0001405
LIPG	5,89092867	1,93128208	0,49660756	4,42884074	0,00000947	0,00015449
AC002116.2	25,5918918	1,19588495	0,27276091	4,41044863	0,0000103	0,00016411
UNG	2362,03983	1,32634165	0,29975081	4,40692892	0,0000105	0,00016607
RAD54B	266,75802	1,16939837	0,26554358	4,39421167	0,0000111	0,00017323
ORC1	691,813587	1,6666604	0,37795945	4,3824423	0,0000117	0,0001824
WDR62	766,596341	1,45094258	0,33134967	4,37240158	0,0000123	0,00018922
CLSPN	1091,54245	1,67501566	0,38017063	4,36742483	0,0000126	0,00019244
SCD	1345,74203	1,35532059	0,31142925	4,35959145	0,000013	0,00019813
WWC1	9,77638638	1,85241231	0,49501321	4,3548267	0,0000133	0,00020148
SOCS1	5198,56908	1,17308325	0,27012128	4,34892689	0,0000137	0,00020477
RNF157	4457,47736	1,28354426	0,30207097	4,33638366	0,0000145	0,00021452
TUBBP1	8,52784924	1,50653657	0,34610586	4,33590032	0,0000145	0,00021481
FANCI	4280,14541	1,21764881	0,28034532	4,33554899	0,0000145	0,00021498
AC125611.3	368,112707	1,08632677	0,25174306	4,32071096	0,0000156	0,00022702
CHAF1B	957,421705	1,31490521	0,30328712	4,31485291	0,000016	0,00023054

BAG2	521,183057	1,05120342	0,24327784	4,30709311	0,0000165	0,00023727
CENPH	576,293978	1,26026279	0,2925594	4,30587288	0,0000166	0,0002382
DUT	4484,90877	1,2199032	0,28278906	4,29737298	0,0000173	0,00024617
EIF4EBP1	1072,5969	1,20523444	0,27988365	4,29345192	0,0000176	0,00024939
FOXRED2	439,287578	1,4681439	0,34151791	4,2862685	0,0000182	0,00025619
ASRGL1	198,029471	1,164368	0,2682786	4,28482002	0,0000183	0,00025747
PIR	89,949917	1,65357487	0,38886029	4,27296141	0,0000193	0,00026824
AL353135.2	14,2246629	1,62814621	0,3797066	4,26149956	0,0000203	0,00027982
ADM2	283,026873	1,01121121	0,23931693	4,24890986	0,0000215	0,0002927
PSPH	366,751383	1,07179051	0,25048272	4,23729156	0,0000226	0,00030506
GGH	647,481775	1,55943325	0,36825399	4,23288001	0,0000231	0,00031019
LRP8	2217,7952	1,10561244	0,26234263	4,22833651	0,0000235	0,00031513
TLCD3A	160,982726	1,43553228	0,33736838	4,22412508	0,000024	0,00031955
SMTN	270,762571	1,126887	0,26663656	4,22404222	0,000024	0,00031955
TUBA1B	60578,4037	1,20501359	0,2849711	4,22013433	0,0000244	0,00032373
KNTC1	1787,11296	1,11477093	0,26350939	4,22033697	0,0000244	0,00032373
KIF18A	417,335287	1,31788213	0,31169429	4,21896245	0,0000245	0,0003247
AC004816.1	14,306372	1,65661376	0,39618463	4,202751	0,0000264	0,0003456
MASTL	864,89905	1,02468418	0,24379548	4,18746011	0,0000282	0,00036448
DTL	2028,0242	1,63425478	0,39575132	4,13128745	0,0000361	0,00044953
POLE2	409,461561	1,53115468	0,369125	4,1304297	0,0000362	0,00044998
TUBG1	2203,28342	1,02452182	0,24807305	4,1290456	0,0000364	0,00045177
FAM72A	220,279994	1,15187674	0,28159687	4,12615562	0,0000369	0,00045593
TEDC2	431,086628	1,64867763	0,39625457	4,12497492	0,0000371	0,00045766
P2RX5	22126,469	1,50476936	0,3635052	4,12437677	0,0000372	0,00045823
ARHGAP11A	1730,04945	1,25299442	0,30371393	4,12055956	0,0000378	0,00046369
CDC25A	699,947246	1,81511065	0,44397787	4,10696078	0,0000401	0,00048693
EXO1	713,754785	1,68789674	0,40358897	4,10386851	0,0000406	0,00049185

TUBA1C	3622,14416	1,09707551	0,26829002	4,09586354	0,0000421	0,0005068
B4GALNT1	10,60565	2,15643736	0,49332317	4,08855336	0,0000434	0,00052029
CCDC74B	104,686214	1,11756828	0,31918457	4,08830793	0,0000435	0,00052045
EZH2	1948,0683	1,01462741	0,24857909	4,0719677	0,0000466	0,00054938
AC007952.4	77,532975	1,16366725	0,29066496	4,06902588	0,0000472	0,00055426
DCTPP1	2597,99471	1,11717813	0,27411709	4,0667583	0,0000477	0,00055819
WARS1	28550,4623	1,08044355	0,26992507	4,0640571	0,0000482	0,00056313
BRI3BP	1335,34543	1,04957051	0,25882536	4,04814242	0,0000516	0,00059269
CDC6	1410,79264	1,63800346	0,40051232	4,04157944	0,0000531	0,00060609
HMGA1	1798,81596	1,24562942	0,30887844	4,02957083	0,0000559	0,00062962
RFC3	814,51005	1,30070738	0,32074068	4,02572616	0,0000568	0,00063763
CKS1B	1636,82627	1,22029692	0,30256448	4,02273939	0,0000575	0,00064432
HELLS	911,07159	1,542782	0,38126874	4,01564698	0,0000593	0,00066022
TCAM1P	25,8600269	1,02260311	0,47239221	4,01360092	0,0000598	0,00066435
EDA2R	20,8387114	1,82530656	0,43498774	4,00318835	0,0000625	0,00069177
HMGB2	8675,27654	1,00558925	0,251096	4,00110979	0,000063	0,00069702
CDT1	1368,90856	1,61856181	0,40331384	3,97889661	0,0000692	0,00075425
FZD5	41,668731	1,30012035	0,32147065	3,97882493	0,0000693	0,00075425
CENPU	902,785896	1,51007305	0,38358497	3,96187243	0,0000744	0,00080079
RAD51AP1	490,051196	1,42774933	0,35682273	3,9615959	0,0000745	0,00080124
PAQR4	1091,18271	1,35723293	0,34178392	3,95995024	0,000075	0,00080489
HDC	30,8090943	2,33219202	0,48736777	3,9581798	0,0000755	0,0008096
POLR3G	120,074947	1,3316655	0,33481957	3,95740384	0,0000758	0,00081112
XRCC2	370,305949	1,40619326	0,35690285	3,94694686	0,0000792	0,0008401
UBE2T	901,685734	1,49786465	0,37668238	3,94064866	0,0000813	0,00085717
AC011511.5	26,6442249	1,29618176	0,33396073	3,94086894	0,0000812	0,00085717
DONSON	949,085575	1,09582141	0,27649212	3,94055698	0,0000813	0,00085717
CDKN1A	2383,78661	1,5829976	0,40776128	3,94030883	0,0000814	0,00085756

MTFR2	320,179139	1,39504069	0,35070288	3,93936383	0,0000817	0,00085995
ELFN1-AS1	19,3850066	1,67751136	0,42667302	3,92620031	0,0000863	0,00089647
PHGDH	1154,77976	1,46015007	0,36922628	3,92534315	0,0000866	0,00089916
THSD8	364,425606	1,19026425	0,30716875	3,92487223	0,0000868	0,0009004
STIL	666,799496	1,43452061	0,36383328	3,92234751	0,0000877	0,00090731
ATF3	271,145157	1,08657261	0,28875395	3,91571619	0,0000901	0,00092945
ERCC6L	216,289004	1,44576283	0,36810749	3,91545896	0,0000902	0,00092992
TTK	499,963879	1,57513627	0,39649228	3,91459441	0,0000906	0,00093175
SLC35G1	79,1619926	1,16368713	0,29752546	3,91427716	0,0000907	0,00093185
TIPIN	806,5352	1,15405363	0,29753383	3,89998518	0,0000962	0,00097923
RAB3D	1128,09782	1,01239501	0,26084934	3,89714692	0,0000973	0,00098867
HSF5	107,39634	1,25325507	0,32196466	3,89543348	0,000098	0,00099502

1305

1306

1307 **Table 2.** List of ST2^{-} CD56^{bright} NK cell signature genes used in this study, Related to Fig. 3C,D,F,G

1308

gene	baseMean	log2FoldChange	lfcSE	stat	pvalue	padj
MARCKSL1	2140,369762	1,740882999	0,116707873	14,91550027	2,61E-50	4,39E-47
SGSM3	8319,280225	1,301010684	0,099219228	13,1115542	2,83E-39	2,71E-36
TMEM123	8464,060835	1,625281824	0,129219167	12,58132481	2,68E-36	2,16E-33
LRRC75B	456,6176087	2,416210354	0,198847881	12,15071388	5,69E-34	3,70E-31
EVA1B	263,1092393	2,229323471	0,188111393	11,85127264	2,12E-32	1,16E-29
IL4R	3450,852494	1,499947728	0,126745269	11,84412664	2,31E-32	1,22E-29
CYSLTR1	649,5300538	1,515430844	0,129159975	11,73268544	8,67E-32	4,26E-29
MAN1C1	565,7106081	3,237435298	0,286233564	11,29381958	1,41E-29	6,17E-27
ANKRD13C	2134,558285	1,002724262	0,089928491	11,15065986	7,11E-29	2,87E-26
P2RX4	2152,637806	1,272120915	0,115924558	10,97495534	5,04E-28	1,92E-25
CD82	977,0473825	2,847624791	0,264383983	10,78862923	3,90E-27	1,38E-24
PPARD	1041,824462	1,179517604	0,111025009	10,62431354	2,30E-26	7,85E-24
CD44	17644,69997	2,466187162	0,235781727	10,46120997	1,30E-25	4,37E-23
CACNB1	672,7485259	1,620194479	0,155622145	10,41380983	2,14E-25	7,09E-23
AKTIP	1505,369451	1,445792576	0,139440905	10,37395255	3,26E-25	1,06E-22
FUCA1	2045,337861	1,842417316	0,17993438	10,23962265	1,32E-24	3,97E-22
LINC00996	319,627706	2,609455123	0,256710702	10,15786989	3,06E-24	8,56E-22
FXYD5	4272,477726	1,196803035	0,121577711	9,843066925	7,34E-23	1,85E-20
AFAP1L2	218,6357125	3,082245531	0,312139865	9,810966072	1,01E-22	2,51E-20
RAB38	243,3177113	3,055826055	0,313133124	9,801295845	1,11E-22	2,70E-20
AHI1	1559,477129	2,477023515	0,255683885	9,685122861	3,49E-22	7,81E-20
SOX4	196,001897	2,237665613	0,23699926	9,444790764	3,56E-21	7,25E-19
KIAA1211L	88,75908207	2,71897675	0,294775003	9,213852772	3,15E-20	5,97E-18
IGFLR1	3854,076961	1,143615923	0,124148381	9,209966716	3,26E-20	6,09E-18
TLE3	1567,104006	2,590685551	0,282744437	9,166413642	4,89E-20	8,80E-18

RARA	600,9572647	1,318907813	0,145484053	9,062144833	1,28E-19	2,22E-17
STBD1	219,2555171	1,822615346	0,209614914	8,717454048	2,85E-18	4,41E-16
FUT8-AS1	67,90486061	2,855822847	0,328357416	8,695225091	3,46E-18	5,29E-16
MMP25	1398,742723	1,40354112	0,162428028	8,639506398	5,65E-18	8,43E-16
FAM102A	2599,12843	1,914468847	0,222371703	8,607765357	7,45E-18	1,09E-15
AL034397.3	264,4978444	2,197245925	0,256021938	8,601655494	7,86E-18	1,14E-15
TMEM200A	142,3148917	2,89847412	0,337566616	8,571643818	1,02E-17	1,47E-15
KIR2DL4	5176,736346	3,205020743	0,372271606	8,56145511	1,11E-17	1,56E-15
SPTBN1	5050,407322	1,454201938	0,169895179	8,562040027	1,11E-17	1,56E-15
GRAMD4	1739,584588	1,256608365	0,148997408	8,426004572	3,58E-17	4,74E-15
AXIN2	122,846397	4,198344719	0,496186938	8,424218323	3,63E-17	4,79E-15
TRAF5	5084,644085	1,264733035	0,151119937	8,371710643	5,68E-17	7,29E-15
AC136475.3	181,4399858	3,322393183	0,393086018	8,331814546	7,96E-17	1,00E-14
AC008691.1	15,3365338	3,974901787	0,471562234	8,271214677	1,33E-16	1,61E-14
PRAM1	324,8694184	3,248314446	0,39599038	8,151417564	3,60E-16	4,12E-14
FOXC1	42,81840529	4,257531481	0,513555488	8,146888353	3,73E-16	4,25E-14
FUT8	857,1317759	2,256320072	0,277545555	8,121125486	4,62E-16	5,20E-14
AREG	49,15236748	2,404981214	0,298520266	8,0837208	6,28E-16	7,04E-14
ANKRD6	380,9412248	1,408207328	0,176085911	8,082307646	6,36E-16	7,08E-14
HVCN1	1192,528257	2,419885321	0,301033606	8,025608906	1,01E-15	1,09E-13
MPZL3	2867,960136	1,96187017	0,244903273	8,005583963	1,19E-15	1,27E-13
LRFN1	903,3538527	1,46235046	0,183524361	7,969598699	1,59E-15	1,66E-13
BACH2	1055,397026	2,043278573	0,256745168	7,956655052	1,77E-15	1,83E-13
IFITM10	79,33410328	2,819037525	0,358126867	7,908149319	2,61E-15	2,67E-13
LMNA	764,4263779	3,588425802	0,460469059	7,795625921	6,41E-15	6,37E-13
MAML2	405,3947041	1,969330901	0,254612167	7,733434442	1,05E-14	1,01E-12
TIAM1	2217,418454	3,446940657	0,443312808	7,712998259	1,23E-14	1,18E-12
LDLRAD2	37,78263563	2,864315899	0,37090984	7,706069704	1,30E-14	1,23E-12

PRCD	141,6670188	2,886854421	0,384456276	7,657090385	1,90E-14	1,76E-12
KLHL6	2736,886324	1,449384166	0,189438168	7,656948369	1,90E-14	1,76E-12
ZFHX3	162,5904485	2,099702068	0,274363937	7,648660179	2,03E-14	1,87E-12
FLNB	1219,316738	2,293855562	0,300509328	7,632018925	2,31E-14	2,10E-12
C19orf38	314,3637498	2,865738545	0,381649932	7,60950385	2,75E-14	2,46E-12
TEC	310,8560866	2,442201965	0,320801105	7,608939573	2,76E-14	2,46E-12
DOK7	143,5755317	2,752814433	0,364946495	7,596460325	3,04E-14	2,68E-12
LDOC1	547,4136479	1,203333137	0,159103248	7,587139728	3,27E-14	2,85E-12
IER5L	207,4254029	3,928176017	0,512131998	7,561144111	4,00E-14	3,43E-12
STARD10	965,4029696	1,517324896	0,202110986	7,524072375	5,31E-14	4,52E-12
CAPN12	1574,643552	1,986846274	0,264452466	7,514838013	5,70E-14	4,81E-12
RRM2P3	33,88671537	1,906501022	0,255080085	7,514772312	5,70E-14	4,81E-12
PLK2	98,37650677	2,344139862	0,312635658	7,475686672	7,68E-14	6,37E-12
PRPF40B	405,9369242	1,255426299	0,168137217	7,466021351	8,27E-14	6,83E-12
IL7R	1849,842269	3,752113699	0,497696008	7,41606311	1,21E-13	9,85E-12
FAAH	346,5778786	1,680102357	0,22747979	7,382156404	1,56E-13	1,24E-11
TNFSF9	132,6527701	3,637122844	0,475030088	7,330987379	2,28E-13	1,78E-11
MBOAT7	1550,633095	1,332621699	0,182816461	7,288449341	3,14E-13	2,39E-11
DST	209,6756475	1,816584497	0,250223788	7,282464592	3,28E-13	2,48E-11
ZBTB46	128,1886131	3,641740392	0,496162257	7,228772817	4,87E-13	3,61E-11
MAFF	2257,925472	1,879053686	0,260093808	7,224527248	5,03E-13	3,70E-11
ZNF217	1450,119102	1,287753617	0,178824246	7,201997933	5,93E-13	4,32E-11
UNC93B1	3043,964328	1,750329949	0,243608534	7,184379072	6,75E-13	4,90E-11
TPCN1	1699,033407	1,53151534	0,213456563	7,17768457	7,09E-13	5,11E-11
ZNF296	727,0590777	1,305088768	0,182369891	7,156348565	8,29E-13	5,90E-11
PLEKHN1	206,4025607	2,085181376	0,292403136	7,122297134	1,06E-12	7,46E-11
SMG6	1585,486005	1,057027036	0,148854315	7,10138665	1,24E-12	8,59E-11
XYLT1	1465,872637	1,156545617	0,163384884	7,077618012	1,47E-12	1,01E-10

SLC39A10	1623,403389	1,212661365	0,173634103	6,988704433	2,77E-12	1,87E-10
HID1	39,66821395	2,205264018	0,320151044	6,966474531	3,25E-12	2,16E-10
RRAD	58,48146211	2,953436907	0,428687381	6,90543153	5,01E-12	3,28E-10
MPG	2611,401069	1,003775495	0,145291907	6,904810892	5,03E-12	3,28E-10
FBXL16	35,19675056	3,730713076	0,511691174	6,896414366	5,33E-12	3,47E-10
PLPP1	233,9239877	1,219327306	0,178811692	6,843240224	7,74E-12	4,92E-10
PLXNA4	961,9891073	2,158678049	0,318267672	6,83276983	8,33E-12	5,26E-10
TBXT	24,26215193	5,06557221	0,664143384	6,814910581	9,43E-12	5,87E-10
METTL24	29,66113697	2,986686143	0,454225853	6,799242063	1,05E-11	6,45E-10
GPR68	3491,357851	1,549838753	0,22953245	6,781940691	1,19E-11	7,20E-10
SNX30	333,4991655	1,840690351	0,272887511	6,764333072	1,34E-11	8,09E-10
PDE6G	738,1239368	1,855810087	0,275709691	6,751372835	1,46E-11	8,76E-10
AL158211.5	55,05019248	3,18301925	0,471540867	6,699949582	2,08E-11	1,22E-09
THEM4	1339,204355	1,240865036	0,187320759	6,627140101	3,42E-11	1,94E-09
GATA6	148,983322	3,806964818	0,557597993	6,618724163	3,62E-11	2,05E-09
SPIN3	579,5682663	2,150287743	0,325929848	6,604060126	4,00E-11	2,23E-09
GOLGA6L10	65,06390646	1,759747802	0,268302629	6,598321389	4,16E-11	2,31E-09
GRAMD1B	353,2229995	2,83284927	0,428341998	6,586356155	4,51E-11	2,49E-09
CD300C	662,9534538	2,141666401	0,329522641	6,574886891	4,87E-11	2,67E-09
S100A13	51,69556697	1,57700331	0,241041752	6,54188058	6,08E-11	3,27E-09
EXT1	752,9336282	1,058061661	0,162404986	6,516422519	7,20E-11	3,81E-09
SH3D21	63,91059322	2,212082091	0,339848211	6,508575435	7,59E-11	4,00E-09
ERCC6	1325,076914	1,196918771	0,184243302	6,498806178	8,10E-11	4,24E-09
SUOX	514,9009048	1,922142601	0,295842521	6,492744365	8,43E-11	4,39E-09
IRF2BPL	951,7592032	1,293991659	0,199419253	6,490984681	8,53E-11	4,43E-09
AL157935.2	12,34158825	2,475195319	0,383015829	6,451818604	1,11E-10	5,67E-09
GPR35	331,9485478	1,26233446	0,196491366	6,414399391	1,41E-10	7,11E-09
ERMP1	6432,990792	1,050931817	0,164670882	6,400523906	1,55E-10	7,69E-09

PPP1R9A	493,7632895	1,981004521	0,309699355	6,391466414	1,64E-10	8,14E-09
TAF9B	820,1818757	1,285949427	0,201407611	6,384789994	1,72E-10	8,42E-09
LRP5	94,50272901	3,172582403	0,489045222	6,380459222	1,77E-10	8,61E-09
ITGAX	12415,82202	2,079106969	0,329943746	6,35380944	2,10E-10	1,01E-08
KLRC2	726,1948602	1,217769369	0,191269433	6,347808523	2,18E-10	1,04E-08
ZNF629	237,397175	1,314223877	0,207922122	6,339709292	2,30E-10	1,09E-08
CXCR3	3176,952781	2,727739219	0,432006382	6,289496674	3,18E-10	1,47E-08
DND1P1	139,7377777	1,591147032	0,253169883	6,281714343	3,35E-10	1,54E-08
RNASE6	49,3304587	1,8336818	0,294251275	6,241170135	4,34E-10	1,95E-08
LINC02273	120,6854075	2,104712474	0,334746798	6,237198999	4,45E-10	2,00E-08
NOD2	627,9389415	1,373877227	0,221025473	6,236011813	4,49E-10	2,01E-08
ZEB1	804,8908063	1,574559748	0,252463737	6,234338719	4,54E-10	2,02E-08
LINC00271	60,35176693	2,032485041	0,326992021	6,22232025	4,90E-10	2,18E-08
COL4A4	136,6893954	2,877693674	0,464567299	6,190854914	5,98E-10	2,60E-08
RHOB	142,5630848	1,646035215	0,266532796	6,153458318	7,58E-10	3,23E-08
WNT11	357,6166372	2,750818924	0,447235458	6,140192481	8,24E-10	3,48E-08
ITM2C	313,5989235	3,078454925	0,495274515	6,138832445	8,31E-10	3,51E-08
PATJ	832,4500235	2,026383599	0,331901279	6,116181619	9,58E-10	3,98E-08
CLSTN3	2662,810035	1,451565636	0,237248483	6,116238957	9,58E-10	3,98E-08
SUPT3H	215,3559279	1,029318783	0,169361342	6,078184656	1,22E-09	4,95E-08
TP53I11	303,9506515	1,927634969	0,330736618	6,072075791	1,26E-09	5,13E-08
ITM2A	2462,385495	1,136864047	0,187341643	6,070902966	1,27E-09	5,16E-08
PI16	42,04003912	4,176725001	0,65065832	6,049442295	1,45E-09	5,84E-08
BEX4	1500,538493	1,086656664	0,180329332	6,028447297	1,66E-09	6,56E-08
RGS10	579,2833941	1,532265566	0,254414155	6,020657274	1,74E-09	6,81E-08
AC002383.1	10,8397303	4,32815078	0,680315877	6,015521954	1,79E-09	7,00E-08
CD55	3052,146888	1,09862975	0,18266267	6,015323622	1,80E-09	7,00E-08
BEX2	385,7628247	1,249224469	0,208923302	6,002445603	1,94E-09	7,52E-08

XIRP1	57,22071206	3,683841193	0,573027442	5,982503354	2,20E-09	8,41E-08
CDHR1	819,9741477	2,677331521	0,444707403	5,959096751	2,54E-09	9,51E-08
CRYBG3	125,5555099	2,063911456	0,35247776	5,942522032	2,81E-09	1,05E-07
RAB43	2036,021922	1,001743046	0,168646318	5,941980609	2,82E-09	1,05E-07
TMEM38A	82,82198594	3,210889069	0,538726068	5,937159296	2,90E-09	1,07E-07
ARMC5	1780,369751	1,389518757	0,234393229	5,927321137	3,08E-09	1,14E-07
CLEC12A-AS1	46,22362818	1,931710213	0,330869574	5,923534282	3,15E-09	1,16E-07
RELL1	724,4778869	1,283650735	0,216901888	5,921056996	3,20E-09	1,17E-07
ACVR2A	307,8483385	1,435989021	0,243605706	5,915557483	3,31E-09	1,21E-07
RCBTB2	3063,875493	2,182264742	0,368944091	5,907303203	3,48E-09	1,27E-07
AL022322.2	67,76634459	1,801975645	0,307307468	5,888891436	3,89E-09	1,41E-07
SCARF1	156,4142594	2,842376226	0,482660895	5,876623721	4,19E-09	1,50E-07
BGLAP	96,04635907	3,538994106	0,589813919	5,862238586	4,57E-09	1,63E-07
SV2A	48,2437807	2,445816786	0,44854443	5,852427352	4,84E-09	1,71E-07
SMIM10L2A	64,30658026	3,508776996	0,594553252	5,837677632	5,29E-09	1,87E-07
PLEC	2056,099146	1,861878277	0,320559179	5,836288724	5,34E-09	1,88E-07
FXYD7	38,81660948	3,469733075	0,578446437	5,830312225	5,53E-09	1,94E-07
RAB3GAP1	663,7483876	1,089492619	0,187676911	5,809340557	6,27E-09	2,17E-07
EXD2	489,2651708	1,22891323	0,21183615	5,806800475	6,37E-09	2,20E-07
PRDM8	497,0459425	1,594431879	0,274486306	5,790720871	7,01E-09	2,41E-07
AL357033.4	101,5975193	1,590155519	0,27616053	5,765928866	8,12E-09	2,74E-07
LTC4S	42,46148258	2,210105354	0,382728867	5,760233058	8,40E-09	2,82E-07
COL9A2	666,9338283	2,977350103	0,517402243	5,751054742	8,87E-09	2,96E-07
AL031736.1	103,687593	1,950697715	0,33843021	5,742233571	9,34E-09	3,10E-07
GAB1	175,9057184	2,737081522	0,477591498	5,708355806	1,14E-08	3,73E-07
SSBP2	719,3021611	1,973183258	0,345798583	5,705182996	1,16E-08	3,79E-07
DEPDC7	126,9076612	2,000178345	0,352564952	5,698178526	1,21E-08	3,93E-07
AHR	1030,419847	2,406975171	0,421207467	5,693457474	1,24E-08	4,01E-07

PLCH2	1656,044125	1,331782742	0,23544833	5,659271744	1,52E-08	4,83E-07
AL132996.1	6,930815148	3,865822551	0,658816638	5,655974876	1,55E-08	4,91E-07
CRTAM	3258,918725	2,879944593	0,498895482	5,635140157	1,75E-08	5,49E-07
EPAS1	235,0594084	1,780244369	0,315446327	5,624532859	1,86E-08	5,82E-07
RPS6KA2	603,4370845	2,081404584	0,375350496	5,615442365	1,96E-08	6,13E-07
AC021066.1	445,2279295	1,806776785	0,322754978	5,588460676	2,29E-08	7,08E-07
SPECC1	1212,882897	1,008531761	0,180580378	5,582913532	2,37E-08	7,28E-07
MTDHP3	18,53111258	3,651885327	0,630130448	5,57811123	2,43E-08	7,47E-07
AL603783.1	43,40415723	2,919117033	0,516839812	5,577366312	2,44E-08	7,48E-07
NBPF15	523,6238388	1,003156505	0,179966039	5,577463011	2,44E-08	7,48E-07
AC073332.1	50,46757368	2,079539706	0,374584686	5,568107727	2,58E-08	7,88E-07
AC011445.1	149,0232011	1,448193495	0,261854134	5,539578792	3,03E-08	9,14E-07
TCF7	3711,66176	2,801294186	0,501319966	5,532091697	3,16E-08	9,52E-07
AL022341.2	64,00754303	2,406238912	0,436859003	5,525605382	3,28E-08	9,82E-07
NELL2	528,3413071	2,958904755	0,536983549	5,519567819	3,40E-08	1,01E-06
GPR155	584,2908913	1,362453331	0,246781698	5,518453369	3,42E-08	1,02E-06
GORASP1	727,874936	1,159369536	0,212809321	5,517578996	3,44E-08	1,02E-06
MAML3	227,3004088	2,910517687	0,520119301	5,507021751	3,65E-08	1,07E-06
NCKAP5L	557,8377929	1,019341234	0,185736999	5,495749561	3,89E-08	1,14E-06
NBPF9	286,8213266	1,104871219	0,201721668	5,487263097	4,08E-08	1,19E-06
AC068580.4	1237,365465	1,09636765	0,199802887	5,481917224	4,21E-08	1,22E-06
PRSS2	20,42490575	3,435662521	0,640356433	5,468191576	4,55E-08	1,31E-06
SEC22B4P	427,8475782	1,068157178	0,195364259	5,467566083	4,56E-08	1,32E-06
AC136475.9	40,38923353	2,683705638	0,492099609	5,467015518	4,58E-08	1,32E-06
KLHDC9	16,03763148	2,554000388	0,46130946	5,46690161	4,58E-08	1,32E-06
PLA2G6	1633,729643	2,025368206	0,371533287	5,451318684	5,00E-08	1,42E-06
NUDT16P1	132,0159874	2,394800836	0,440749668	5,433913468	5,51E-08	1,56E-06
IFITM3	7923,417658	1,451337304	0,267556571	5,43083565	5,61E-08	1,58E-06

MTM1	1010,089782	1,886289418	0,347656721	5,420132252	5,96E-08	1,68E-06
GPR82	337,6226796	2,635019703	0,481344315	5,419871453	5,96E-08	1,68E-06
ATP6V0E2-AS1	108,2815423	1,244807485	0,230542859	5,410393293	6,29E-08	1,76E-06
LINC01871	1830,467521	1,540975424	0,285096179	5,408546324	6,35E-08	1,78E-06
LSR	887,6666794	2,840944598	0,518173198	5,401460927	6,61E-08	1,85E-06
AL034550.2	33,02488769	3,172151524	0,559528571	5,395879874	6,82E-08	1,90E-06
AC092368.3	24,78169397	1,512806742	0,283628302	5,379991707	7,45E-08	2,06E-06
TPD52L1	51,71867641	2,422752867	0,455664353	5,373551856	7,72E-08	2,13E-06
CD2	9315,600078	1,454866474	0,272244595	5,363995817	8,14E-08	2,24E-06
PFKFB3	1945,504031	1,000897819	0,187849186	5,329454109	9,85E-08	2,65E-06
LINC02446	16,30915541	2,489644747	0,459313591	5,324837854	1,01E-07	2,72E-06
ANKDD1B	17,25372673	1,915061785	0,364217268	5,324244425	1,01E-07	2,72E-06
EPHX1	54,71961291	2,458322408	0,471892105	5,292055384	1,21E-07	3,18E-06
EPHA1	89,4450334	1,590839766	0,303668555	5,283878035	1,26E-07	3,32E-06
PALD1	72,54013307	2,564431066	0,484668735	5,283191913	1,27E-07	3,33E-06
GSN	11477,76579	1,080001767	0,204600157	5,282113632	1,28E-07	3,34E-06
SLC17A9	1020,722123	2,025156259	0,383167497	5,274721728	1,33E-07	3,48E-06
ZNF667	63,99101562	3,275472613	0,616486896	5,226061181	1,73E-07	4,42E-06
SPACA9	113,6159267	2,142499804	0,408667207	5,222418166	1,77E-07	4,50E-06
CSF2	167,7107889	3,291839501	0,596805233	5,214685992	1,84E-07	4,67E-06
ZNF471	57,49951783	2,226779851	0,434540854	5,214527878	1,84E-07	4,67E-06
ARMCX2	60,84843318	1,884167269	0,360777333	5,214744992	1,84E-07	4,67E-06
EGR3	43,79934598	2,259073472	0,432640676	5,206379511	1,93E-07	4,85E-06
TTC23	29,86479356	1,512348688	0,295236661	5,206164654	1,93E-07	4,85E-06
BEND5	33,96012583	2,096798976	0,408007954	5,199110676	2,00E-07	5,03E-06
TRPM8	20,34419262	3,04250246	0,678290192	5,195196907	2,05E-07	5,12E-06
WDR86-AS1	5,171232188	3,921026082	0,684325649	5,193465345	2,06E-07	5,16E-06

SLC49A3	485,7237538	1,312431718	0,253372909	5,184921568	2,16E-07	5,39E-06
TUBA8	95,46203126	2,550813663	0,490022933	5,170630572	2,33E-07	5,79E-06
RNF144A	1772,527623	1,289472324	0,250586361	5,162317942	2,44E-07	6,03E-06
SPRY2	473,2348813	2,107772018	0,408888309	5,147224675	2,64E-07	6,51E-06
DDIT4	5551,55676	1,362385866	0,26530604	5,144237245	2,69E-07	6,61E-06
SLC44A1	1742,706472	1,401151872	0,273392571	5,125205954	2,97E-07	7,23E-06
ASPH	249,8983469	1,797842619	0,35231292	5,105993649	3,29E-07	7,92E-06
AC009404.1	43,90260786	1,29603386	0,254206162	5,101933528	3,36E-07	8,08E-06
ENPP3	119,5988475	2,667883964	0,57024697	5,093649621	3,51E-07	8,39E-06
CD27	111,4046967	3,032675704	0,579396161	5,06209634	4,15E-07	9,84E-06
CPNE7	81,84795563	1,838326943	0,363674022	5,0473816	4,48E-07	1,05E-05
LINC02391	9,538284846	2,131988111	0,422294001	5,046154098	4,51E-07	1,06E-05
MFGE8	399,3689337	1,248535075	0,247873273	5,045848157	4,52E-07	1,06E-05
AC004687.3	18,53533533	3,779035129	0,68637623	5,04379158	4,56E-07	1,07E-05
SLC29A4	26,32821855	2,370306808	0,468206092	5,043496764	4,57E-07	1,07E-05
TRO	241,9601661	1,037435872	0,207147565	5,021933504	5,12E-07	1,19E-05
AC011298.1	12,69198312	3,717939806	0,684965986	5,015416738	5,29E-07	1,22E-05
AC136475.5	16,14527145	2,820416285	0,563897138	5,015266466	5,30E-07	1,22E-05
COX6A2	11,17509384	3,840578061	0,686505729	4,995326291	5,87E-07	1,35E-05
AC097658.2	6,571846465	2,389027138	0,470204318	4,983528216	6,24E-07	1,42E-05
PLCB4	8,966236706	3,114548233	0,662253761	4,977668738	6,44E-07	1,46E-05
FXYD2	28,56930801	3,374607679	0,679677749	4,973572964	6,57E-07	1,49E-05
MS4A1	103,7166229	2,651249066	0,544912467	4,960162463	7,04E-07	1,59E-05
SRGAP3	102,6996534	2,09325268	0,424847963	4,953356723	7,29E-07	1,64E-05
IL9RP3	32,18469003	2,965586928	0,614113692	4,945474988	7,60E-07	1,70E-05
EGR2	775,1497977	1,551361391	0,312263	4,943510388	7,67E-07	1,72E-05
CASS4	376,6299138	1,107652538	0,224036719	4,943290919	7,68E-07	1,72E-05
CAV1	12,3243057	3,000225407	0,669579558	4,936992385	7,93E-07	1,77E-05

SEPTIN11	3368,522987	1,230166792	0,249533059	4,93445316	8,04E-07	1,79E-05
DAPP1	453,4751878	1,810976987	0,378679342	4,933798851	8,06E-07	1,79E-05
KCTD9	622,9600217	1,554305672	0,315884338	4,932125087	8,13E-07	1,81E-05
NR4A3	60,41180688	2,390151939	0,482092819	4,931824622	8,15E-07	1,81E-05
AL390719.1	21,22682362	2,173717679	0,438728664	4,924569418	8,45E-07	1,87E-05
AC093890.1	84,29101585	1,850806298	0,37780216	4,919792993	8,66E-07	1,92E-05
LINC01862	165,8059183	3,407342196	0,647630517	4,918208601	8,73E-07	1,93E-05
NPTX2	11,95920836	2,674611464	0,647295525	4,903056914	9,44E-07	2,07E-05
AC246785.2	54,40084889	1,103043325	0,224853183	4,902309554	9,47E-07	2,07E-05
GNG7	32,13907297	2,162926917	0,455478684	4,901646418	9,50E-07	2,08E-05
FHL1	356,3105433	1,851953834	0,378469867	4,898587642	9,65E-07	2,11E-05
TNFSF11	290,4070602	2,662973414	0,535577669	4,898267525	9,67E-07	2,11E-05
E2F3	2431,09033	1,106357893	0,227053379	4,881546688	1,05E-06	2,27E-05
SERPINE1	24,51291118	3,069040041	0,611586793	4,879453656	1,06E-06	2,29E-05
AL512625.1	136,192134	1,160967664	0,239929247	4,87860271	1,07E-06	2,30E-05
LEF1	2008,647706	2,61189181	0,527151981	4,872815174	1,10E-06	2,36E-05
DCAF4	454,5373992	1,152808831	0,236887987	4,871929897	1,11E-06	2,37E-05
PIK3R6	267,3136241	2,728241743	0,551094203	4,869987304	1,12E-06	2,39E-05
TNFSF10	2868,030902	1,088892881	0,223705676	4,865157215	1,14E-06	2,45E-05
A1BG	168,3731151	1,775440392	0,365395825	4,855055251	1,20E-06	2,56E-05
AC016026.1	86,36717872	1,052261414	0,217943588	4,848636915	1,24E-06	2,64E-05
PGBD1	81,40353523	1,717651033	0,362680229	4,847121884	1,25E-06	2,65E-05
MMRN1	259,7084239	3,018811421	0,620565044	4,841825249	1,29E-06	2,72E-05
CCR2	145,1278363	2,860956803	0,574266949	4,83652106	1,32E-06	2,78E-05
RGS9BP	34,79056254	2,361203239	0,496212139	4,830697487	1,36E-06	2,86E-05
LGALS9C	706,5233468	1,509910795	0,322621982	4,828798788	1,37E-06	2,88E-05
SUCLG2-AS1	107,4804422	1,589844771	0,330428536	4,814550363	1,48E-06	3,07E-05
PGGHG	7170,992647	1,625079721	0,338907522	4,784349433	1,72E-06	3,54E-05

EFHC2	306,4969901	1,666384281	0,349250247	4,779806872	1,75E-06	3,61E-05
GNG4	13,38166738	3,909794942	0,683043142	4,773653198	1,81E-06	3,71E-05
UBE2Q2P2	175,2414379	1,404562422	0,295652145	4,76984627	1,84E-06	3,77E-05
TNFRSF10D	45,93736542	2,132218736	0,478037828	4,756439585	1,97E-06	4,02E-05
ZNF667-AS1	191,2023662	2,490988306	0,525674202	4,7365302	2,17E-06	4,38E-05
CUEDC1	35,54985212	2,292075626	0,481057487	4,724454283	2,31E-06	4,63E-05
EGLN3	44,92095041	2,24550515	0,479632739	4,711643955	2,46E-06	4,90E-05
INSC	48,77728206	3,098483111	0,623070967	4,709394843	2,48E-06	4,95E-05
EMILIN1	128,8480127	1,639857566	0,347426603	4,704790036	2,54E-06	5,05E-05
MAL	39,57340648	3,464877836	0,669770372	4,694105682	2,68E-06	5,29E-05
RORC	26,13664694	2,777760689	0,587674155	4,684977087	2,80E-06	5,50E-05
PTK2	351,4638039	2,477553128	0,521587879	4,684769133	2,80E-06	5,50E-05
GYPE	142,7763228	1,891528989	0,401385726	4,684246085	2,81E-06	5,51E-05
AGAP3	949,5526516	1,041453001	0,222716515	4,677427311	2,90E-06	5,67E-05
NLRP6	362,0418812	1,688567398	0,382816417	4,676545909	2,92E-06	5,69E-05
CCR3	57,93643764	2,803902646	0,582266843	4,674047945	2,95E-06	5,75E-05
MYO7A	33,55637115	3,737964548	0,684756816	4,66937877	3,02E-06	5,86E-05
NEIL1	1497,44199	1,453142161	0,310129545	4,667908927	3,04E-06	5,90E-05
ZMAT4	216,068965	2,640467911	0,558154412	4,643769643	3,42E-06	6,54E-05
GATA6-AS1	11,54308557	3,066840867	0,629454234	4,630479567	3,65E-06	6,93E-05
KLRC1	9685,022474	1,004146993	0,21694846	4,629659228	3,66E-06	6,95E-05
TNFSF4	139,7637985	2,011664798	0,427744978	4,626434948	3,72E-06	7,02E-05
JUP	58,15443641	2,526880336	0,546290366	4,616890407	3,90E-06	7,28E-05
BTBD6P1	302,4428418	2,666889986	0,563167772	4,614916427	3,93E-06	7,32E-05
KLHL29	33,08738174	1,946606948	0,416347485	4,61404557	3,95E-06	7,34E-05
LINC01619	61,33308047	2,086410116	0,459723481	4,610883455	4,01E-06	7,44E-05
PER2	289,3529778	1,149889389	0,249251779	4,609300045	4,04E-06	7,49E-05
NAB2	282,4119613	1,650115906	0,354901133	4,605926938	4,11E-06	7,58E-05

PDK4	62,19623696	2,612015818	0,625512614	4,597283482	4,28E-06	7,87E-05
OR2W3	8,537974039	2,71906961	0,575346458	4,588680942	4,46E-06	8,17E-05
RNA5-8SN2	83,66427081	1,424126424	0,309865244	4,576279252	4,73E-06	8,61E-05
TRIM47	230,944992	2,515587478	0,57857664	4,576015626	4,74E-06	8,62E-05
PDE9A	28,46432687	2,11835182	0,463611347	4,5757863	4,74E-06	8,62E-05
RAMP1	1416,771374	2,003743871	0,436861022	4,569071259	4,90E-06	8,87E-05
FES	14096,02622	1,218324888	0,267207028	4,565206498	4,99E-06	9,01E-05
AC012435.2	34,70171456	2,115485105	0,462083466	4,556526026	5,20E-06	9,35E-05
CAMK1	712,271817	1,318506905	0,289591149	4,541444188	5,59E-06	9,97E-05
CKMT2	21,75960717	2,975202182	0,64829	4,540229443	5,62E-06	0,000100095
CYP2E1	41,85003279	1,868522619	0,4155738	4,538337814	5,67E-06	0,000100908
MCF2L	98,84718277	2,428602121	0,531561162	4,537497838	5,69E-06	0,000101221
HDAC11	197,7692003	1,658304137	0,367992609	4,521049269	6,15E-06	0,000108744
AC092171.3	4,066207505	3,35422722	0,680565705	4,517883731	6,25E-06	0,000110189
LINC01232	60,31393813	1,043585838	0,231126021	4,512542166	6,41E-06	0,000112804
UBR5-AS1	44,37993739	1,718926174	0,381103323	4,504273936	6,66E-06	0,000116878
WNT6	5,052215367	3,331058752	0,675564228	4,500825894	6,77E-06	0,000118378
DIO3OS	25,74357413	3,117712453	0,653715159	4,496033198	6,92E-06	0,000120658
FNBP1L	19,56801807	2,777742174	0,598214518	4,494566007	6,97E-06	0,000121283
JHY	255,9646704	1,520655684	0,340394715	4,494675056	6,97E-06	0,000121283
XCL2	7701,308734	1,762187493	0,390203808	4,49211141	7,05E-06	0,000122479
CSTF2T	3840,28611	1,005275341	0,22378182	4,490371606	7,11E-06	0,000123377
PRKAR2B	149,6290659	2,645619867	0,579069628	4,480688106	7,44E-06	0,000128777
PLS3	37,18201753	2,874024246	0,664410669	4,478669708	7,51E-06	0,000129778
CITED4	54,10013354	1,04923707	0,233115122	4,465966524	7,97E-06	0,00013737
MGAT5B	72,42671081	2,704211638	0,596935983	4,462644629	8,10E-06	0,00013928
BMS1P1	120,6512927	1,155984636	0,261025163	4,453962399	8,43E-06	0,000144666
DOCK1	19,87347216	2,858351435	0,618826085	4,453308541	8,46E-06	0,000144984

MPV17L	18,52482589	2,933379987	0,630792433	4,438740939	9,05E-06	0,000153713
KANSL1L-AS1	57,80704568	1,175597107	0,265021626	4,438865951	9,04E-06	0,000153713
FAM117B	398,6916273	1,703561568	0,38370197	4,431446356	9,36E-06	0,00015834
AC009133.3	89,18313721	1,272998877	0,288556644	4,428772591	9,48E-06	0,000159779
AC008014.1	81,58722507	1,565423115	0,352980341	4,420221681	9,86E-06	0,00016568
PAOX	277,1754213	1,163805828	0,264060277	4,410719008	1,03E-05	0,000172546
P4HA2	62,19190001	2,074598291	0,470662803	4,403734272	1,06E-05	0,000177903
CCDC121	55,15150199	1,36373148	0,310334972	4,399393755	1,09E-05	0,000180899
IL3	7,263746933	3,032465126	0,685089311	4,39804176	1,09E-05	0,000181879
HOXA5	29,22251332	2,663573703	0,628071499	4,396650806	1,10E-05	0,000182746
TNFRSF11A	900,3745533	3,043200414	0,652565419	4,393640665	1,11E-05	0,000184991
PCNX2	244,8780474	1,353694323	0,30927685	4,37962019	1,19E-05	0,000196172
KRT81	219,3263906	1,852860789	0,420643076	4,376345734	1,21E-05	0,000198816
AC123912.4	57,7867272	3,215074261	0,670750072	4,370088695	1,24E-05	0,000203932
BMF	108,750818	1,85337081	0,424311083	4,354033382	1,34E-05	0,000217868
HSPG2	17,117014	2,187090022	0,677115263	4,335947056	1,45E-05	0,000235248
SLC5A2	15,49691469	2,370559637	0,57441768	4,324722237	1,53E-05	0,000247153
RASSF2	2129,258914	1,4305824	0,330369984	4,321751259	1,55E-05	0,000250104
CEP68	758,1683459	1,69136332	0,390381931	4,320330329	1,56E-05	0,000251116
NEK6	534,3137535	1,209174135	0,281884172	4,313087311	1,61E-05	0,000259282
AL136456.1	15,04858929	2,661349463	0,605572047	4,297893561	1,72E-05	0,000275504
CYGB	340,0955644	2,588938845	0,590623579	4,292018938	1,77E-05	0,000282226
UBASH3A	71,54453592	2,887247625	0,635371147	4,289809408	1,79E-05	0,000284823
CSPG4P12	36,1560947	1,837829876	0,435732667	4,287569921	1,81E-05	0,000287255
NFIX	60,68310508	2,522417396	0,573915819	4,28194832	1,85E-05	0,000293454
PECAM1	2770,661028	1,234226615	0,29372387	4,27280116	1,93E-05	0,000304801
TTLL10	55,17994789	3,165533647	0,677545215	4,266103255	1,99E-05	0,000312867
CARD10	195,7946157	3,162507469	0,681788746	4,254657742	2,09E-05	0,000328161

BASP1	89,17467743	2,459015851	0,534617824	4,252059772	2,12E-05	0,000331342
AC093157.1	224,0533513	1,180037207	0,276519418	4,250369494	2,13E-05	0,000333594
AC079779.1	58,29398965	2,129901217	0,592652134	4,246268326	2,17E-05	0,000338968
WASIR2	8,636171076	2,893649754	0,687707799	4,245385515	2,18E-05	0,000339256
CELSR1	44,13666181	2,481443117	0,603597699	4,245644287	2,18E-05	0,000339256
PKIA	78,85937452	2,204573982	0,521138808	4,238829798	2,25E-05	0,00034824
PDGFA	21,16065015	2,465664476	0,576959244	4,220608974	2,44E-05	0,000376173
BEX5	89,58593359	1,367130389	0,322809632	4,216438277	2,48E-05	0,000382609
CLEC3B	9,930720348	2,837184486	0,656641233	4,211959984	2,53E-05	0,000389978
AK8	8,325888658	2,258884646	0,536740694	4,201875242	2,65E-05	0,000405598
AC005083.1	9,836329602	2,579657893	0,645084134	4,201039134	2,66E-05	0,00040679
INPP5F	829,2714252	1,197923774	0,28491769	4,190833732	2,78E-05	0,000423278
HOXA-AS3	29,76508842	2,251069243	0,535071714	4,188372622	2,81E-05	0,000427249
PDCD4	11931,50272	1,092133935	0,260805255	4,186306354	2,84E-05	0,000430181
FUT6	3,392327544	2,858222968	0,677162137	4,18386062	2,87E-05	0,000433859
AL022238.4	222,1358653	1,115870744	0,267411959	4,183134943	2,88E-05	0,00043492
CSPG4P10	50,37921758	1,015984266	0,242249925	4,177084633	2,95E-05	0,000445644
IGLV2-18	3,924084235	2,611510241	0,663150589	4,173288094	3,00E-05	0,000451786
TLCD2	26,04526924	1,633004101	0,410515131	4,169477262	3,05E-05	0,000458039
AC025164.2	773,1323373	1,46411102	0,353146935	4,16917934	3,06E-05	0,000458298
AC068775.1	884,7281123	1,09932535	0,260790028	4,165733973	3,10E-05	0,000463895
MVB12B	297,7737086	1,406102328	0,347569303	4,156290574	3,23E-05	0,000479572
TTC24	68,77921346	2,267286146	0,562949671	4,149431782	3,33E-05	0,000492719
EPS8	127,5161962	1,415747403	0,355555925	4,13439404	3,56E-05	0,000521907
CARD19	1476,40296	1,100074256	0,26648286	4,126729715	3,68E-05	0,000537257
PLD1	141,5092009	1,383133178	0,339080294	4,125699483	3,70E-05	0,000538894
RETREG1	94,16902923	2,07510904	0,512433511	4,114913381	3,87E-05	0,000560662
MCC	133,7813786	1,435245654	0,362675489	4,109445865	3,97E-05	0,000572868

STXBP1	166,6807384	1,773062233	0,430974083	4,105823205	4,03E-05	0,000580547
ZEB1-AS1	164,9176877	1,566477904	0,388516549	4,102143778	4,09E-05	0,000589145
NECTIN3	65,65558893	2,109821104	0,522511446	4,100453329	4,12E-05	0,000593043
BMP8B	158,3523606	1,797732771	0,428864179	4,094667742	4,23E-05	0,000605456
TMEM14C	657,2655348	1,810962691	0,442101686	4,077193222	4,56E-05	0,000647929
EPHA4	1050,413239	1,557123797	0,38537098	4,065706375	4,79E-05	0,000676663
FAM30A	12,43469716	2,62472664	0,687276262	4,064282968	4,82E-05	0,00068015
LGALS3BP	455,2933785	2,01736213	0,498440034	4,063485753	4,83E-05	0,000681702
CNR2	2219,199414	2,444235085	0,585082679	4,058692112	4,93E-05	0,000692456
ZNF843	15,55036673	2,364271664	0,592664421	4,057948375	4,95E-05	0,000693699
AC036176.1	50,40960634	1,284314447	0,317099019	4,055862318	4,99E-05	0,000698464
CYP4F22	115,5672067	1,023809783	0,254208061	4,05374212	5,04E-05	0,000703365
SIX4	5,032002761	2,972599722	0,687818501	4,049103353	5,14E-05	0,000714977
DTX1	44,33735311	2,597561359	0,615597976	4,038247269	5,39E-05	0,000744769
PCBP3	14,05993545	2,732766327	0,655409566	4,033752225	5,49E-05	0,000757091
COL15A1	46,51217042	2,389977593	0,542911588	4,032154516	5,53E-05	0,000761736
AL138828.1	4,740326734	2,687186184	0,658844736	4,030351437	5,57E-05	0,000767079
AL135818.2	33,98399152	1,492962774	0,370720041	4,027813163	5,63E-05	0,000774348
SERPINB9P1	37,81299154	1,718317668	0,425459062	4,022438429	5,76E-05	0,00079062
H3-2	22,33116103	1,607520491	0,393806175	4,018284767	5,86E-05	0,00080359
LTB	7685,961389	1,885747477	0,465054567	4,015437499	5,93E-05	0,000811148
MEST	60,3144696	1,50647934	0,379673843	4,006372315	6,17E-05	0,00083779
HOXA10	474,6676523	1,586323541	0,395748298	4,00277112	6,26E-05	0,000848934
KL	6,183304183	2,588017678	0,687354751	3,999147664	6,36E-05	0,000861015
SELL	61133,19386	1,046801587	0,263254611	3,99281777	6,53E-05	0,000881824
NR2F6	281,6955243	1,506947823	0,37795197	3,99255195	6,54E-05	0,000882222
RGS6	4,488837285	2,58082069	0,666501808	3,987713893	6,67E-05	0,000897999
YWHAEP7	38,3378469	2,636322159	0,645170748	3,984996126	6,75E-05	0,00090592

CHMP4C	34,73443287	2,848940037	0,671522152	3,970921553	7,16E-05	0,000954791
ABTB2	42,18544019	1,874409248	0,473912327	3,968552991	7,23E-05	0,000961785

1309

1310 **Table 3.** List of ST2^{-} CD56^{dim} NK cell signature genes used in this study, Related to Fig. 3C,D,F,G

1311

gene	baseMean	log2FoldChange	lfcSE	stat	pvalue	padj
FGFBP2	8144,153518	3,202150845	0,320967185	10,00234058	1,49E-23	9,84E-20
RNF166	8329,004271	1,572015459	0,157231451	10,01458146	1,32E-23	9,84E-20
RASGRP2	4442,914764	1,388044602	0,146010973	9,525583883	1,64E-21	6,51E-18
DPEP2	1526,11809	1,609829657	0,190756897	8,483359095	2,19E-17	4,34E-14
AL353622.1	297,1803946	1,685555006	0,200170725	8,443427493	3,08E-17	5,56E-14
KLF3	2317,609775	1,540112022	0,183942681	8,40503739	4,28E-17	7,07E-14
CEP78	4905,929088	1,044810306	0,126366368	8,259780569	1,46E-16	2,07E-13
LINC00944	44,76489599	3,21482747	0,372462803	8,19595732	2,49E-16	3,29E-13
DYRK1B	672,4335557	1,118315017	0,137280114	8,165574615	3,20E-16	3,86E-13
P2RY8	7887,303735	1,486780838	0,189003159	7,86287299	3,75E-15	3,24E-12
GPA33	161,1699077	2,418507998	0,327658938	7,546200536	4,48E-14	3,07E-11
AC245407.2	406,0213999	1,859932789	0,248929722	7,516379506	5,63E-14	3,72E-11
TMEM71	1574,466452	1,954352228	0,268749796	7,358825676	1,86E-13	1,12E-10
AL138824.1	129,6429159	2,422070604	0,336058541	7,33023171	2,30E-13	1,30E-10
LINC00861	3061,05769	1,53354884	0,210763177	7,323411026	2,42E-13	1,33E-10
KLF2	6970,676213	1,560628347	0,216566128	7,216426459	5,34E-13	2,71E-10
WAKMAR2	491,0159819	1,331281734	0,186211266	7,186350801	6,65E-13	3,30E-10
RASSF1-AS1	238,3238734	1,416845962	0,196731197	7,170698638	7,46E-13	3,52E-10
MCM3AP-AS1	326,1585037	1,138706429	0,161235728	7,053431474	1,75E-12	7,37E-10
AC005332.2	94,85373685	2,095310385	0,293433439	6,976915203	3,02E-12	1,11E-09
BISPR	1681,320381	1,060832931	0,152324166	6,960487766	3,39E-12	1,22E-09
SELPLG	21499,71541	1,283065741	0,185716133	6,934799516	4,07E-12	1,39E-09
OAS1	1195,66649	1,211755432	0,175809612	6,871013811	6,37E-12	2,07E-09
AL662844.4	967,2315141	1,207738148	0,177139872	6,840280625	7,90E-12	2,53E-09
IFIT2	1117,024786	2,133274979	0,315695154	6,834721634	8,22E-12	2,59E-09

RASSF1	11231,77473	1,301637387	0,192592714	6,758344733	1,40E-11	3,90E-09
STMN3	137,9011327	2,372036606	0,352935904	6,73337158	1,66E-11	4,44E-09
AC073130.3	171,1204581	1,663210743	0,247089371	6,720080459	1,82E-11	4,56E-09
HSBP1L1	213,0495397	1,096455411	0,163684666	6,690234449	2,23E-11	5,46E-09
KIFC3	745,2824955	2,12908314	0,321380577	6,679504561	2,40E-11	5,66E-09
AL592295.5	158,8162533	1,063282332	0,160343558	6,661930468	2,70E-11	6,16E-09
HEATR9	73,23745131	2,555095193	0,387866469	6,65222127	2,89E-11	6,36E-09
AC055839.2	298,5800799	1,540998324	0,233523327	6,636494986	3,21E-11	7,00E-09
NDRG1	1077,893796	1,288213421	0,195811703	6,60289876	4,03E-11	8,38E-09
PLEKHG3	8342,958982	1,360164232	0,206675366	6,586993772	4,49E-11	9,18E-09
PARP12	6641,277294	1,200871467	0,18278299	6,561481629	5,33E-11	1,07E-08
FGR	17120,1803	1,4607729	0,222708926	6,556003566	5,53E-11	1,09E-08
ZFHX2-AS1	761,7303199	1,065192305	0,162302597	6,536673788	6,29E-11	1,19E-08
THRA	284,6004293	1,592549138	0,2455052	6,533669042	6,42E-11	1,20E-08
ICAM2	3207,579092	1,124983666	0,172111497	6,529980219	6,58E-11	1,22E-08
MHENCR	224,0159648	1,361939827	0,209491017	6,521826752	6,95E-11	1,28E-08
RENBP	199,7535366	1,483512111	0,229877225	6,484212226	8,92E-11	1,62E-08
TTC38	8039,041486	1,003443505	0,159254813	6,304267394	2,90E-10	4,54E-08
NATD1	671,0286088	1,052857164	0,167698493	6,275188997	3,49E-10	5,25E-08
CTSF	1165,042147	1,941891463	0,322774126	6,247305527	4,18E-10	6,09E-08
SFXN3	1817,137939	1,061585468	0,170287364	6,239116516	4,40E-10	6,35E-08
DLGAP1-AS1	330,5404792	1,279252449	0,205533663	6,233047148	4,57E-10	6,41E-08
TTLL3	2088,501966	1,21159376	0,194420136	6,232022848	4,60E-10	6,41E-08
AC244157.2	11,20080967	3,129269147	0,478217362	6,211872602	5,24E-10	6,97E-08
PATL2	4331,057083	2,073692218	0,339076125	6,142247184	8,14E-10	1,01E-07
SNAI3	591,4513799	1,664734223	0,274430177	6,141609469	8,17E-10	1,01E-07
ZMYND10	90,55930117	1,479130226	0,24144219	6,144421879	8,03E-10	1,01E-07
ZNF276	8281,915905	1,111608858	0,18130732	6,140495038	8,23E-10	1,01E-07

TRIM22	16223,92092	1,132720837	0,186423812	6,070675197	1,27E-09	1,47E-07
AL139246.5	210,2164121	1,289055593	0,214307842	6,02576554	1,68E-09	1,81E-07
BTN3A3	7879,327212	1,001665785	0,167620932	5,979652651	2,24E-09	2,27E-07
CCDC88C	5657,368226	1,023107223	0,171581502	5,974768528	2,30E-09	2,33E-07
SLAMF6	4918,979345	1,245100796	0,210034001	5,943449696	2,79E-09	2,74E-07
FCGR2A	84,56463711	2,695351865	0,468057246	5,934925165	2,94E-09	2,83E-07
CDC14B	109,090885	2,543603082	0,417798191	5,929046971	3,05E-09	2,91E-07
DEGS2	171,5630993	2,213052873	0,37606735	5,890150226	3,86E-09	3,54E-07
FAM13A-AS1	86,14944071	1,321665729	0,224337026	5,88294354	4,03E-09	3,60E-07
LINC002481	1047,622692	1,077615531	0,183488496	5,87767994	4,16E-09	3,65E-07
NLRP1	11216,96825	1,109626639	0,189979648	5,855860413	4,75E-09	4,06E-07
EFEMP2	692,2367593	1,341301299	0,231765649	5,815466941	6,05E-09	4,96E-07
AC006369.1	101,647403	1,990066631	0,35352843	5,813465678	6,12E-09	4,96E-07
TRGV10	614,0797893	1,416106431	0,241708205	5,811665992	6,19E-09	4,97E-07
PRR29	306,0053646	1,386872293	0,238445664	5,79664335	6,77E-09	5,35E-07
ZFP36L2	18485,19308	1,390293461	0,239873773	5,788011561	7,12E-09	5,58E-07
METTL7A	1308,623924	1,73695712	0,300854347	5,780965031	7,43E-09	5,80E-07
SEPTIN4	75,97567771	2,698194832	0,452517403	5,75264716	8,79E-09	6,63E-07
AL391987.4	20,05432848	2,197526065	0,378590689	5,734426497	9,78E-09	7,21E-07
BCL9L	506,2869482	1,200452362	0,211099255	5,706615393	1,15E-08	8,25E-07
C3orf18	189,7095457	1,494737274	0,261434877	5,677302098	1,37E-08	9,52E-07
DNAI2	26,98773266	2,158699082	0,377378171	5,675041668	1,39E-08	9,62E-07
AC008555.4	342,8896863	1,305132998	0,230246837	5,671671372	1,41E-08	9,74E-07
AC083862.3	93,04402387	1,605951846	0,285482801	5,666288702	1,46E-08	9,98E-07
AOAH	15162,22478	1,177424409	0,212304547	5,666244743	1,46E-08	9,98E-07
SCIMP	212,0349226	2,783228915	0,450582846	5,664457042	1,47E-08	1,01E-06
A2M-AS1	33,70740077	2,023754653	0,369565554	5,654876374	1,56E-08	1,04E-06
PROCR	189,2710625	1,782388913	0,308461157	5,655020804	1,56E-08	1,04E-06

HLA-DPB1	3374,062135	1,455744026	0,254509239	5,591878485	2,25E-08	1,37E-06
THEMIS2	6429,654639	1,318426828	0,243695999	5,581361969	2,39E-08	1,45E-06
TTYH2	119,2345397	1,912936214	0,330242527	5,570418879	2,54E-08	1,50E-06
FCHO2	354,5028786	1,313542877	0,235595382	5,550212185	2,85E-08	1,64E-06
SYNE1	7987,350074	1,037980237	0,187983316	5,549434563	2,87E-08	1,64E-06
ANO8	97,04963606	1,230117118	0,221829997	5,547661657	2,90E-08	1,65E-06
AL731571.1	505,1583218	1,013699118	0,182893325	5,543829085	2,96E-08	1,66E-06
ARVCF	833,3125729	2,408541464	0,439432257	5,524252065	3,31E-08	1,81E-06
SMAD7	2965,651036	1,11518809	0,202018956	5,511917559	3,55E-08	1,91E-06
UCP3	56,41155725	1,573797693	0,285729882	5,507325675	3,64E-08	1,95E-06
LIME1	942,3741088	1,479021292	0,267520994	5,506762372	3,65E-08	1,95E-06
AC133552.2	182,303471	1,054617444	0,192419877	5,500330174	3,79E-08	1,99E-06
NUAK2	1515,700571	1,857743056	0,334990288	5,499802944	3,80E-08	2,00E-06
AP001372.2	131,5564837	1,148468837	0,210424808	5,469934728	4,50E-08	2,30E-06
AL160269.1	17,96116089	2,732927978	0,50061574	5,464840779	4,63E-08	2,36E-06
MC1R	484,7686664	1,07744908	0,196701472	5,458544783	4,80E-08	2,40E-06
AC015911.3	80,38809773	1,337714978	0,247579608	5,45226435	4,97E-08	2,47E-06
CLIC3	9459,677847	1,481450713	0,279632872	5,441172466	5,29E-08	2,57E-06
PRR5	1701,267869	1,29351842	0,235458066	5,439890922	5,33E-08	2,59E-06
C8G	45,28819125	1,659126755	0,308272489	5,436019139	5,45E-08	2,63E-06
VIPR2	140,3095731	2,66019421	0,459253371	5,43117563	5,60E-08	2,68E-06
AMZ2P1	484,3583591	1,158245381	0,213752863	5,421662242	5,90E-08	2,77E-06
TMEM191A	149,1107394	1,328338074	0,245783935	5,419654336	5,97E-08	2,77E-06
AC093010.2	133,6541972	1,438341241	0,262590937	5,414098905	6,16E-08	2,82E-06
LINC01801	99,14112127	1,834082888	0,337712839	5,409646324	6,31E-08	2,86E-06
CXXC4	7,761928407	3,341815889	0,592915329	5,401131918	6,62E-08	2,96E-06
COL6A2	1751,980505	2,12446352	0,391644071	5,398399147	6,72E-08	3,00E-06
LINC00565	51,79099498	2,056481532	0,380334703	5,383884267	7,29E-08	3,17E-06

AC021188.1	181,0353108	1,059744646	0,197249743	5,382760231	7,34E-08	3,18E-06
ZNF683	1353,273478	2,206563322	0,407730698	5,365112229	8,09E-08	3,39E-06
HCG27	22,85714239	2,036093232	0,387623816	5,365334247	8,08E-08	3,39E-06
LINC00943	31,06372798	3,170285752	0,524871488	5,363474766	8,16E-08	3,40E-06
AC015911.11	643,1416956	1,104234871	0,207477992	5,354340959	8,59E-08	3,53E-06
RASA3	14648,7847	1,227943988	0,230592384	5,350087119	8,79E-08	3,59E-06
MXD4	4367,991898	1,008548164	0,189256948	5,34861958	8,86E-08	3,60E-06
TSPAN32	1680,349979	1,79932189	0,336957099	5,343106309	9,14E-08	3,68E-06
CARMIL3	114,0695523	2,419235059	0,442115745	5,337392111	9,43E-08	3,77E-06
AC008878.3	449,526451	1,286863372	0,24350788	5,302891786	1,14E-07	4,37E-06
DBP	1128,896084	1,281597154	0,24346066	5,294708607	1,19E-07	4,55E-06
BBS2	1317,400007	1,010588346	0,191435061	5,286580295	1,25E-07	4,69E-06
LEXM	191,9846548	1,794520893	0,34204509	5,279096728	1,30E-07	4,84E-06
ZBP1	2571,005471	1,248883048	0,237996161	5,27659424	1,32E-07	4,86E-06
ADGRG1	24045,91616	2,134403793	0,408032775	5,273768679	1,34E-07	4,92E-06
DGKD	7479,620703	1,010624725	0,191786194	5,273526694	1,34E-07	4,92E-06
KLF9	95,97313961	1,239751056	0,234357911	5,271941387	1,35E-07	4,95E-06
AL645933.3	72,22059645	1,355849793	0,256626744	5,26739582	1,38E-07	5,05E-06
LINC00299	1692,671679	1,19453555	0,22752385	5,265035978	1,40E-07	5,10E-06
PHOSPHO1	155,6505971	1,102879801	0,209418228	5,260066897	1,44E-07	5,22E-06
VASH1	473,3051921	1,054677812	0,194473484	5,257675292	1,46E-07	5,28E-06
AL365272.1	94,70735444	1,693224309	0,322038434	5,241850783	1,59E-07	5,63E-06
KDM7A	806,6152019	1,000202276	0,191750705	5,240127635	1,60E-07	5,67E-06
AC026748.1	43,85490864	2,347312926	0,472272602	5,23597803	1,64E-07	5,77E-06
AC004408.2	17,0308697	2,529599962	0,597942865	5,232422875	1,67E-07	5,85E-06
NMUR1	2270,621657	1,684435022	0,324979943	5,230283425	1,69E-07	5,91E-06
LY9	479,5011827	2,118962474	0,391487208	5,228320333	1,71E-07	5,95E-06
TSPOAP1	3229,099018	1,739234161	0,330229789	5,221416885	1,78E-07	6,12E-06

CDC42-AS1	31,27226099	1,79126482	0,358407045	5,218163321	1,81E-07	6,20E-06
AL590560.3	30,87246874	2,067096386	0,398254939	5,208159089	1,91E-07	6,44E-06
C9orf139	1590,305386	1,005446539	0,192864819	5,19139162	2,09E-07	6,92E-06
AC023908.3	109,2582264	1,041530409	0,20068853	5,186997842	2,14E-07	7,04E-06
LINC00987	56,43830273	2,101577291	0,388294364	5,160013637	2,47E-07	7,86E-06
SLC43A2	246,8527537	1,658615653	0,308859536	5,157946714	2,50E-07	7,91E-06
LINC00528	455,6077964	1,04871322	0,2034194	5,149984738	2,61E-07	8,16E-06
AC009133.1	143,5085013	1,162587828	0,223297213	5,144641867	2,68E-07	8,37E-06
ATP8A1	2191,085121	1,016084287	0,197428	5,142980308	2,70E-07	8,42E-06
SORL1	15644,15909	1,237782888	0,241760048	5,13654422	2,80E-07	8,59E-06
AC008115.3	12,80872293	1,749697322	0,341449513	5,121549903	3,03E-07	9,07E-06
TLR1	991,0522492	1,011983935	0,19931512	5,097226114	3,45E-07	1,00E-05
NME4	398,7327413	1,185412126	0,246136621	5,078882468	3,80E-07	1,08E-05
LINC02580	103,136312	1,927552183	0,381713593	5,075481389	3,87E-07	1,09E-05
FCMR	3082,195454	1,525517697	0,30064693	5,06963301	3,99E-07	1,12E-05
ADAMTS10	1817,806232	1,476035116	0,291159586	5,06860452	4,01E-07	1,12E-05
AXIN1	2828,725292	1,107000537	0,21911331	5,054831921	4,31E-07	1,19E-05
PPM1N	111,0466079	1,86650293	0,365824576	5,048706704	4,45E-07	1,22E-05
AC017104.6	281,1891744	1,924773209	0,390438273	5,043971505	4,56E-07	1,24E-05
AC084018.2	126,5141249	1,028639788	0,204398709	5,041739495	4,61E-07	1,26E-05
ADHFE1	1716,108649	1,300878706	0,261954489	5,026136826	5,00E-07	1,34E-05
CALCOCO1	8382,387021	1,036633552	0,20669138	5,018369601	5,21E-07	1,38E-05
YPEL3	5250,87534	1,182445039	0,23676953	5,002213151	5,67E-07	1,48E-05
AC020656.2	18,1122843	1,867029789	0,377135657	4,988305634	6,09E-07	1,55E-05
AC087741.1	361,5262212	1,184731562	0,240995022	4,978428649	6,41E-07	1,62E-05
ASPRV1	58,1557482	1,222666349	0,244679157	4,968705871	6,74E-07	1,69E-05
MAP2K6	110,4938357	1,232926195	0,251886494	4,966838123	6,81E-07	1,70E-05
AC245100.8	344,612282	1,124740314	0,228653101	4,952502178	7,33E-07	1,79E-05

IL13RA1	81,74065765	2,92075194	0,514790173	4,939134248	7,85E-07	1,90E-05
AC134669.1	372,670439	1,042972577	0,211665566	4,925676539	8,41E-07	1,98E-05
IFIT1	167,5701181	1,990677333	0,432179887	4,91394281	8,93E-07	2,08E-05
BTN3A1	11982,80094	1,076439364	0,219833583	4,910972132	9,06E-07	2,10E-05
C13orf46	219,4481016	1,604370654	0,343040709	4,908335023	9,19E-07	2,12E-05
IL24	14,13899697	1,829517236	0,368439861	4,904722928	9,36E-07	2,15E-05
TXNIP	87373,28167	1,198611463	0,24632488	4,892742155	9,94E-07	2,25E-05
PPP2R5C	10495,0938	1,212018087	0,248196189	4,881872109	1,05E-06	2,35E-05
PRR5-ARHGAP8	30,04910832	2,233599954	0,459502379	4,857117848	1,19E-06	2,60E-05
TRIM73	113,5137089	1,326773633	0,270785003	4,832941441	1,35E-06	2,83E-05
MST1L	35,53330089	1,843963043	0,39785379	4,826925457	1,39E-06	2,90E-05
AC009093.10	70,90865127	1,303881935	0,271860718	4,825710292	1,40E-06	2,91E-05
NR1D2	1901,099841	1,061516657	0,220954674	4,805364677	1,54E-06	3,14E-05
SLFN12L	388,6582447	1,016747552	0,212823659	4,804996628	1,55E-06	3,14E-05
DAPK2	315,8775139	2,269275673	0,46000889	4,803430519	1,56E-06	3,16E-05
AL162457.1	60,01120291	1,80702327	0,371410401	4,798244632	1,60E-06	3,22E-05
NHSL2	1708,883997	1,543158551	0,327110587	4,794206828	1,63E-06	3,27E-05
UNC5CL	93,2975135	1,57197324	0,329561404	4,788580335	1,68E-06	3,33E-05
AL162458.1	165,1223187	1,127248748	0,23570295	4,789075463	1,68E-06	3,33E-05
AC010319.1	43,13147385	1,502921542	0,313091723	4,786588652	1,70E-06	3,36E-05
DLGAP1-AS2	58,74548733	1,427003542	0,297323381	4,786150878	1,70E-06	3,36E-05
ZNF208	25,17114763	1,843243073	0,394563582	4,783253633	1,72E-06	3,40E-05
AC243829.1	40,37717938	2,533252857	0,52705675	4,780751422	1,75E-06	3,43E-05
CCDC65	186,1724057	2,427617547	0,513646417	4,779372081	1,76E-06	3,45E-05
SAT1	3820,59353	1,023904591	0,214341376	4,773329599	1,81E-06	3,52E-05
ZNF831	1478,234274	1,148277783	0,240483824	4,772403024	1,82E-06	3,53E-05
AC018809.1	30,58052564	1,127351416	0,235538174	4,758501657	1,95E-06	3,71E-05
FRMPD3	25,27426586	2,242602646	0,492422158	4,745952303	2,08E-06	3,90E-05

C1orf21	3800,709353	1,152410123	0,243213472	4,745811927	2,08E-06	3,90E-05
AC099489.1	97,36576781	1,972012994	0,414899076	4,739572019	2,14E-06	3,99E-05
PLCD1	824,4581922	1,334017381	0,282996846	4,739078882	2,15E-06	3,99E-05
SIRT4	98,34753543	1,075089499	0,227828607	4,733254327	2,21E-06	4,07E-05
AP003068.2	69,49145467	1,045748728	0,221320079	4,731441888	2,23E-06	4,09E-05
MTSS1	2929,102962	1,654146357	0,351096483	4,727358026	2,27E-06	4,15E-05
AL590560.2	120,164635	1,814906046	0,398136941	4,708077351	2,50E-06	4,48E-05
AC124016.2	116,854978	1,002133543	0,214280142	4,704480502	2,55E-06	4,54E-05
AC025279.1	104,2758127	1,381314656	0,294837335	4,703887732	2,55E-06	4,55E-05
AL773545.3	27,83370224	1,160252068	0,246928811	4,693325472	2,69E-06	4,74E-05
PSD2	17,42910173	1,849647571	0,390947834	4,681260096	2,85E-06	4,95E-05
AC023794.4	11,47496082	1,601383024	0,339309844	4,680697826	2,86E-06	4,95E-05
COLGALT2	870,3854753	1,353701533	0,298558899	4,673802619	2,96E-06	5,05E-05
ATG9B	111,1433503	1,447918986	0,316929422	4,673272382	2,96E-06	5,05E-05
FCGBP	212,86402	1,405748668	0,304885636	4,664369744	3,10E-06	5,24E-05
LINC00954	421,6966756	1,163749282	0,248363315	4,660070335	3,16E-06	5,31E-05
SULF2	74,31806132	2,635487063	0,508138654	4,656477327	3,22E-06	5,39E-05
PROX2	60,31267389	1,344959973	0,29151711	4,63502145	3,57E-06	5,86E-05
HSPA7	98,06520416	2,172463402	0,47461447	4,6257089	3,73E-06	6,05E-05
AC092070.2	271,9266929	1,044125945	0,225528349	4,625397712	3,74E-06	6,05E-05
IFT172	739,4401397	1,046835161	0,226649969	4,61768802	3,88E-06	6,22E-05
LRRN1	199,3817219	1,67634591	0,347861825	4,613286527	3,96E-06	6,30E-05
AC107884.1	149,9546605	1,098534222	0,238546131	4,607222473	4,08E-06	6,43E-05
LRFN2	17,33028618	2,70347866	0,589952673	4,602924909	4,17E-06	6,54E-05
LINC00891	99,51639127	1,211701174	0,27010786	4,596032167	4,31E-06	6,73E-05
FCGRT	188,1205837	1,714697178	0,365707243	4,593517411	4,36E-06	6,79E-05
LINC-PINT	939,3163	1,052297189	0,231429274	4,586378535	4,51E-06	6,97E-05
UNC45B	67,03005005	1,69186889	0,370619754	4,578527977	4,68E-06	7,19E-05

FCGR2B	178,910675	2,286289763	0,494827636	4,573149683	4,80E-06	7,34E-05
AC010883.2	20,891705	1,984927898	0,446983453	4,562862989	5,05E-06	7,61E-05
OPRD1	7,304310896	2,099294135	0,457757727	4,558500739	5,15E-06	7,75E-05
GPRASP1	292,3099084	1,65327553	0,351655055	4,558420211	5,15E-06	7,75E-05
PRSS40A	19,76720964	2,409698917	0,534900922	4,549321221	5,38E-06	8,02E-05
AC211476.12	52,38657243	1,113237922	0,242282423	4,548969966	5,39E-06	8,02E-05
RTCA-AS1	86,85366497	1,308702077	0,290320204	4,545842086	5,47E-06	8,10E-05
CCDC114	62,46447889	1,596195989	0,350021629	4,545020059	5,49E-06	8,12E-05
AL353748.3	22,42083074	1,620815243	0,371708927	4,53980668	5,63E-06	8,27E-05
AC015911.10	459,6133838	1,073288441	0,239562632	4,536841491	5,71E-06	8,35E-05
AP000977.1	104,011099	1,901781356	0,427486371	4,535458552	5,75E-06	8,40E-05
P2RY6	102,6792379	2,707602737	0,563857161	4,529894188	5,90E-06	8,57E-05
FRAT1	637,5847984	1,044245964	0,230046085	4,523603261	6,08E-06	8,78E-05
MAN1B1-DT	90,43292212	1,17205302	0,266235582	4,521034025	6,15E-06	8,87E-05
DLG4	58,07181287	1,200925482	0,267174539	4,506728855	6,58E-06	9,29E-05
KRT2	24,47030025	1,962531153	0,45089209	4,503145747	6,70E-06	9,42E-05
CD68	340,2825221	2,88669529	0,563558472	4,496760346	6,90E-06	9,66E-05
AC015911.8	32,80239405	1,306274083	0,294328639	4,493626462	7,00E-06	9,77E-05
TLR8	63,06937408	2,818121661	0,544355561	4,493254349	7,01E-06	9,78E-05
ZNF540	192,2027719	1,014889414	0,226165718	4,492982309	7,02E-06	9,79E-05
AC114490.1	68,7453404	1,42591301	0,315481587	4,492207674	7,05E-06	9,81E-05
ZEB2	5870,147002	1,905679567	0,428102631	4,490713028	7,10E-06	9,85E-05
SGSM1	415,2285547	1,377020187	0,307687888	4,487318345	7,21E-06	9,94E-05
HELZ2	1472,231384	1,081424223	0,242364264	4,476578523	7,58E-06	0,000102887
AC010175.1	27,9370756	1,801279253	0,435967861	4,468299007	7,88E-06	0,000105815
AZIN2	87,19863322	1,544194386	0,352785449	4,467055383	7,93E-06	0,000106216
C11orf21	3310,830889	1,394613926	0,312979942	4,45381841	8,44E-06	0,00011133
KLRC4	422,5199519	1,085847636	0,246319418	4,448547078	8,65E-06	0,000113795

AC008750.7	26,8318274	1,615791861	0,364256153	4,44163176	8,93E-06	0,000116874
SERPINA1	465,6871084	2,858234421	0,560442559	4,440305821	8,98E-06	0,00011723
AC022182.2	150,9571258	1,087910973	0,246185903	4,437422784	9,10E-06	0,000118576
RNF43	227,8255452	1,259155595	0,285216739	4,43645344	9,15E-06	0,000119033
KLRC4-KLRK1	1187,083535	1,055601882	0,244961622	4,435937577	9,17E-06	0,00011924
LINC00612	9,628627634	2,245717697	0,47550919	4,434097608	9,25E-06	0,000120027
ZNF600	6875,594315	1,157301054	0,259148588	4,428094487	9,51E-06	0,000122773
PIK3IP1	3313,24148	1,549054891	0,352505797	4,42026686	9,86E-06	0,000126646
SMTNL1	26,20968107	1,206617562	0,272854977	4,419653143	9,89E-06	0,000126924
AC010247.2	108,6006819	1,751829787	0,408572456	4,416610391	1,00E-05	0,000128474
FPR2	32,26783206	2,812957924	0,586331833	4,414977997	1,01E-05	0,000129113
TBKBP1	190,9601071	1,155598435	0,269633612	4,410544963	1,03E-05	0,000131278
FBXO32	634,638113	1,334966847	0,300758638	4,409183759	1,04E-05	0,000131915
EZH1	2760,488621	1,024724935	0,233506286	4,398972741	1,09E-05	0,000136894
MST1P2	44,49123567	1,487308001	0,338995118	4,391979895	1,12E-05	0,000140659
CERCAM	358,6930088	2,05338782	0,465546825	4,369907416	1,24E-05	0,000152669
ZNNT1	14,06611698	1,666753235	0,384730813	4,365328721	1,27E-05	0,000155134
HHIPL1	12,29385891	2,440397057	0,586643925	4,36195048	1,29E-05	0,000157065
AGBL2	172,1027624	1,091825321	0,251245593	4,342605766	1,41E-05	0,000168555
AJM1	493,903758	1,166318095	0,270096934	4,337255959	1,44E-05	0,000172086
MMP23B	565,0281546	1,426836318	0,330894457	4,336378185	1,45E-05	0,000172493
ACRBP	71,76783533	1,5565221	0,354867671	4,335078283	1,46E-05	0,000173278
LILRA1	34,58448064	2,671567669	0,590158482	4,33373998	1,47E-05	0,000173918
AC015813.2	194,8450986	1,409014415	0,321690641	4,333027371	1,47E-05	0,000174273
TNNT3	49,39452397	1,804851787	0,41390741	4,329582053	1,49E-05	0,000176365
ARHGAP8	41,14702571	1,869067694	0,391968748	4,328443884	1,50E-05	0,000176883
AC087500.1	71,25157823	1,36274409	0,313124684	4,328552407	1,50E-05	0,000176883
SIGLEC14	32,97944356	2,867917613	0,586000779	4,314342775	1,60E-05	0,0001858

GIPR	247,2273223	1,265795748	0,294605051	4,311569226	1,62E-05	0,000187271
ITPKB-IT1	11,65616568	1,94870385	0,442908753	4,304491259	1,67E-05	0,000192127
AL031432.2	48,63230437	1,149306495	0,267555358	4,303230646	1,68E-05	0,000192889
FCN1	240,7170617	2,239097406	0,572694685	4,300606497	1,70E-05	0,000194625
AC241377.4	88,72225019	1,163268268	0,257997161	4,29405576	1,75E-05	0,000199312
SMARCD3	82,5657991	1,061315237	0,245133676	4,290751423	1,78E-05	0,000201632
CHI3L1	105,0187819	2,764764411	0,561411352	4,290005909	1,79E-05	0,000202171
CXCL9	1631,844563	3,019144376	0,567702029	4,286376323	1,82E-05	0,000205034
CCL4L2	2083,779693	1,332132681	0,317476168	4,280361404	1,87E-05	0,000209541
AL109955.1	56,45528254	1,22339593	0,287083275	4,280156044	1,87E-05	0,000209541
AC012020.1	150,8591323	1,13377389	0,262738046	4,279761268	1,87E-05	0,000209791
AC117503.5	55,09409353	1,086407585	0,258588869	4,27956127	1,87E-05	0,00020986
CLEC10A	73,08940149	2,590400054	0,552820393	4,271991036	1,94E-05	0,000215653
DLEC1	189,4312435	1,269736394	0,295617882	4,270105333	1,95E-05	0,000217241
LAX1	1875,573381	1,124027965	0,265052092	4,269530701	1,96E-05	0,000217679
MTMR9LP	120,9932721	1,196541494	0,279272188	4,250639616	2,13E-05	0,000233348
AC008555.1	65,24832511	1,529956752	0,355594055	4,24861174	2,15E-05	0,00023508
AL031432.4	52,55290791	1,406199828	0,328327625	4,248006873	2,16E-05	0,000235456
ERBB2	2779,98432	1,771240615	0,422205266	4,237211366	2,26E-05	0,00024371
IFIT3	988,5316983	1,879000492	0,446826736	4,225013506	2,39E-05	0,000253305
ST3GAL5-AS1	15,98539508	1,361023574	0,322771102	4,225133523	2,39E-05	0,000253305
AC015911.7	168,4716196	1,194825632	0,286871494	4,221939215	2,42E-05	0,000255829
NLRC4	20,05947594	2,21351362	0,491287507	4,221693233	2,42E-05	0,000255972
C1QB	392,594276	2,765195687	0,57671314	4,217893765	2,47E-05	0,000259494
NSG1	213,3118137	2,151324676	0,465034021	4,200775413	2,66E-05	0,000275964
SBK1	2498,439639	1,486623003	0,352244724	4,198557899	2,69E-05	0,000278098
CETP	25,78379367	1,520827665	0,34856314	4,197411794	2,70E-05	0,000279071
MORN3	119,5276288	1,181763759	0,283665883	4,196401452	2,71E-05	0,000280027

SNX29P2	64,91047058	1,145671423	0,271929173	4,192631513	2,76E-05	0,000283689
AC022382.2	13,66233815	1,420709546	0,337932477	4,192213526	2,76E-05	0,000283842
U73169.1	44,52090523	1,071515801	0,256254032	4,191664825	2,77E-05	0,000284017
OR52N4	23,66026102	1,561418814	0,377858277	4,175564778	2,97E-05	0,000300827
NF1	645,8109695	1,044720041	0,252128524	4,164946871	3,11E-05	0,000311834
ZNF528-AS1	80,98846976	1,268779464	0,305086055	4,161081028	3,17E-05	0,000315726
C9orf163	18,5394897	1,187612285	0,286313822	4,159935506	3,18E-05	0,000316677
TET1	95,91593596	1,087796479	0,269314783	4,154274202	3,26E-05	0,000323323
CEBPA	273,3535858	1,693595605	0,383895284	4,152059581	3,29E-05	0,000325817
LGALS2	79,70384392	3,037782072	0,581743211	4,146918286	3,37E-05	0,0003314
SIRPA	69,69050234	2,514324763	0,548528424	4,145239844	3,39E-05	0,000333341
PLXDC1	148,4655896	1,737290221	0,37078693	4,143083583	3,43E-05	0,000335165
MAFB	77,03530969	2,44252124	0,582044745	4,14144348	3,45E-05	0,000337238
MARCKS	50,14277391	2,558047711	0,565758684	4,132939356	3,58E-05	0,000347048
LINC02384	974,945981	1,646170751	0,423241969	4,128697116	3,65E-05	0,000351807
AL160313.2	18,36002482	1,9082612	0,443445282	4,127559352	3,67E-05	0,000353379
TCAF2P1	90,61487765	1,196699269	0,344802197	4,118903513	3,81E-05	0,000364591
PER3	406,3538786	1,176375143	0,286096826	4,117082009	3,84E-05	0,000367152
ARHGEF25	12,10795433	1,523866138	0,369421632	4,11067572	3,95E-05	0,000375858
AC010894.5	15,68235509	1,429634561	0,352352394	4,104378682	4,05E-05	0,000384238
AC138150.2	20,99619197	1,611050011	0,395209006	4,096971637	4,19E-05	0,000394637
AC008033.3	24,92576769	1,644614108	0,439318701	4,090677198	4,30E-05	0,000403584
S1PR1	5902,533667	1,650275277	0,405233926	4,089638087	4,32E-05	0,000404631
AC010332.3	220,6792336	1,18054779	0,287886468	4,087329077	4,36E-05	0,000408292
AL732406.1	25,77180853	2,525015641	0,595819635	4,082382507	4,46E-05	0,000416102
ZEB2-AS1	20,92822888	2,041743092	0,543004141	4,078380522	4,54E-05	0,000421781
A2M	46,10435988	1,855720802	0,465311273	4,077395203	4,55E-05	0,000422936
C1QA	275,1619046	2,666743726	0,577682916	4,072474985	4,65E-05	0,000430965

ALDH2	138,8625881	2,151838446	0,478658617	4,07101691	4,68E-05	0,00043319
LINC00469	44,735068	2,329501796	0,595299585	4,066003525	4,78E-05	0,000440019
ABTB1	3730,092258	1,015826688	0,250840392	4,060212195	4,90E-05	0,000450033
TGFBI	240,632952	2,378503177	0,564127078	4,04868559	5,15E-05	0,000466731
HEXD-IT1	99,19477023	1,606417503	0,393003783	4,047096326	5,19E-05	0,000468839
SECTM1	210,7848666	2,539037872	0,566820489	4,038806098	5,37E-05	0,00048264
FCGR1B	32,76756643	2,529744718	0,598428639	4,038521574	5,38E-05	0,000483007
HCK	238,8229275	2,62929151	0,577984795	4,036712715	5,42E-05	0,000485864
AL627422.2	7,307006393	2,088340758	0,579863734	4,033784066	5,49E-05	0,000491075
TMEM132C	15,95285903	2,113240572	0,570097812	4,028123874	5,62E-05	0,000499218
INGX	56,6903233	1,013427798	0,252357648	4,024988721	5,70E-05	0,000503984
AC011468.5	33,83511075	1,00624306	0,25045443	4,02197368	5,77E-05	0,000508793
CCL5	26076,1303	1,350996157	0,338240824	4,018892107	5,85E-05	0,000513853
DNAH10OS	40,39125171	1,458902435	0,369652043	4,017319822	5,89E-05	0,00051619
LITAF	23187,8389	1,162951381	0,291672676	4,00566205	6,18E-05	0,000536211
AC006252.1	52,37109194	1,009691775	0,250258005	4,004858797	6,21E-05	0,000537282
CTSL	74,21962201	2,454853756	0,540016838	4,001871625	6,28E-05	0,000542219
Z97989.1	67,93343703	1,135059575	0,283732596	3,995354494	6,46E-05	0,00055494
SNPH	180,8298809	1,253589867	0,315616339	3,994005513	6,50E-05	0,000557626
LINC00896	28,77510339	1,411251209	0,353359802	3,991520666	6,57E-05	0,000562285
PLBD1	20,7191469	2,333156757	0,597824193	3,990912588	6,58E-05	0,000563
AC009093.8	58,26159984	2,08156925	0,511004232	3,989005573	6,64E-05	0,000566811
SYNGR1	567,9251608	1,927252588	0,483645475	3,98663967	6,70E-05	0,000571506
AC099521.3	4,465709563	1,915216771	0,507221182	3,985714789	6,73E-05	0,00057349
LINC00243	64,48078132	1,561970772	0,389064624	3,985374808	6,74E-05	0,000574066
AC092636.2	7,528712191	2,192861718	0,592925011	3,98377413	6,78E-05	0,000577452
AC002316.1	1373,011225	1,781229551	0,444075125	3,979749852	6,90E-05	0,000585806
AMY2B	265,8743418	1,086094794	0,269209238	3,977767361	6,96E-05	0,000589217

EFNA1	14,24715828	1,423949984	0,353903706	3,976513335	6,99E-05	0,000591301
AL592295.4	142,3120406	1,031011265	0,262967147	3,973726899	7,08E-05	0,000595923
LSMEM1	18,07762195	1,192849374	0,300746055	3,970909637	7,16E-05	0,000601029
CD4	240,2007002	2,606279363	0,593337825	3,96790605	7,25E-05	0,000606599
C1QC	207,6228252	2,627950954	0,578340915	3,966688121	7,29E-05	0,000608936
AGPAT4	825,0728962	1,142423688	0,292463785	3,951534591	7,77E-05	0,000641791
NPC1	6856,804572	1,1169577	0,283898687	3,951619429	7,76E-05	0,000641791
SSBP3-AS1	83,55414745	1,35851243	0,348467799	3,949429756	7,83E-05	0,000645846
SPTBN5	56,12225854	1,790237666	0,449479988	3,94387235	8,02E-05	0,000658542
LRRC25	99,37734494	2,366414987	0,554275373	3,943665224	8,02E-05	0,000658838
MGAM2	16,39325032	2,038434496	0,600942011	3,936225634	8,28E-05	0,000675674
LIPC	100,0814985	1,466979253	0,372709729	3,932402949	8,41E-05	0,000684541
PRR5L	5668,248956	1,120823026	0,286527703	3,922323325	8,77E-05	0,000708018
LYZ	2603,852795	2,274736707	0,559041505	3,921639446	8,79E-05	0,000709165
AL445228.3	17,73035404	1,353675163	0,341398838	3,910800302	9,20E-05	0,000734566
CCDC183	36,65153314	1,398895017	0,37414863	3,902339346	9,53E-05	0,000753179
LINC00921	253,0803091	1,17283326	0,298308603	3,900763022	9,59E-05	0,000757195
AC106782.1	18,21332579	1,688685299	0,428966603	3,89942032	9,64E-05	0,000759893
PLIN1	28,93255006	1,540497579	0,401704587	3,892711527	9,91E-05	0,000778133
AC108704.2	273,4213432	1,200214784	0,31201904	3,891357084	9,97E-05	0,000781872
LILRB2	146,8986618	2,51266224	0,5753606	3,87920882	0,000104797	0,000813637
FAM110C	211,470031	1,787405297	0,45720726	3,879197894	0,000104801	0,000813637
COL6A4P2	11,74889994	1,809747089	0,570450663	3,86995067	0,000108857	0,000839866
AC092117.1	95,12539326	1,010526045	0,260581465	3,861426274	0,000112727	0,000863341
AC107375.1	27,79797232	1,208929691	0,315845007	3,849790212	0,000118219	0,000896747
H2AC3P	7,187114823	1,946149143	0,495613703	3,846985969	0,00011958	0,000904992
FCGR1A	120,6255376	2,35160559	0,598788438	3,846140739	0,000119993	0,000907772
CARNS1	481,2979576	1,02262037	0,26340231	3,842597591	0,000121739	0,00091818

MAP3K6	269,7151428	1,021393561	0,265297573	3,837253772	0,000124418	0,000934477
AC067945.4	14,57270036	1,306885021	0,34569316	3,83336978	0,0001264	0,000946495
ITGA5	7566,222291	1,017538868	0,267460512	3,82982707	0,000128233	0,000956795
HSD11B1-AS1	10,3404823	1,498716783	0,39565234	3,829069372	0,000128629	0,000958948
AC009951.4	24,76922044	1,812496874	0,465994527	3,826523032	0,000129966	0,000965545
ADAMTS6	6,127241271	2,131827374	0,582871238	3,824732893	0,000130914	0,000971133
SERPING1	254,6799424	2,48752146	0,58399494	3,820698331	0,000133074	0,000984581

1312

1313

Table 4. List of NK cell signature genes used in this study (from *(48)*), Related to Fig. 7A-D, fig. S9E

Name	Gene symbols
NK cell signature	NCR3, KLRB1, PRF1, CD160, NCR1

Supplementary information

Fig. S1. IL-33 in combination with IL-12 strongly activates NK cell secretory and cytotoxic functions

(A-C) Quantification of IFN-γ secretion by healthy donors' blood NK cells upon stimulation with IL-33, IL-18, IL-1α or IL-1β alone (10 ng/mL) or in combination with **(A)** IL-15 (10 ng/mL), IL-2 (500 UI/mL), IFN-α (500 UI/mL), **(B)** anti-NKp30 (1 μg/mL), anti-NKp46 (1 μg/mL) agonistic antibodies or **(C)** K562 target cells for 24 h. Histogram bars represent the median (n = 4 individual experiments). Friedman test with Dunn's multiple comparisons test was performed.

(D-G) Healthy donors' blood NK cells were isolated from the blood of healthy donors and activated for 24 h with IL-33, IL-18, IL-1α or IL-1β (0.1 to 100 ng/mL of each) alone or in combination with **(d)** IL-12 (10 ng/mL), **(E)** IL-2 (500 UI/mL), **(F)** IL-15 (10 ng/mL) or **(G)** IFN-α (500 UI/mL) prior to supernatant collection and IFN-γ quantification by ELISA. Results are expressed as mean +/- SEM (n = 4 to 8 individual experiments). One-way ANOVA with Tukey's multiple comparisons test was performed for each cytokine concentration from 1 ng/mL.

(H) Healthy donors' blood NK cells were activated as described above and supernatants were collected at several time points prior to IFN-γ quantification by ELISA (n = 1).

(I) Healthy donors' blood NK cells were activated with indicated cytokines (10 ng/mL for each cytokine) for 24 h and co-cultured with calcein-loaded K562 target cells for 4 h at indicated effector to target ratios. Calcein release in the supernatant was quantified by fluorometry to calculate lysis percentage. Results are expressed as mean +/- SEM (n = 3 individual experiments).

(J) Healthy donors' blood NK cells activated with indicated cytokines (10 ng/mL for each cytokine) for 24 h were exposed to K562 cells in a direct cytotoxic assay. Percentage of CD107+ NK cells are shown. Results are expressed as mean + SEM (n = 2 individual experiments).

Fig. S2. IL-12 induces ST2 expression on a subset of NK cells in a STAT4-dependent manner

Healthy donors' blood NK cells were activated as indicated (10 ng/mL of each cytokine).

(A) Healthy donors' blood NK cells were activated by different cytokine combinations in the presence of anti-ST2 (10 μg/mL), anti-IL-18 (1 μg/mL), control mIgG1 antibodies (1 or 10 μg/mL as control for anti-IL-18 or anti-ST2, respectively) or IL-1RA antagonist (100 ng/mL). Supernatants were collected after 24 h and IFN-γ secretion was quantified by ELISA. Results are expressed as mean + SD and are representative of three individual experiments. Two-way ANOVA with Tukey's multiple comparisons test was performed.

(B) *IL1RL1/ST2* and *IL1RAcP* relative mRNA expression was analyzed by RT-qPCR at indicated times. Results are expressed as mean + SD and are representative of two individual experiments. Two-way ANOVA with Tukey's multiple comparisons test was performed.

(C) NK cells were treated or not with lisofylline (500 μM) for 24 h prior to activation with IL-12 (0.1 to 10 ng/mL) for 5 min and p-STAT4 intracellular levels were analyzed by flow cytometry (n = 3 individual experiments).

(D) *In silico* analysis of putative STAT4 binding sites in *ST2* promoter region. Dissimilarity indicates the deviation between the identified sequence and the STAT4 consensus binding site. RE and RE query values indicate the probability to randomly finding the motif respectively considering a model with equiprobability of the four nucleotides and a model with the same nucleotide frequency as the query sequence. A value of 0.001 means that the hit is only expected to occur by chance once in 1 Mb of sequence.

Fig. S3. IL-33 preferentially activates a subset of CD56^{dim} NK cells

(A) Healthy donors' blood NK cells were activated with IL-12 (10 ng/mL) or not (medium) for 5 min and p-STAT4 intracellular levels were analyzed by flow cytometry on gated CD56^{bright} vs CD56^{dim} subsets. Data are representative of three individual experiments.

(B) FACS-sorted CD56^{bright} and CD56^{dim} healthy donors' blood NK cells were activated with medium or IL-12 alone for 24 h prior to the addition of IL-33, IL-18, IL-1α or IL-1β, supplemented or not with IL-12. Each cytokine was used at 10ng/mL. p38 (MAPK) and S6 (mTOR) phosphorylation as analyzed 5 min

or 1 h after the addition of IL-1 family cytokines, respectively. Representative histogram plots (left) and quantification (%) (right) of p-p38^{+} or p-S6^{+} NK cells after cytokine activation. Histogram bars indicate the median. Two-way ANOVA with Bonferroni's multiple comparisons test was performed; n = 4 to 5 experiments.

(C) Healthy donors' blood NK cells were activated as indicated for 24 h, each cytokine was used at 10 ng/mL. CD69 surface and IFN-γ intracellular expression was analyzed by flow cytometry. CD56 surface expression levels were used to discriminate CD56^{bright} and CD56^{dim} NK cells. Representative dot plots (left) and quantification (%) (right) of CD69^{+} IFN-γ^{+} NK cells after cytokine activation. Histogram bars indicate the median. Two-way ANOVA test with Bonferroni's multiple comparisons test was performed; n = 4 experiments.

Fig. S4. ST2^{+} NK cells display a unique gene signature compared to CD56^{bright} and CD56^{dim} NK cells

(A) Heatmap representing all differentially-expressed genes (upregulated and downregulated) (n=2399 genes) in each sorted healthy donors' blood NK cell subset compared to the two other subsets following IL-12 activation (n = 3 individual donors).

(B) Expression levels of DEG (up and down) presented in heatmap in Fig. 3E.

Fig. S5. Unsupervised clustering of sc-RNAseq datasets

UMAP plots of NK cells clusters annotated from human melanoma metastases (GSE139249) *(42)* and mouse lung tumors (GSE123534) *(43)* sc-RNAseq public datasets.

Fig. S6. Gating strategy to identify NK cells in tumor cell suspensions by flow cytometry

(A) Tumor cell suspensions were stained for CD45, CD3, CD56, and CD7 expression and tumor-infiltrating NK cells were identified using gating strategy as illustrated. Cell viability was determined using Zombie dye (Biolegend).

(B) Cell suspensions were obtained from fresh breast tumors to analyze NK cell frequency among total infiltrating cells by flow cytometry according to BC molecular types (n = 46 patients). Kruskal Wallis test with Dunn's multiple comparisons test was performed.

Fig. S7 | IL-12 sensitizes mouse splenic NK cells to the production of IFN-γ in response to IL-33

(A) Splenic cells were activated with IL-12 (20 ng/mL) or not for 24 h prior to flow cytometry analysis of ST2 surface expression (black line) or corresponding isotypic control (grey). CD45, NK1.1, and CD3 were used to identify NK cells. Representative histogram plots (left) and quantification (%) (right) of $ST2^+$ NK cells after medium or IL-12 culture. Horizontal bars represent the mean + SEM (n = 4 individual mice). Paired two-tailed Student's *t*-test was performed.

(B) Splenic cells were activated as indicated (20 ng/mL of each cytokine) for 24 h prior to flow cytometry analysis of IFN-γ intracellular expression. CD45, NK1.1, and CD3 were used to identify NK cells. Plots are representative of four individual experiments with 3 to 4 mice/experiment and results for each individual mouse are presented in the right panel. Results are expressed as mean + SEM. One-way repeated measures ANOVA with Tukey's multiple comparisons test was performed.

Fig. S8. Antitumoral effect of IL-33 and IL-12 combination is dependent on NK cells in *Rag2*-KO mice

(A) *Rag2*-KO mice were injected intra-peritoneally with NaCl or anti-NK1.1 depleting antibody prior to intra-mammary injection with $2.5x10^5$ E0771 cells on day 0 and then treated in the tumor area with NaCl or a combination of 10 ng/mouse rmIL-12 and 100 ng/mouse rmIL-33 twice a week from day 2 to day 23. Primary tumor growth was monitored in non-depleted *Rag2*-KO mice treated with NaCl (n = 3) or with rmIL-12 and rmIL-33 combination (n = 3) or in NK cell-depleted WT mice treated with NaCl (n = 3) or with rmIL-12 and rmIL-33 combination (n=4). Two-way ANOVA with Tukey's multiple comparisons test was performed.

(B) Kaplan-Meier survival plots of non-depleted *Rag2*-KO mice treated with NaCl (n = 3) or with rmIL-12 and rmIL-33 combination (n = 3) or in NK cell-depleted WT mice treated with NaCl (n = 3) or with

rmIL-12 and rmIL-33 combination (n=4). Mice were sacrificed when longest side of primary tumor reached 17 mm. Log-rank test was performed and the p-value is indicated for non-depleted mice treated with rmIL-12 + rmIL-33 vs NK cell-depleted mice treated with rmIL-12 + rmIL-33.

(C) Serum was retrieved from blood collected at day 5, 4hrs after NaCl or cytokine injection into the peritumoral area. IFN-γ concentration was measured by ELISA in the serum of non-depleted *Rag2*-KO mice treated with NaCl (n = 3) or with rmIL-12 and rmIL-33 combination (n = 3) or in NK cell-depleted WT mice treated with NaCl (n = 3) or with rmIL-12 and rmIL-33 combination (n = 4). Histogram bars represent the median. Kruskal Wallis test with Dunn's multiple comparisons test was performed.

Fig. S9. IL-33 is associated with increased overall patient survival for several cancers

(A) Summary of p-values associated with the log rank test performed to evaluate prognostic value of *IL33* and *IL1RL1* (ST2) in 32 human TCGA cancer data sets (the same as in Fig. 6A, MESO: Mesothelioma ; UVM: Uveal Melanoma were added). Data are represented as a bubble map showing positive (green) or negative (red) impact on progression-free survival. Dots size represents p-values obtained by log-rank test.

(B) Patients from TCGA database were stratified as high or low for *IL33* and progression-free survival was analyzed in all cancer data sets. Kaplan-Meier survival curves for ACC, BRCA, KIRP, LIHC, SKCM, THCA, and UCEC patients are represented and p-values were obtained with log-rank test.

(C) Patients from TCGA database were stratified as high or low for *IL1RL1* (ST2) and progression-free survival was analyzed in all cancer data sets. Kaplan-Meier survival curves for BRCA, KIRC, KIRP, LIHC, and UVM patients are represented and p-values were obtained with log-rank test.

(D) Multivariate Cox analysis of *IL33* impact on prognosis in breast cancers from TCGA dataset regarding the age, molecular subtype, and stage of the tumors p-values were obtained with log-rank test.

(E) Kaplan-Maier curves for progression-free survival for $NK^{high}/IL33^{high}$, $NK^{high}/IL33^{low}$ and $NK^{low}/IL33^{high}$ scores as compared to $NK^{low}/IL33^{low}$ in cancer datasets from TCGA that showed statistical significance in Fig. 7B. p-values were obtained with log-rank test.

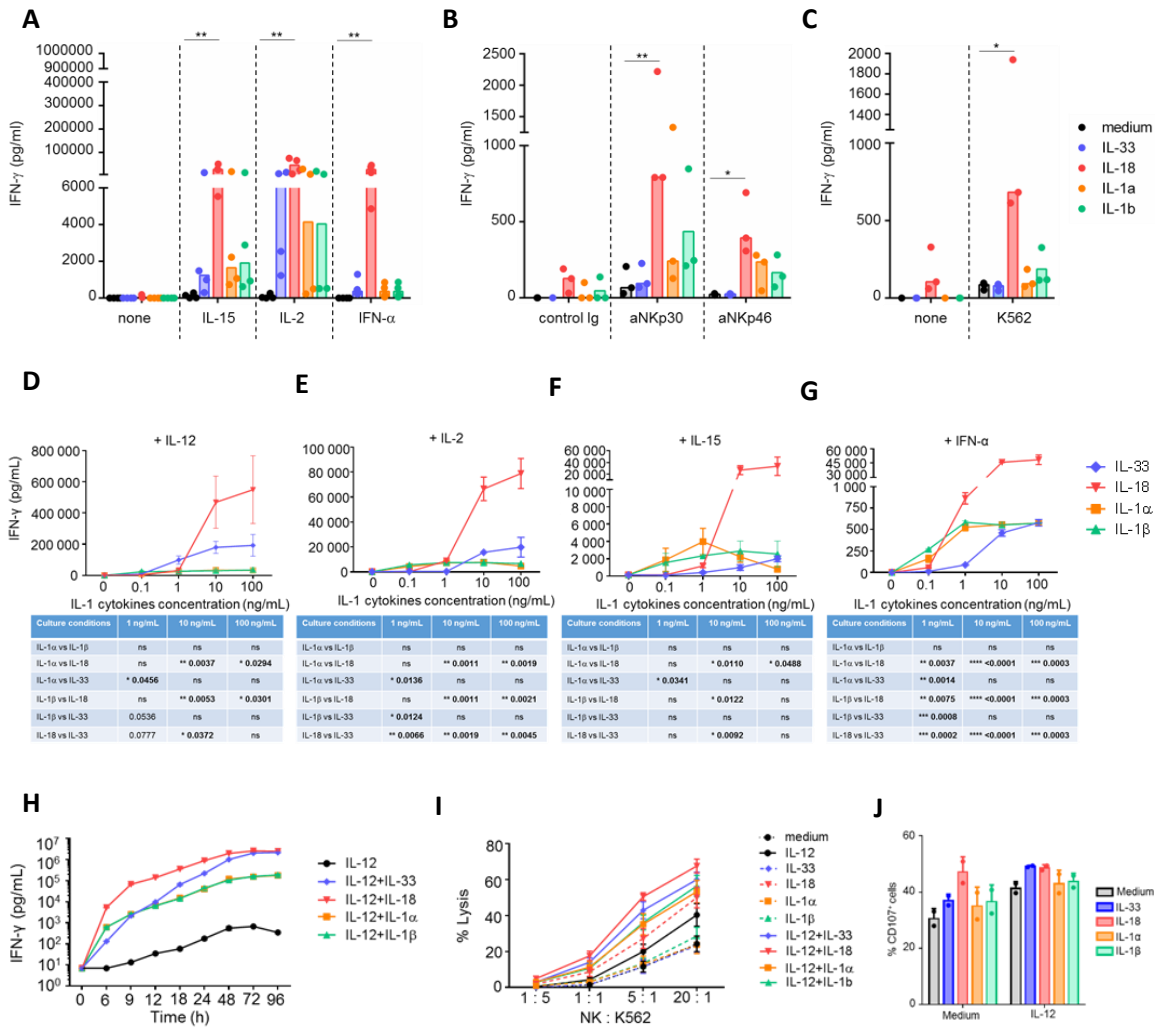

132

133 **Fig. S1. IL-33 in combination with IL-12 strongly activates NK cell secretory and cytotoxic functions**

134 **(A-C)** Quantification of IFN-γ secretion by healthy donors' blood NK cells upon stimulation with IL-33, IL-18, IL-1α

135 or IL-1β alone (10 ng/mL) or in combination with **(A)** IL-15 (10 ng/mL), IL-2 (500 UI/mL), IFN-α (500 UI/mL), **(B)**

136 anti-NKp30 (1 µg/mL), anti-NKp46 (1 µg/mL) agonistic antibodies or **(C)** K562 target cells for 24 h. Histogram bars

137 represent the median (n = 4 individual experiments). Friedman test with Dunn's multiple comparisons test was

138 performed.

139 **(D-G)** Healthy donors' blood NK cells were isolated from the blood of healthy donors and activated for 24 h with

140 IL-33, IL-18, IL-1α or IL-1β (0.1 to 100 ng/mL of each) alone or in combination with **(D)** IL-12 (10 ng/mL), **(E)** IL-2

141 (500 UI/mL), **(F)** IL-15 (10 ng/mL) or **(G)** IFN-α (500 UI/mL) prior to supernatant collection and IFN-γ quantification

142 by ELISA. Results are expressed as mean +/- SEM (n = 4 to 8 individual experiments). One-way ANOVA with

143 Tukey's multiple comparisons test was performed for each cytokine concentration from 1 ng/mL.

(H) Healthy donors' blood NK cells were activated as described above and supernatants were collected at several time points prior to IFN-γ quantification by ELISA (n = 1).

(I) Healthy donors' blood NK cells were activated with indicated cytokines (10 ng/mL for each cytokine) for 24 h and co-cultured with calcein-loaded K562 target cells for 4 h at indicated effector to target ratios. Calcein release in the supernatant was quantified by fluorometry to calculate lysis percentage. Results are expressed as mean +/- SEM (n = 3 individual experiments).

(J) Healthy donors' blood NK cells activated with indicated cytokines (10 ng/mL for each cytokine) for 24 h were exposed to K562 cells in a direct cytotoxic assay. Percentage of CD107+ NK cells are shown. Results are expressed as mean + SEM (n = 2 individual experiments).

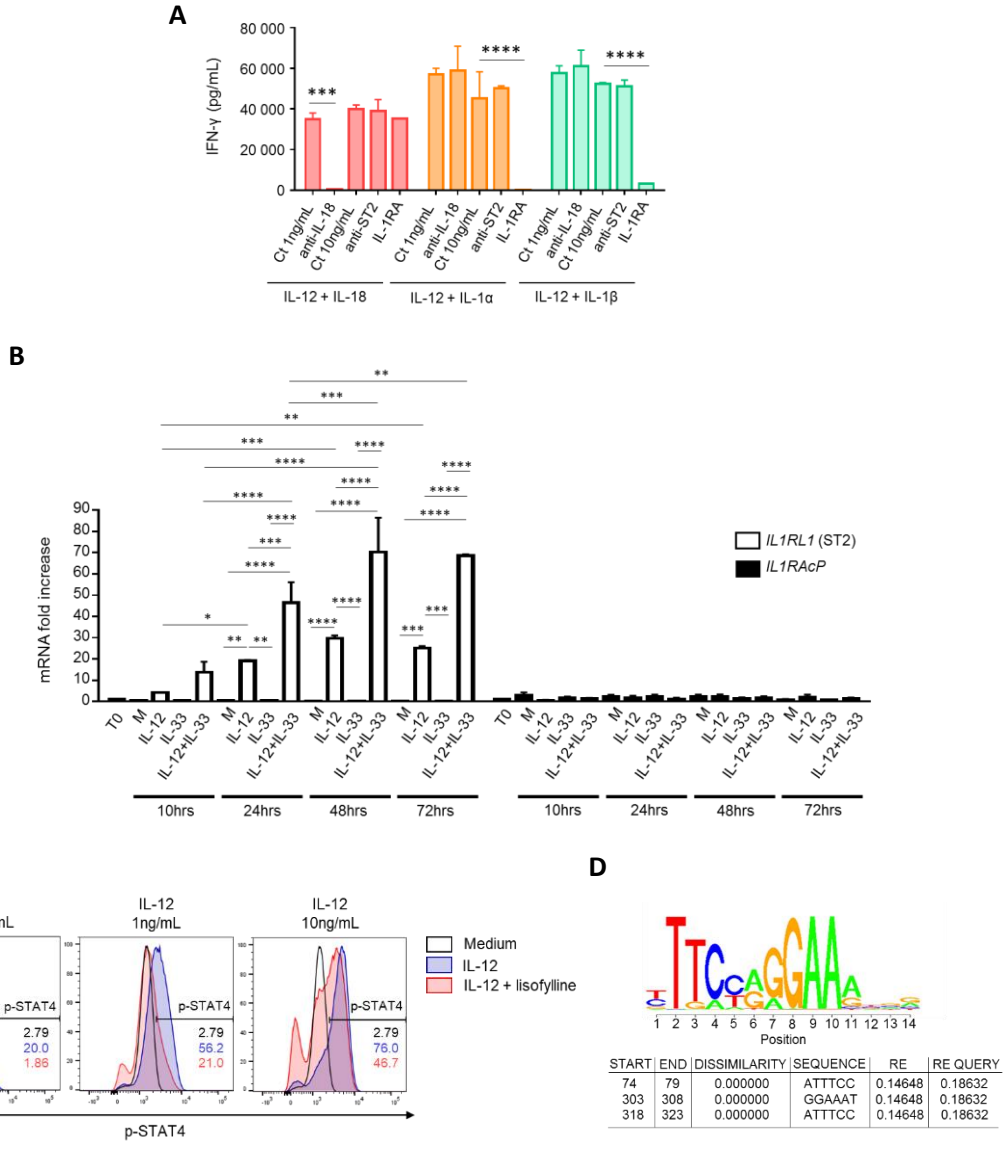

Fig. S2. IL-12 induces ST2 expression on a subset of NK cells in a STAT-4-dependent manner

Healthy donors' blood NK cells were activated as indicated (10 ng/mL of each cytokine).

(A) Healthy donors' blood NK cells were activated by different cytokine combinations in the presence of anti-ST2 (10 µg/mL), anti-IL-18 (1 µg/mL), control mIgG1 antibodies (1 or 10 µg/mL as control for anti-IL-18 or anti-ST2, respectively) or IL-1RA antagonist (100 ng/mL). Supernatants were collected after 24 h and IFN-γ secretion was quantified by ELISA. Results are expressed as mean + SD and are representative of three individual experiments. Two-way ANOVA with Tukey's multiple comparisons test was performed.

(B) *IL1RL1/ST2* and *IL1RAcP* relative mRNA expression was analyzed by RT-qPCR at indicated times. Results are expressed as mean + SD and are representative of two individual experiments. Two-way ANOVA with Tukey's multiple comparisons test was performed.

(C) NK cells were treated or not with lisofylline (500 μM) for 24 h prior to activation with IL-12 (0.1 to 10 ng/mL) for 5 min and p-STAT4 intracellular levels were analyzed by flow cytometry (n = 3 individual experiments). **(D)** *In silico* analysis of putative STAT-4 binding sites in *ST2* promoter region. Dissimilarity indicates the deviation between the identified sequence and the STAT-4 consensus binding site. RE and RE query values indicate the probability to randomly finding the motif respectively considering a model with equiprobability of the four nucleotides and a model with the same nucleotide frequency as the query sequence. A value of 0.001 means that the hit is only expected to occur by chance once in 1 Mb of sequence.

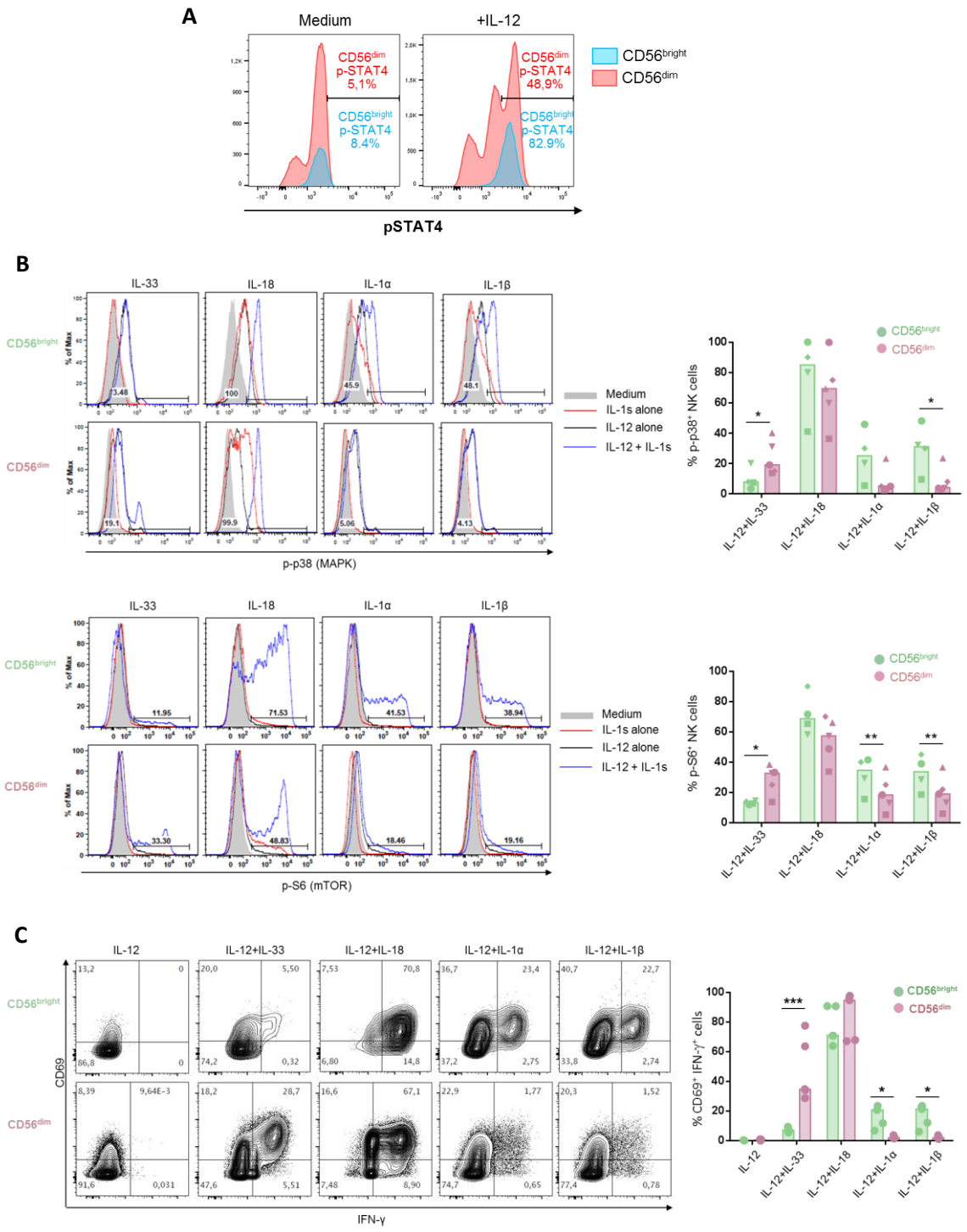

Fig. S3. IL-33 preferentially activates a subset of CD56^{dim} NK cells

(A) Healthy donors' blood NK cells were activated with IL-12 (10 ng/mL) or not (medium) for 5 min and p-STAT-4 intracellular levels were analyzed by flow cytometry on gated CD56^{bright} vs CD56^{dim} subsets. Data are representative of three individual experiments.

(B) FACS-sorted CD56^{bright} and CD56^{dim} healthy donors' blood NK cells were activated with medium or IL-12 alone for 24 h prior to the addition of IL-33, IL-18, IL-1α or IL-1β, supplemented or not with IL-12. Each cytokine was used at 10ng/mL. p38 (MAPK) and S6 (mTOR) phosphorylation as analyzed 5 min or 1 h after the addition of IL-1 family cytokines, respectively. Representative histogram plots (left) and quantification (%) (right) of p-p38^{+} or p-S6^{+} NK cells after cytokine activation. Histogram bars indicate the median. Two-way ANOVA with Bonferroni's multiple comparisons test was performed; n = 4 to 5 experiments.

(C) Healthy donors' blood NK cells were activated as indicated for 24 h, each cytokine was used at 10 ng/mL. CD69 surface and IFN-γ intracellular expression was analyzed by flow cytometry. CD56 surface expression levels were used to discriminate CD56^{bright} and CD56^{dim} NK cells. Representative dot plots (left) and quantification (%) (right) of CD69^{+} IFN-γ^{+} NK cells after cytokine activation. Histogram bars indicate the median. Two-way ANOVA test with Bonferroni's multiple comparisons test was performed; n = 4 experiments.

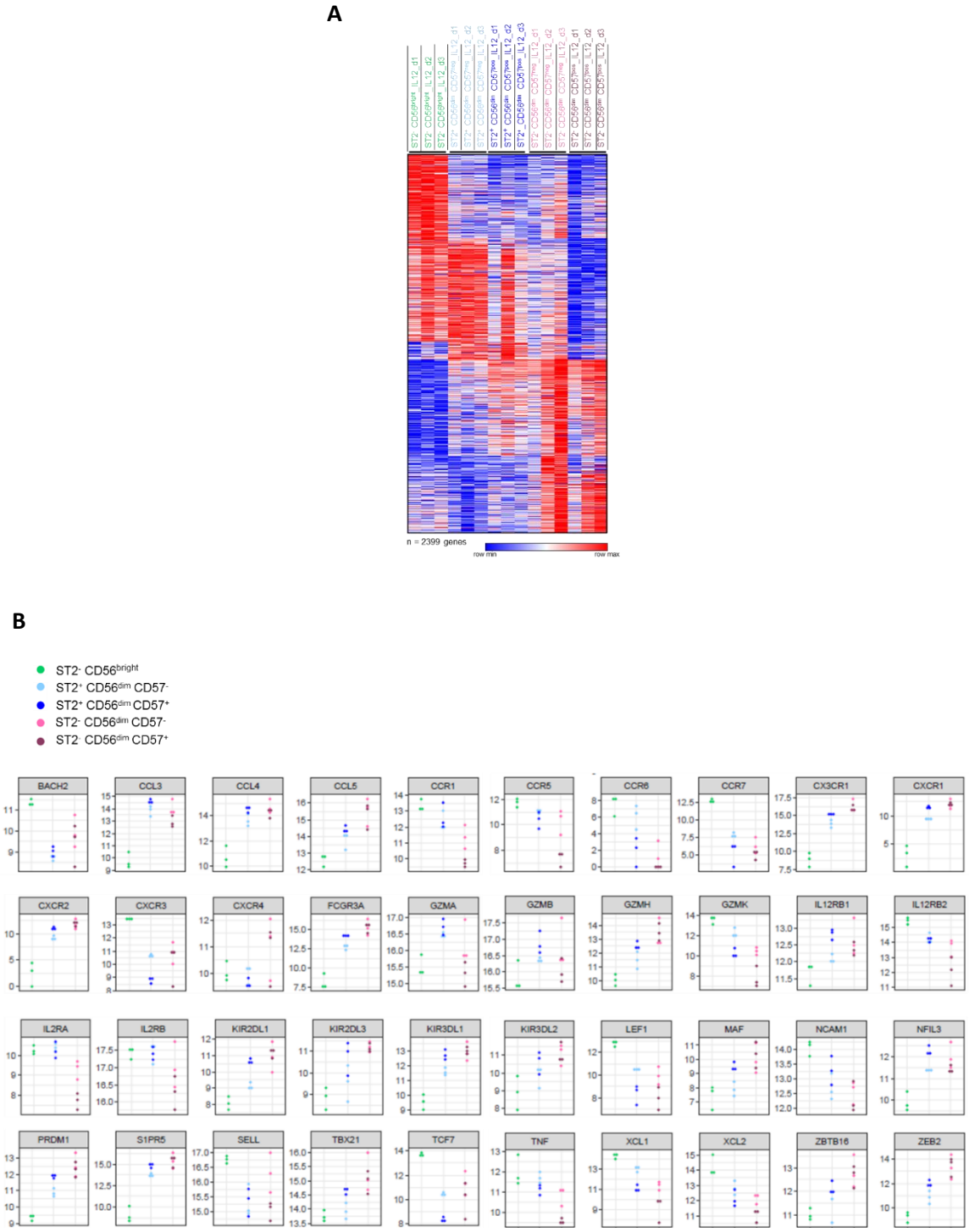

Fig. S4. ST2^{+} NK cells display a unique gene signature compared to CD56^{bright} and CD56^{dim} NK cells

(A) Heatmap representing all differentially-expressed genes (upregulated and downregulated) (n=2399 genes) in each sorted healthy donors' blood NK cell subset compared to the two other subsets following IL-12 activation (n = 3 individual donors).

(B) Expression levels of DEG (up and down) presented in heatmap in Fig. 3E.

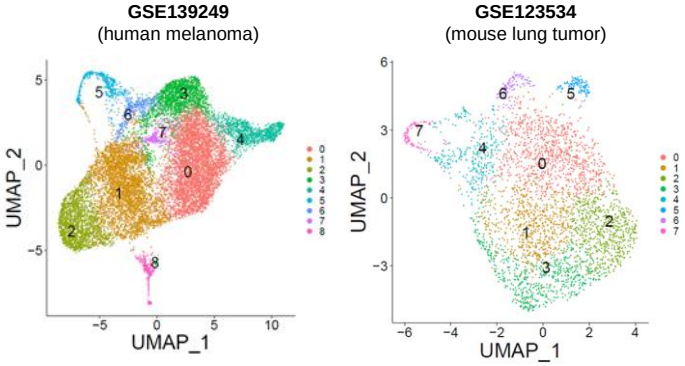

Fig. S5. Unsupervised clustering of sc-RNAseq datasets

UMAP plots of NK cells clusters annotated from human melanoma metastases (GSE139249) *(42)* and mouse lung tumors (GSE123534) *(43)* sc-RNAseq public datasets.

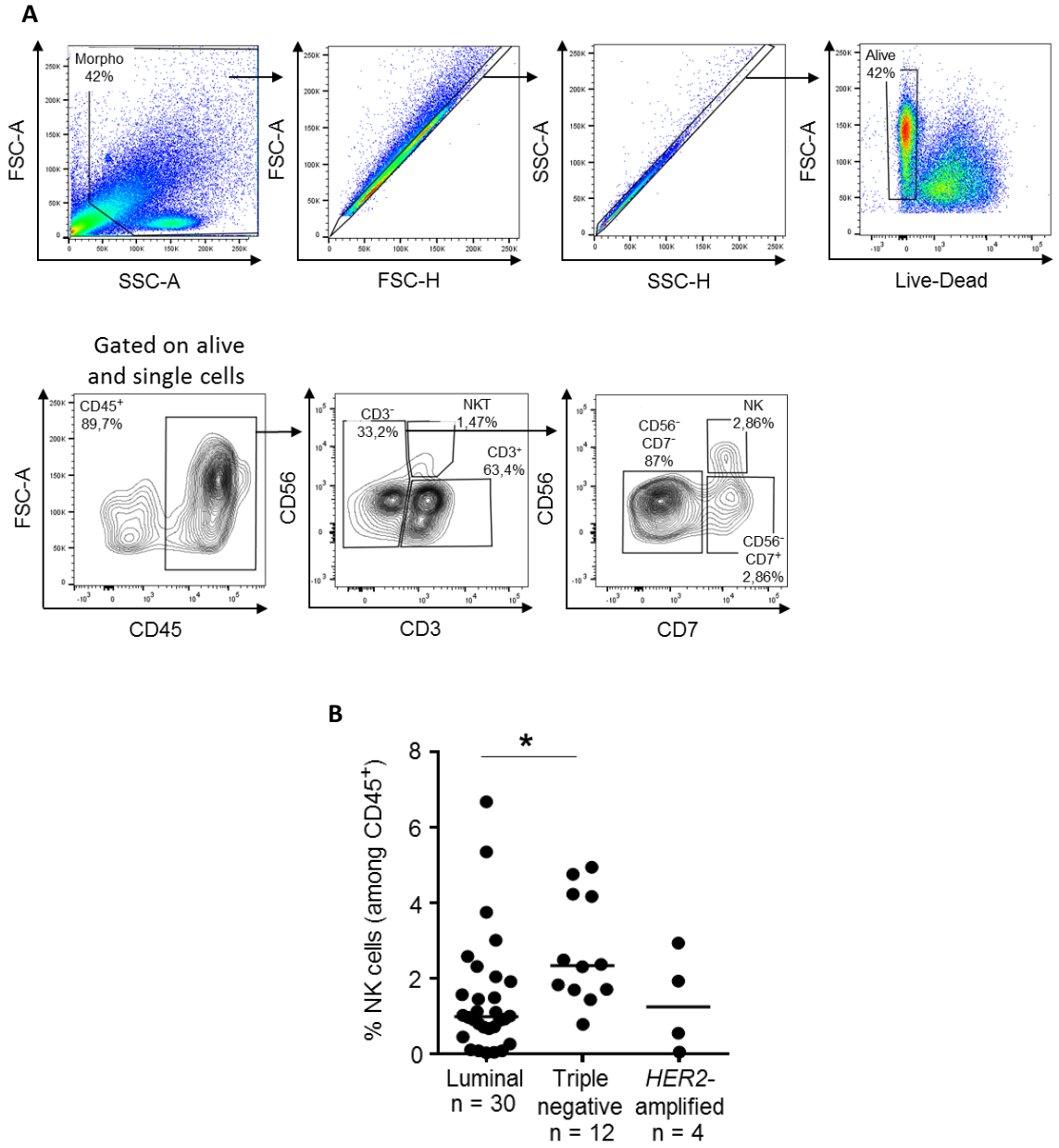

Fig. S6. Gating strategy to identify NK cells in tumor cell suspensions by flow cytometry

(A) Tumor cell suspensions were stained for CD45, CD3, CD56, and CD7 expression and tumor-infiltrating NK cells were identified using gating strategy as illustrated. Cell viability was determined using Zombie dye (Biolegend). **(B)** Cell suspensions were obtained from fresh breast tumors to analyze NK cell frequency among total infiltrating cells by flow cytometry according to BC molecular types (n = 46 patients). Kruskal Wallis test with Dunn's multiple comparisons test was performed.

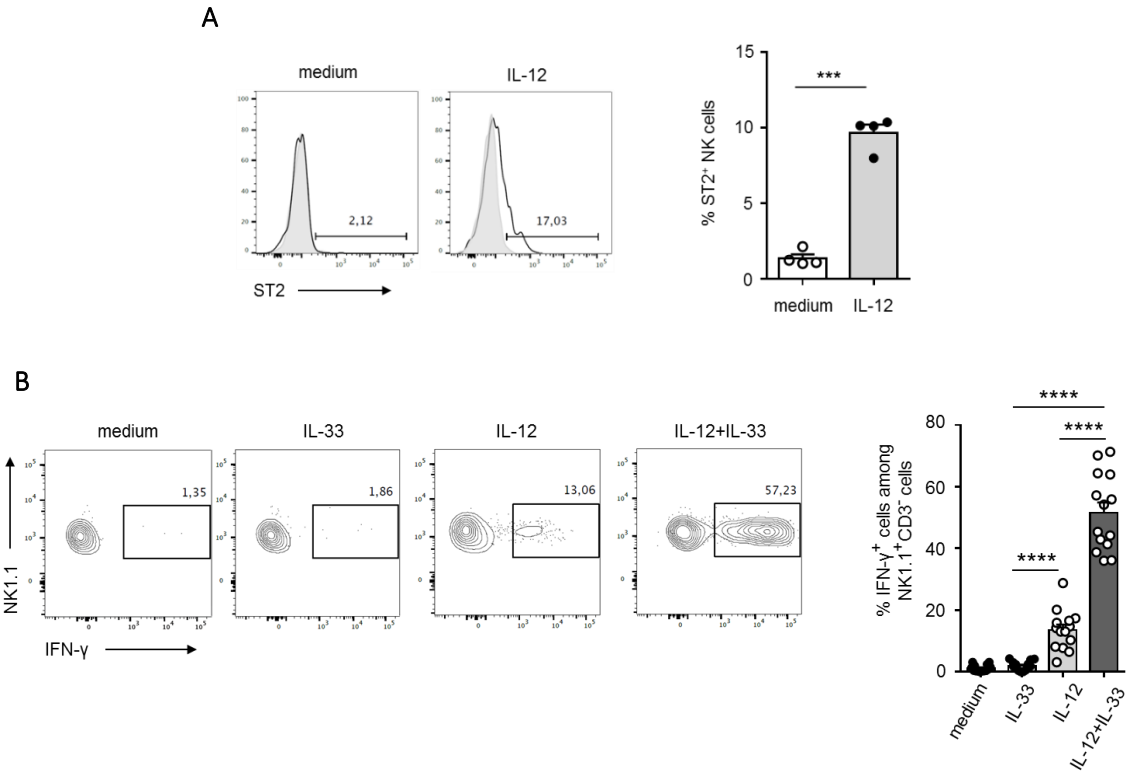

Fig. S7. IL-12 sensitizes mouse splenic NK cells to the production of IFN-γ in response to IL-33

(A) Splenic cells were activated with IL-12 (20 ng/mL) or not for 24 h prior to flow cytometry analysis of ST2 surface expression (black line) or corresponding isotypic control (grey). CD45, NK1.1, and CD3 were used to identify NK cells. Representative histogram plots (left) and quantification (%) (right) of $ST2^+$ NK cells after medium or IL-12 culture. Horizontal bars represent the mean + SEM (n = 4 individual mice). Paired two-tailed Student's *t*-test was performed.

(B) Splenic cells were activated as indicated (20 ng/mL of each cytokine) for 24 h prior to flow cytometry analysis of IFN-γ intracellular expression. CD45, NK1.1, and CD3 were used to identify NK cells. Plots are representative of four individual experiments with 3 to 4 mice/experiment and results for each individual mouse are presented in the right panel. Results are expressed as mean + SEM. One-way repeated measures ANOVA with Tukey's multiple comparisons test was performed.

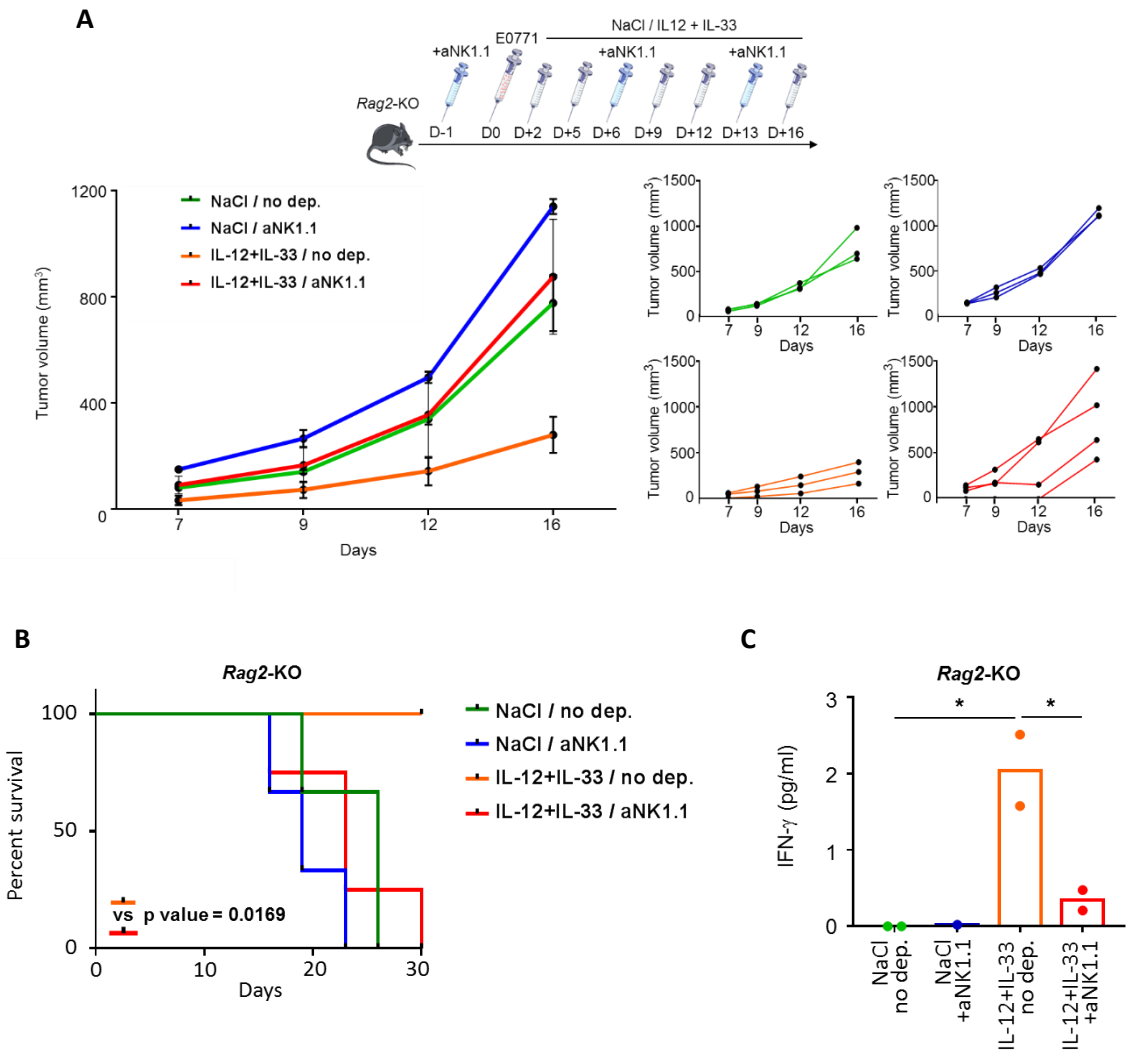

Fig. S8. Antitumoral effect of IL-33 and IL-12 combination is dependent on NK cells in *Rag2*-KO mice

(A) *Rag2*-KO mice were injected intra-peritoneally with NaCl or anti-NK1.1 depleting antibody prior to intra-mammary injection with 2.5x10^5 E0771 cells on day 0 and then treated in the tumor area with NaCl or a combination of 10 ng/mouse rmIL-12 and 100 ng/mouse rmIL-33 twice a week from day 2 to day 23. Primary tumor growth was monitored in non-depleted *Rag2*-KO mice treated with NaCl (n = 3) or with rmIL-12 and rmIL-33 combination (n = 3) or in NK cell-depleted WT mice treated with NaCl (n = 3) or with rmIL-12 and rmIL-33 combination (n=4). Two-way ANOVA with Tukey's multiple comparisons test was performed.

(B) Kaplan-Meier survival plots of non-depleted *Rag2*-KO mice treated with NaCl (n = 3) or with rmIL-12 and rmIL-33 combination (n = 3) or in NK cell-depleted WT mice treated with NaCl (n = 3) or with rmIL-12 and rmIL-33 combination (n=4). Mice were sacrificed when longest side of primary tumor reached 17 mm. Log-rank test was

performed and the p-value is indicated for non-depleted mice treated with rmIL-12 + rmIL-33 vs NK cell-depleted mice treated with rmIL-12 + rmIL-33.

(C) Serum was retrieved from blood collected at day 5, 4hrs after NaCl or cytokine injection into the peritumoral area. IFN-γ concentration was measured by ELISA in the serum of non-depleted *Rag2*-KO mice treated with NaCl (n = 3) or with rmIL-12 and rmIL-33 combination (n = 3) or in NK cell-depleted WT mice treated with NaCl (n = 3) or with rmIL-12 and rmIL-33 combination (n = 4). Histogram bars represent the median. Kruskal Wallis test with Dunn's multiple comparisons test was performed.

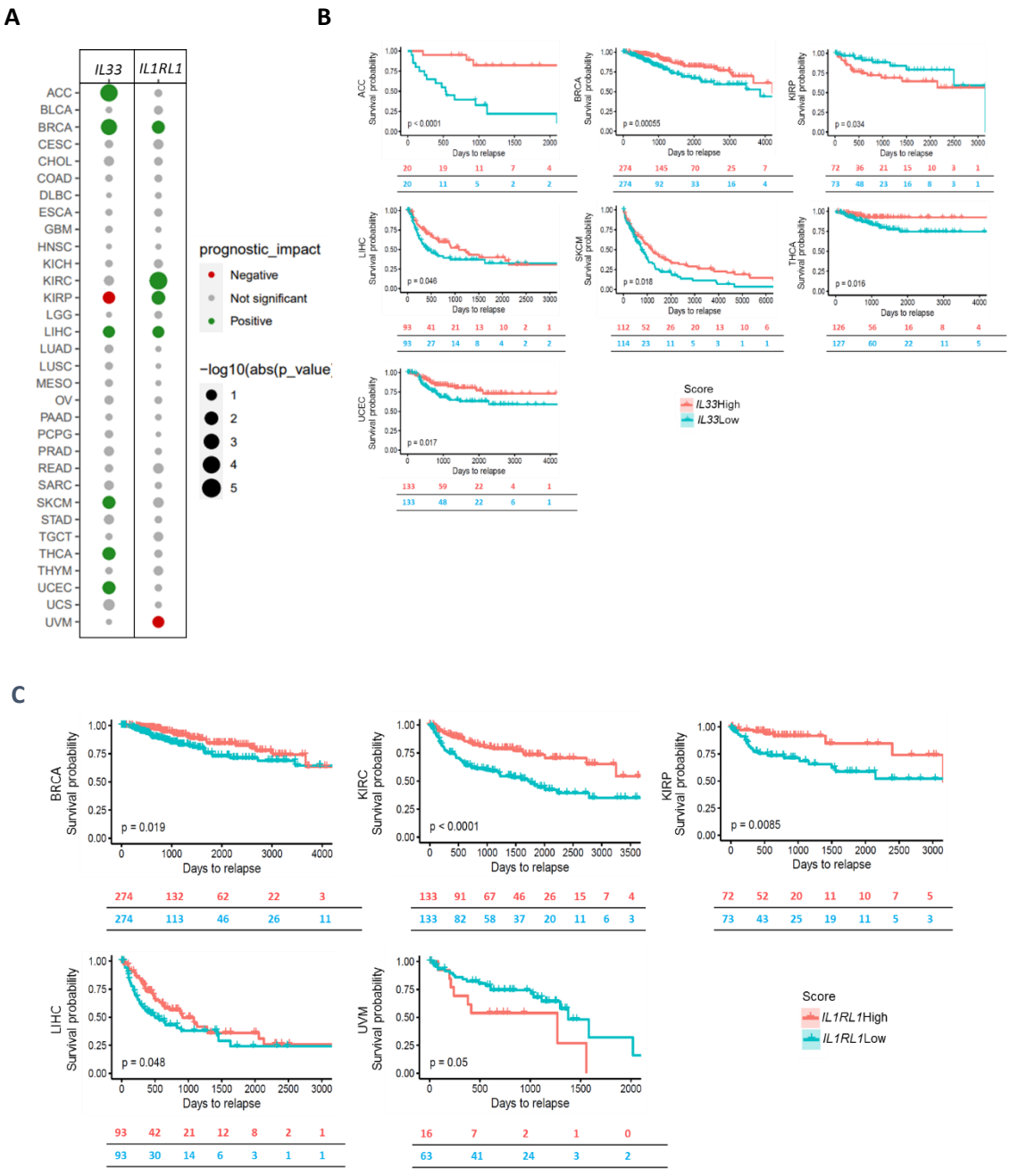
A
IL33
IL1RL1
ACC
BLCA
BRCA
CESC
CHOL
COAD
DLBC
ESCA
GBM
HNSC
KICH
KIRC
KIRP
LGG
LIHC
LUAD
LUSC
MESO
OV
PAAD
PCPG
PRAD
READ
SARC
SKCM
STAD
TGCT
THCA
THYM
UCEC
UCS
UVM
prognostic_impact
Negative
Not significant
Positive
−log10(abs(p_value
1
2
3
4
5
B
ACC
Survival probability
p < 0.0001
BRCA
p = 0.00055
KIRP
p = 0.034
LIHC
p = 0.046
SKCM
p = 0.018
THCA
p = 0.016
UCEC
p = 0.017
Days to relapse
Score
IL33High
IL33Low
C
BRCA
p = 0.019
KIRC
p < 0.0001
KIRP
p = 0.0085
LIHC
p = 0.048
UVM
p = 0.05
Score
IL1RL1High
IL1RL1Low

D

Variable		N	Hazard ratio	p
Age_cat	(25,45]	150	Reference	
	(45,65]	500	0.71 (0.44, 1.16)	0.171
	(65,75]	166	0.76 (0.40, 1.45)	0.406
	(75,90.1]	106	1.17 (0.58, 2.35)	0.654
Molecular_subtype	Basal	167	Reference	
	Her2	71	0.80 (0.39, 1.66)	0.551
	LumA	495	0.57 (0.35, 0.91)	0.019
	LumB	189	0.43 (0.23, 0.80)	0.008
Stage	1	152	Reference	
	2	536	2.03 (0.95, 4.33)	0.067
	3	218	4.94 (2.28, 10.70)	<0.001***
	4	16	20.39 (7.94, 52.35)	<0.001***
IL33_cat	Low	229	Reference	
	Intermediate1	227	0.46 (0.26, 0.81)	0.007**
	Intermediate2	234	0.65 (0.38, 1.10)	0.107
	High	232	0.45 (0.26, 0.79)	0.006**

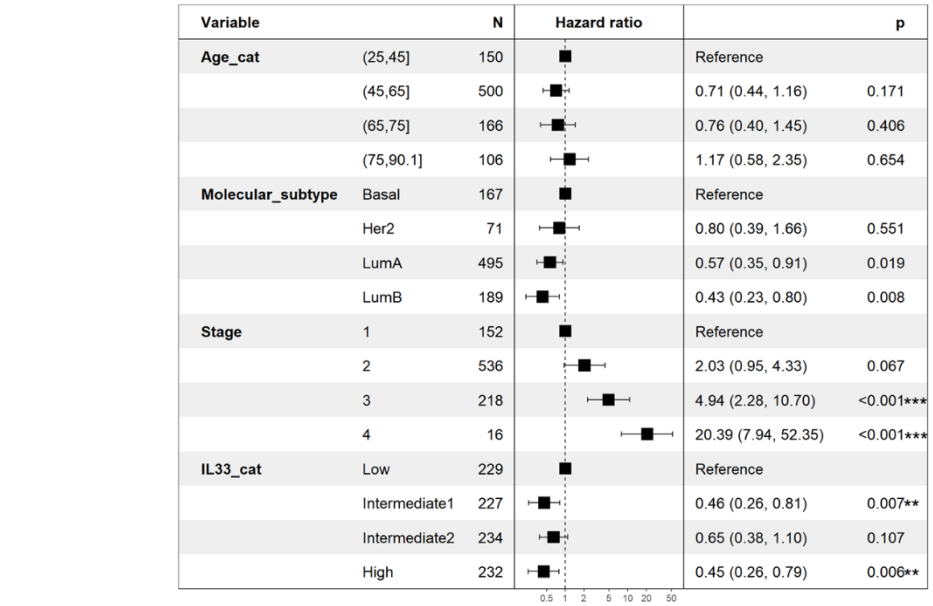

E

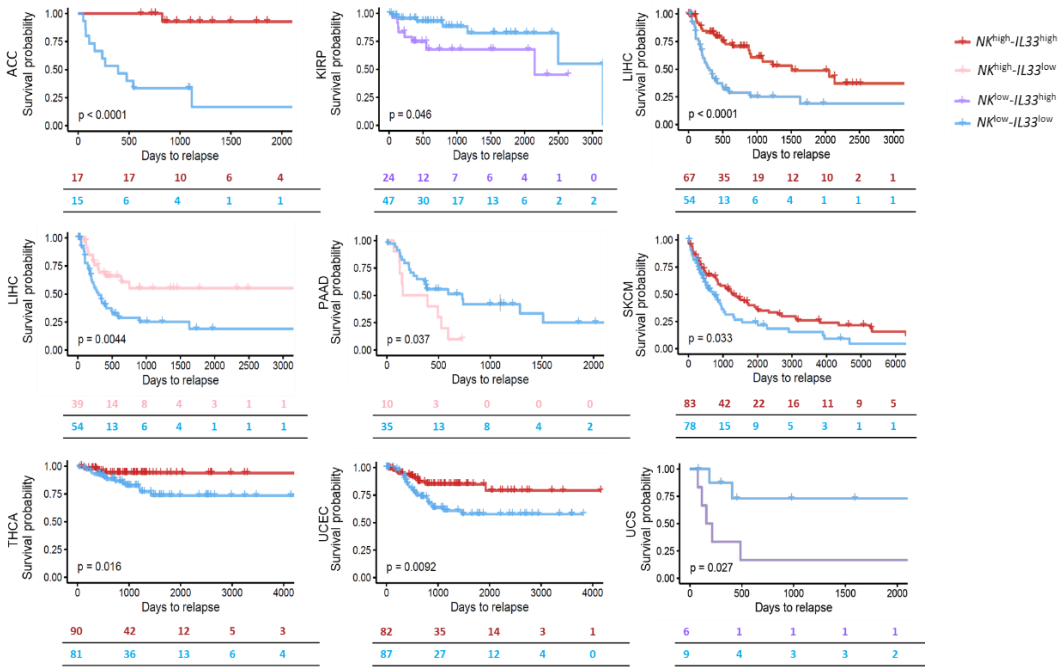

Fig. S9. IL-33 is associated with increased overall patient survival for several cancers

(A) Summary of p-values associated with the log rank test performed to evaluate prognostic value of *IL33* and *IL1RL1* (ST2) in 32 human TCGA cancer data sets (the same as in Fig. 6A, MESO: Mesothelioma ; UVM: Uveal Melanoma were added). Data are represented as a bubble map showing positive (green) or negative (red) impact on progression-free survival. Dots size represents p-values obtained by log-rank test.

(B) Patients from TCGA database were stratified as high or low for *IL33* and progression-free survival was analyzed in all cancer data sets. Kaplan-Meier survival curves for ACC, BRCA, KIRP, LIHC, SKCM, THCA, and UCEC patients are represented and p-values were obtained with log-rank test.

(C) Patients from TCGA database were stratified as high or low for *IL1RL1* (ST2) and progression-free survival was analyzed in all cancer data sets. Kaplan-Meier survival curves for BRCA, KIRC, KIRP, LIHC, and UVM patients are represented and p-values were obtained with log-rank test.

(D) Multivariate Cox analysis of *IL33* impact on prognosis in breast cancers from TCGA dataset regarding the age, molecular subtype, and stage of the tumors p-values were obtained with log-rank test.

(E) Kaplan-Maier curves for progression-free survival for $NK^{high}/IL33^{high}$, $NK^{high}/IL33^{low}$ and $NK^{low}/IL33^{high}$ scores as compared to $NK^{low}/IL33^{low}$ in cancer datasets from TCGA that showed statistical significance in Fig. 7B. p-values were obtained with log-rank test.

Table S1. Reagent and resources table

REAGENT OR RESOURCE	SOURCE	IDENTIFIER
Flow cytometry antibodies (Human)		
Anti-CD3-BV711	BD Bioscience	Clone UCHT1 Mouse IgG1 κ
Anti-CD3-PerCP	Miltenyi	Clone BW264/56, Mouse IgG2a κ
Anti-CD3-V450	BD Bioscience	Clone UCHT1 Mouse IgG1 κ
Anti-CD4-BB515	BD Bioscience	Clone RPAT4 Mouse IgG1 κ
Anti-CD4-FITC	BD Bioscience	Clone RPAT4 Mouse IgG1 κ
Anti-CD7-BV650	BD Bioscience	Clone M-T701, Mouse IgG1 κ
Anti-CD7-BV711	BD Bioscience	Clone M-T701, Mouse IgG1 κ
Anti-CD7-FITC	Beckman Coulter	Clone 8h8.1, Mouse IgG2a κ
Anti-CD8-PerCP-Cy5.5	BD Bioscience	Clone RPA T8, Mouse IgG1 κ
Anti-CD14-BV510	BD Bioscience	Clone MϕP9, Mouse IgG2b κ
Anti-CD16-V500	BD Bioscience	Clone 3G8, Mouse IgG1 κ
Anti-CD25-PE	BD Bioscience	Clone M-A251, Mouse IgG1 κ
Anti-CD45-AF700	BD Bioscience	Clone HI30, Mouse IgG2b κ
Anti-CD45-BV510	BD Bioscience	Clone HI30, Mouse IgG2b κ
Anti-CD56-PEVio770	Miltenyi	Clone AF12-7H3, Mouse IgG1 κ
Anti-CD56-VioBright-FITC	Miltenyi	Clone AF12-7H3, Mouse IgG1 κ
Anti-CD57-APC	BD Bioscience	Clone HNK-1, Mouse IgM κ
Anti-CD69-APC	BD	Clone FN50, Mouse IgG1 κ
Anti-CD127-APC	eBioscience	Clone eBioRDR5, Mouse IgG1 κ
Anti-CD158(KIR2DL1/S1/S3/S5)-PE-Cy7	Biolegend	CloneHP-A4, Mouse IgG2b κ
Anti-CD158e1(KIR3DL1)-PE-Cy7	Biolegend	Clone DX9, Mouse IgG1 κ
Anti-IFNg-BV421	Biolegend	Clone 4SB3, Mouse IgG1 κ
Anti-IL-1R1-BV421	BD Bioscience	Clone 89412, Mouse IgG1 κ
Anti-IL-18Ra-PE	BD Bioscience	Clone H44, Mouse IgG1 κ
Anti-p-p38-PE	BD Bioscience	Clone 36/p38, Mouse IgG1 κ

Anti-p-p65-PE	BD Bioscience	Clone K10-895.12.50, Mouse IgG2b κ
Anti-p-S6	Cell Signaling Technology	Clone D57.2.2E, Rabbit IgG
Anti-p-STAT4-PE	BD Bioscience	Clone 38/p-Stat4, Mouse IgG2b κ
Anti-ST2-PE	R&D	Polyclonal goat
Flow cytometry antibodies (Mouse)		
anti-CD11b-APCeFluor 780	eBioscience	Clone M1/70, Rat IgG2b κ
anti-CD27-PerCPeFluor 710	eBioscience	Clone LG.7F9, Haster IgG
anti-IFN-γ-PE	Biolegend	Clone XMG1.2, Rat IgG1 κ
anti-IL-1R-BV421	BD Bioscience	Clone 4E2, Rat IgG2a κ
anti-IL-18Rα-PE	eBioscience	Clone P3TUNYA, Rat IgG2a κ
anti-NK1.1-APC	BD Bioscience	Clone PK136, Mouse IgG2a κ
anti ST2-PE	BD Bioscience	Clone U29-93, Rat IgG2a κ
Other antibodies		
Anti-goat	Agilent	E0466
Anti-IL-18	MBL	Clone 125-2H, Mouse IgG1 κ
Anti-IL-33	R&D	Clone AF3625, Goat
Anti-NK1.1	BioXCell	Clone PK136
Anti-NKp30	R&D	Clone 210845 Mouse IgG2a κ
Anti-NKp46	R&D	Clone 195314, Mouse IgG2b κ
Anti-PanCK	Agilent	clone AE1-AE3,
Anti-p-STAT4	Cell SIgnaling Technology	Y693, Rabbit IgG
Anti-ST2	R&D	Clone 97203, Mouse IgG1 κ
Reagents		
Calcein	Invitrogen	C1430
CTV	Invitrogen	C34557

Continued

REAGENT OR RESOURCE	**SOURCE**	**IDENTIFIER**
DAPI	Invitrogen	D1306

DNAse I	Sigma-Aldrich	D4263
GolgiPlug	BD bioscience	555029
Lisofylline	Cayman chemicals	10010785
Lymphocyte Separation Medium	Eurobio	CMSMSL0101
Pharm LyseTM Buffer	BD Biosciences	555899
Lyse/fix Buffer Phosflow	BD Biosciences	558049
Perm Buffer III Phosflow	BD Biosciences	558050
RPMI 1640 Medium, GlutaMAX	Gibco	61870036
Sulfinpyrazone	Sigma-Aldrich	S9509
Type IV collagenase	Sigma-Aldrich	C5138
Zombie Dye Aqua	Biolegend	423101
Cytokines		
Recombinant Human IFN-α2b	Schering-Plough	
Recombinant Human IL-1α	Peprotech	200-01A
Recombinant Human IL-1β	Peprotech	200-01B
Recombinant Human IL-1RA	Peprotech	200-01RA
Recombinant Human IL-2	Chiron	
Recombinant Human IL-12	Miltenyi	130-096-704
Recombinant Human IL-15	Peprotech	200-15
Recombinant Human IL-18	MBL	B003-5
Recombinant Human IL-33	Miltenyi	130-109-378
Recombinant Mouse IL-1α	Miltenyi	130-094-050
Recombinant Mouse IL-1β	Miltenyi	130-094-053
Recombinant Mouse IL-12	Miltenyi	130-096-707
Recombinant Mouse IL-12 (*in vivo*)	R&D	419-ML
Recombinant Mouse IL-18	MBL	B002-5
Recombinant Mouse IL-33	Miltenyi	130-112-958
Recombinant Mouse IL-33 (*in vivo*)	Biolegend	580502

Kits		
Bio-Plex Pro™ Human Cytokine 17-plex	BioRad	M5000031YV
ChIP-IT High Sensitivity	Active Motif	53040
Extra Sensitive IFN gamma Mouse ELISA Kit	ThermoFischer	BMS609
FoxP3/Transcription Factor Staining Set	eBioscience	00-5523-00
Human IFN-γ DuoSet ELISA kit	R&D	DY285B
iScript Reverse Transcription kit	BioRad	1708840
MycoAlertTM Mycoplasma Detection Kit	Lonza	LT07-118
NK Cell Isolation Kit, human	Miltenyi	130-092-657
NucleoSpin RNA Kit	Macherey-Nagel	740955
Oligonucleotides		
GADD45α TaqMan	ThermoFischer	Hs00169255_m1
Negative Primer Set 1 and 2	Active Motif	71001 and 71002
IL1Rap TaqMan	ThermoFischer	Hs00895050_m1
IL1RL1 TaqMan	ThermoFischer	Hs00249384_m1
IL1RL1 (promoter) Forward	Agilent	5'-GTGATCATCGGGTTCAGCTTATC-3'
IL1RL1 (promoter) Reverse	Agilent	5-'GCTTTACTAAATACAACAGCCAGCCT-3'
SimpleChIP Human *PRF1* Primers	Cell Signaling Technology	9014S

263